

**Studies of the Spatial Organization of Metabolism in
Shewanella oneidensis and *Pseudomonas aeruginosa*
Biofilms**

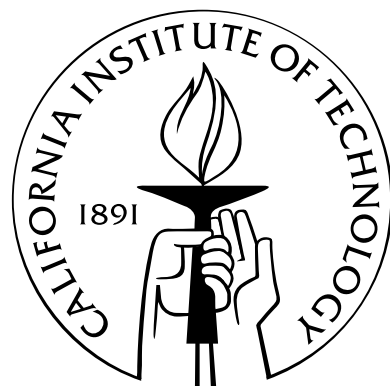
Thesis by

Tracy K. Teal

In Partial Fulfillment of the Requirements

for the Degree of

Doctor of Philosophy



California Institute of Technology

Pasadena, California

2008

(Defended May 24, 2007)

© 2008

Tracy K. Teal

All Rights Reserved

Abstract

Bacteria grow in the environment as surface-attached microbial communities. These communities are pervasive and resilient in the face of changing and challenging environmental conditions. Because of their community organization and three-dimensional structure, conditions within a biofilm are heterogenous, exposing the bacterial cells to individual microenvironments depending on their location in the biofilm and the biomass of the structure. Communities are therefore thought to be metabolically stratified. To understand how communities are organized with regard to growth activity and metabolic state and what role endogenous compounds might play in this organization, this thesis explores the spatiometabolic organization and dynamics of *Shewanella oneidensis* biofilms and the roles that acyl-homoserine lactones and phenazines might have in *Pseudomonas aeruginosa* communities.

Using unstable fluorescent reporters to measure growth activity and protein synthesis and conducting quantitative image analysis, domains of activity were determined for developing *S. oneidensis* biofilms. Biofilm structures reproducibly stratify with respect to growth activity and metabolism as a function of structure size. Within domains of growth-inactive cells, genes upregulated under anaerobic conditions are expressed demonstrating that cells in the nutrient-limited regions of the biofilm are not dead, but are capable of generating enough energy to persist.

To determine if these growth-inactive cells are able to respond dynamically to changes in environmental conditions and what types of nutrients affect growth activity profiles, *S. oneidensis* biofilms were exposed to increased concentrations of an electron acceptor and an electron donor. Cells in the growth-inactive regions were able to respond to nutrient changes, but were more affected by a change in electron acceptor than electron donor.

To investigate the role of small molecules in biofilm community organization, the degradation of acyl-homoserine lactone (AHL), was studied. This molecule is an important part of the quorum sensing signaling network in *P. aeruginosa* where the bacteria both produce and sense this molecule. When bacteria sense a specific concentration of the AHL, they are induced to form a biofilm or initiate a community wide response. To determine what role AHL degradation has on the community response, a mutant that constitutively degrades the compound was characterized and expression profiles for degradation were compared between this strain and wild type communities. Genes for AHL degradation were expressed in the middle of biofilm colonies suggesting that degradation may be an important part of the community response network. It was also shown that AHLs can be used as a substrate for growth, so nutrient-limited cells might also be able to use AHLs to generate energy.

Finally, to investigate whether endogenously produced redox-active small molecules could potentially play a role in energy maintenance in communities, the SoxR sensing system was studied. This system is typically thought to regulate the response to superoxide radicals. In *P. aeruginosa* and other organisms outside the class of enterics, however, recent evidence suggested that they may instead play a role in the sensing of redox-active small molecules produced under conditions of low nutrients and high cell density. To determine the ubiquity of this response mechanism, bioinformatic analyses were conducted to discover SoxR binding sites across all genomes containing SoxR. Predictions for binding sites and the mechanism of regulation, redox-active molecule induction, were confirmed in the Gram-positive bacterium *Streptomyces coelicolor*.

This work brings us closer to understanding how cells persist and retain the capacity to dynamically regulate their metabolism in biofilm communities. Using reporter assays and quantitative analyses, studies can be done to determine metabolic organization within communities and further investigate the role that endogenous small molecules can play in community organization.

Contents

Abstract	iii
1 Introduction	1
1.1 Overview	2
2 Background	5
2.1 Bacterial communities in the environment	5
2.2 Biofilm formation	6
2.3 Spatial organization of biofilm communities	8
2.4 The role of small molecules in biofilm development and maintenance	9
2.4.1 Quorum sensing	10
2.4.2 Redox active compounds	10
2.4.3 <i>Shewanella oneidensis</i> as a model organism for the study of metabolic organization in biofilms	11
2.4.4 <i>Pseudomonas aeruginosa</i> as a model organism for the study of community response to endogenous small molecules	12
2.5 Summary	13
3 Spatiometabolic stratification of <i>Shewanella oneidensis</i> biofilms	14
3.1 Abstract	14
3.2 Introduction	15
3.3 Materials and Methods	16
3.3.0.1 Bacterial strains, plasmids and media.	16
3.3.0.2 Plasmid stability determination.	17
3.3.0.3 GFP expression and stability measurements.	17
3.3.0.4 Determination of respiration rates.	17

3.3.0.5	Biofilm experiments.	18
3.3.0.6	LIVE/DEAD stain.	18
3.3.0.7	<i>mtrB</i> expression with varying oxygen levels.	18
3.3.0.8	Quantitative analysis of biofilm images.	19
3.4	Results	20
3.4.0.9	Development of <i>S. oneidensis</i> biofilms	20
3.4.0.10	LIVE/DEAD stain for <i>S. oneidensis</i> biofilms	20
3.4.0.11	Patterns of growth activity in biofilms using the <i>rrnB</i> P1 reporter .	21
3.4.0.12	Patterns of metabolism under anaerobic conditions in biofilms using the <i>mtrB</i> reporter	23
3.4.0.13	Quantitative analysis of expression patterns	25
3.5	Discussion	25
3.6	Acknowledgements	27
3.7	Supplemental methods	27
3.7.0.14	Mini-Tn7 Derivative Construction and Characterization.	27
4	Metabolic dynamics and heterogeneity in <i>Shewanella oneidensis</i> biofilms	30
4.1	Abstract	30
4.2	Introduction	31
4.3	Material and Methods	31
4.3.1	Bacterial strains, plasmids and media.	31
4.3.2	Measurements of growth and fluorescence	32
4.3.3	Fermentor experiments	32
4.3.4	NADH and NAD ⁺ measurements	33
4.3.5	Growth activity response to the addition of fumarate	33
4.3.6	Growth activity of <i>S. oneidensis</i> DSP10 and <i>S. oneidensis</i> NP-FC-1 in aerobic and anaerobic conditions	34
4.3.7	Biofilm experiments	34
4.3.8	Quantitative image analysis	35
4.4	Results	35
4.4.1	Growth and growth activity of <i>S. oneidensis</i> DSP10 and <i>S. oneidensis</i> NP- FC-1 in aerobic and anaerobic conditions	35
4.4.2	Fermentor measurements of growth, dissolved oxygen and NADH/NAD ⁺ ratios	35

4.4.3	Growth activity response to the addition of fumarate	37
4.4.4	Biofilm growth activity profiles with the addition of fumarate or lactate.	39
4.4.5	Profiles of growth activity in biofilms of the <i>S. oneidensis</i> fumarate reductase mutant, NP-FC-1	40
4.5	Discussion	40
5	Conclusion	43
5.1	Summary	43
5.1.1	What is the spatial and temporal stratification of growth and metabolic states within a biofilm? In particular, can cells decouple metabolism from growth? . .	43
5.1.2	Does nutrient availability affect growth and metabolic stratification dynamically? .	44
5.1.3	How are small molecules used differently within different regions of a biofilm? .	44
5.1.4	Might redox-active small molecule production and sensing be a ubiquitous process that could be utilized for metabolism under biofilm conditions? . . .	44
5.2	Future directions	45
A	Development of <i>Shewanella oneidensis</i> biofilms	48
A.1	Abstract	48
A.2	Introduction	48
A.3	Methods	49
A.3.1	Setup of flow cell system	49
A.3.2	Media	50
A.3.3	Cultures	50
A.3.4	Imaging	50
A.3.5	Image processing	51
A.3.6	Quantitative image analysis	51
B	Supplemental tables for Chapter 6	54
B.1	Pyscangen table	54
B.2	Pyscangenes table	80
Bibliography		95

List of Figures

2.1	Stages of biofilm development.	8
3.1	Time course of <i>S. oneidensis</i> biofilm development. Cells are expressing a constitutive GFP. The first four panels are x-y slices at the base of the developing biofilm structure. The final panel is a z-profile through the structure. Scale bar is 10 μ m.	20
3.2	LIVE/DEAD staining in <i>S. oneidensis</i> biofilms. Green is the live stain, Syto9, and red is the dead stain, propidium iodide. Grid marks are 10 μ m. (A) At 60 μ m in diameter most cells continue to stain as live. (B) At ~80 μ m in diameter cells throughout the biofilm start to stain dead. (C) At ~140 μ m in diameter almost all cells in the middle of the biofilm are stained as dead.	21
3.3	Fluorescence levels and absorbance at OD ₆₀₀ for <i>S. oneidensis</i> MR-1 (diamonds), <i>S. oneidensis</i> DKN308 constitutively expressing GFP (squares), and <i>S. oneidensis</i> DKN310 expressing GFP(AAV) from a ribosomal promoter, representing growth activity (circles). OD ₆₀₀ is indicated by dashed lines, and fluorescence by solid lines. As cells grow through exponential phase, fluorescence levels increase, but when stationary phase is reached, fluorescence levels from the constitutively expressing GFP remain high whereas fluorescence from the growth active version decreases rapidly. Error bars represent standard deviations of triplicate cultures; in some cases the error is smaller than the size of the symbol.	22

4.2	Representative curve of growth, dissolved oxygen concentration and NADH/NAD ⁺ ratios for <i>S. oneidensis</i> MR-1 cultures grown in a chemostat. The solid gray line is NADH/NAD ⁺ ratio. The dashed black line with the solid black triangles is dissolved oxygen concentration, where 1.0 represents the maximum concentration in air, 21% oxygen. The dashed black line with the open squares is growth as measured by OD ₆₀₀ . Oxygen concentrations decrease as cell density increases, and there is a brief drop in the NADH/NAD ⁺ ratios during this transition in cell density and oxygen concentration.	37
4.3	Fluorescence levels and OD ₆₀₀ for <i>S. oneidensis</i> MR-1 pTK4 grown aerobically with and without fumarate. OD ₆₀₀ is indicated by dashed lines and fluorescence by solid lines. pTK4 fum 420 cultures were switched to media containing fumarate at 420 minutes, indicated by the arrow on the graph. pTK4 fum cultures were grown in media containing fumarate through the whole experiment.	38
4.4	Representative images of <i>S. oneidensis</i> MR-1 pTK4 biofilms with no change in media (A and B), with the addition of 2mM fumarate (C and D) or with the addition of 20mM fumarate (E and F). Images A, C and F are the biofilms at 48 hours before a change in conditions. Images B, D and F are 56 hours, 6 hours after the media change. Green fluorescence is fluorescence from the ribosomal reporter pTK4 and indicates regions of growth activity. In panels A and B, no change in the media is made and there is a slight decrease in fluorescence intensity at 56 hours. In panels C and D, there is a slight increase in the intensity and region of fluorescence at 56 hours when the biofilm has been exposed to 2mM fumarate. In panels E and F there is a greater increase in the intensity and region of fluorescence after exposure to 20mM fumarate.	39
4.5	Representative images of the fumarate reductase mutant, <i>S. oneidensis</i> NP-FC-1 pTK4, biofilms before and after the addition of 20mM fumarate to the media. Panel A is 48 hours and panel B is at 56 hours, 6 hours after the addition of fumarate. Green fluorescence is fluorescence from the ribosomal reporter pTK4 and indicates regions of growth activity. After the addition of fumarate, colonies of <i>S. oneidensis</i> NP-FC-1 pTK4 maintain their growth activity, but significantly decrease in size.	41
A.1	Setup of biofilm once flow-through system on the biofilm cart.	49
A.2	Excitation and emission spectra for the enhanced fluorescent proteins. From Patterson, Day and Piston [73].	52

List of Tables

B.1	The number of sites found in intergenic regions and within genes for thresholds 1.0 - 13.0 in each genome containing SoxR.	54
B.2	The soxbox sites found in genomes containing SoxR. Column 1 is the site energy of the site. Column 2 is the sequence of the site. Column 3 is the operon position, whether the named operon is to the left or the right of the soxbox site. Column 4 is the distance from the soxbox site to the start of the operon. Column 5 are the genes contained in the adjacent operon.	80

Chapter 1

Introduction

“One of the extraordinary things about life is the sort of places it’s prepared to put up with living. Anywhere it can get some kind of a grip, whether its the intoxicating seas of Santragiinus V, where the fish never seem to care whatever the heck kind of direction they swim in. the fire storms of Frastra, where, they say, life begins at 40,000 degrees, or just burrowing around in the lower intestine of a rat for the sheer unadulterated hell of it, life will always find a way of hanging on somewhere.” - Douglas Adams, Mostly Harmless

Bacteria living in the environment face the challenge of living in communities under nutrient-limited conditions. Even areas we think of as being nutrient-rich such as our intestines, become nutrient-limiting when high numbers of bacteria are present, competing for resources. In particular, while it is often thought that bacteria live most of their lives as individual planktonic cells, it has recently been discovered that most bacteria live their lives in surface-attached microbial communities, or biofilms [24]. Biofilm communities have been shown to be prevalent in environments from hydrothermal vents and caves to the lungs of patients with cystic fibrosis [20, 27]. Because these bacteria aggregate together they are creating an environment where they are limiting themselves for nutrients [108]. Why this bacterial lifestyle would be preferred then is not understood. It is known however that bacteria living in biofilms are much more resistant to changes in environmental conditions, antibiotics and anti-microbial agents [97]. There must therefore be something to account for their ubiquity and persistence in the environment.

Because of the inherent nutrient limitation and heterogeneity in biofilm communities, the metabolic state of cells must be different than that of an exponentially growing cell in a nutrient replete environment. It has been suggested that sub-populations of cells within biofilms are actually dead, having sacrificed themselves for the community, invoking a type of hierarchical selection argument.

However, it is likely that while cells may not be able to generate enough energy to grow and divide, they are generating enough energy to maintain their lives. What processes must occur to generate this maintenance energy are not well understood. Small molecules have been reliably shown to be endogenously generated under such conditions of low-nutrients and high cell density [15]. Some of these small molecules have been shown to be involved in activating community wide responses, such as in quorum sensing [4], where bacteria produce and sense a small molecule that triggers bacteria to form biofilms at a given threshold concentration. Other redox-active compounds are known to act as both antibiotics and as molecules that can aid in the transport of nutrients, and the roles of many others remain unexplored. It is becoming apparent that these endogenously produced small molecules play multiple roles in bacterial survival, and may be extremely important factors in the maintenance of biofilm communities.

With these maintenance processes in bacterial communities largely not understood, I set out to explore the spatial organization and dynamics of metabolic states within bacterial biofilms and to further investigate what types of processes and compounds might be important for maintaining populations of cells in these environments. I proposed to address the following questions:

1. What is the spatial and temporal stratification of growth and metabolic states within a biofilm?
In particular, can cells decouple metabolism from growth?
2. Does nutrient availability affect growth and metabolic stratification dynamically?
3. How are small molecules used differently within different regions of a biofilm?
4. Might redox-active small molecule production and sensing be a ubiquitous process that could be utilized for metabolism under biofilm conditions?

1.1 Overview

In this thesis I present our progress in answering these questions. **Chapter 2** reviews what we know about biofilm communities and the role of small molecules in bacterial metabolism and population signaling. This begins with a discussion of the pervasiveness and resilience of bacterial biofilms in the environment and the effects of biofilm communities on human health and industrial processes. This is followed by a review on biofilm formation, and it highlights what is known about how biofilm structures form, grow and detach. Next I focus on the heterogeneity within biofilm communities and discuss how diffusion and metabolism within biofilm structures has an effect on the microen-

vironments of cells within the biofilm. I review studies that have been conducted to explore the spatial organization of these communities with regards to their growth activity and some specific processes. I then discuss the role of endogenous small molecules, produced under conditions of low nutrients and high cell density, highlighting their role in biofilm formation and community response, as in quorum sensing, and the potential role of redox-active compounds in metabolic maintenance. Finally, I introduce two model organisms, *Shewanella oneidensis* and *Pseudomonas aeruginosa* and describe their merits as model organisms for the study of metabolic organization in biofilms and community response to endogenous small molecules. The chapter concludes with a brief summary focusing on what will be presented in this dissertation.

Chapter 3 presents our findings on the metabolic stratification of *Shewanella oneidensis* biofilms. We employed unstable fluorescent reporters to measure growth activity and protein synthesis *in vivo* over the course of *S. oneidensis* biofilm development and created a quantitative routine to compare domains of activity in independently grown biofilms. In these experiments we observed that biofilm structures reproducibly stratify with respect to growth activity and metabolism as a function of size. In order to determine if cells in the middle of a biofilm were dead as is often thought to be the case, we compared regions of growth activity with those of active protein synthesis under anaerobic conditions. Within domains of growth-inactive cells, genes typically upregulated under anaerobic conditions are expressed well after growth has ceased, indicating that cells in all regions of the biofilm are persisting and are able to turn on metabolic programs appropriate to their local microenvironment and developmental stage. This chapter was published in Applied and Environmental Microbiology 72(11): 7324-30.

In **Chapter 4** we characterize how nutrient availability affects *S. oneidensis* biofilm metabolic organization and whether previously growth inactive cells are able to respond dynamically to changing nutrient conditions. We measured oxygen levels, cell number and NADH/NAD⁺ ratios to correlate oxygen availability with metabolic state. We then determined whether the addition of an electron acceptor can affect the growth activity of stationary phase, oxygen-limited planktonic cells. Finally, we quantitatively characterized the growth activity profiles of *S. oneidensis* biofilms in response to an electron acceptor, fumarate, and an electron donor, lactate. We also determined the effect of fumarate on a *S. oneidensis* fumarate reductase mutant biofilm.

In **Chapter 5** we describe a variant of *Pseudomonas aeruginosa* PAO1_{lagless}, that constitutively degrades long chain acyl-homoserine lactones (AHL), the molecules used in quorum sensing. We compare long-chain AHL accumulation and growth on long chain AHLs in wild-type *P. aeruginosa*

and the variant PAO1_{lagless}. Using microarray analysis, we determine the genes differentially expressed in each strain. Finally, we examine the expression of PA1032, a gene required for AHL degradation, in wild-type *P. aeruginosa* and PAO1_{lagless} under planktonic and biofilm conditions and determine the profiles of expression in biofilm conditions. This work was done in collaboration with Dr. Jean Huang and Dr. Jared Leadbetter.

In **Chapter 6**, we investigate whether SoxR may be regulated by redox-active small molecules endogenously produced under conditions of low-nutrients and high cell density, rather than by superoxides as the paradigm from *E. coli* would suggest. Using known binding sites for SoxR, we construct a position weight matrix (PWM) and use this PWM to find binding sites across all bacterial genomes. We then determine the specific genes that are being regulated by SoxR and categorize them according to function. To test our bioinformatics hypotheses, we determine the response of predicted SoxR regulated genes in *Streptomyces coelicolor* to actinorhodin, an endogenously produced redox-active compound. This work was done in collaboration with Dr. Lars E. P. Dietrich.

Chapter 7 contains a summary of the main findings of the work in this thesis, concluding remarks and potential directions for future work.

Two appendices are included. Appendix A describes the methods for growing *S. oneidensis* biofilms in more detail . Appendix B includes complete tables from Chapter 7.

Chapter 2

Background

2.1 Bacterial communities in the environment

Over the last decade our vision of microorganisms as cells swimming alone in the environment has shifted to the realization that most bacteria spend their lives as surface-attached microbial communities, or biofilms. These microbial biofilms are ubiquitous, resilient, responsive to their environment and able to communicate through chemical signalling [97]. Biofilms are generally described three-dimensional structures, often with pillar-like formations, consisting of bacterial cells and an extra-cellular matrix which holds the microcolonies together. Through the structure runs a network of open-water channels which can transport nutrients and waste products [75]. These complex differentiated communities are remarkably persistent in the face of changing environmental conditions and exposure to toxins [97]. Bacterial biofilms can be found in almost every environment. They have been characterized in regions as extreme as acidic hot springs, acid mine drainage and Antarctica to environments as mundane as shower curtains and the surfaces of our teeth [47, 51, 81, 114]. The presence of fossilized stromatolites suggests that the biofilm lifestyle is also an ancient one, having existed for thousands of years [34].

Biofilms are of particular importance in industrial systems and human health. Biofilms can contribute significantly to industrial processes such as waste water treatment, paper milling and potentially to biofuel production, or they can be destructive, clogging pipes and rusting surfaces [72]. In human health, biofilms of *Pseudomonas aeruginosa* form in the lungs of patients with cystic fibrosis [20, 67, 113]. (For a review of cystic fibrosis pathology see Boucher 2007 [12].) Plaque, leading to gingivitis, is a biofilm comprised of hundreds of species of bacteria [51]. Biofilms form on catheters and medical implants, on contact lenses and in wound infections [21]. Bacteria in these communities are up to one hundred times more resistant to antibiotics and other anti-microbial

agents than infections of planktonic cells.

It had been thought that the extracellular matrix that the cells produce was forming a diffusion barrier to toxins such as antibiotics and anti-microbial agents, but numerous studies have shown that this diffusion limitation alone cannot account for the remarkable resilience of these communities. An alternative factor that may account for the persistence of biofilms is that of the heterogeneity of the population and the potential for a subpopulation of cells in a less active metabolic state [11, 56, 97]. Nutrient diffusion, metabolism and microscale interactions create microenvironments within the community. Biofilm communities are therefore heterogeneous and spatially stratified, so that activity levels and biochemical processes occur differentially according to the location of a cell in the biofilm and overall mass of the biofilm structure [107]. Yet this metabolic heterogeneity is not well understood. In particular the spatial organization of growth and metabolic states and the dynamics of these states has not been well-characterized. In addition little is understood about the maintenance requirements or processes essential for growth of cells in these nutrient-limited communities. In order to understand the role of bacteria in the environment, i.e. how they affect nutrient cycling, trophic organization and other environmental processes, or to affect a biofilm community, for the purpose of using them in industrial processes or treating people with biofilm infections, it is important to understand the metabolic and maintenance processes being utilized and the organization of these processes within a community.

2.2 Biofilm formation

Biofilms formation proceeds much like a developmental process. As seen in Figure 2.1, bacteria attach to a surface and as more cells attach, they begin to form an extracellular matrix comprised of polysaccharides, extracellular DNA and other components [117]. In biofilms exhibiting the standard mushroom morphology seen in lab conditions and shown in Figure 2.1, the stalk of the mushroom is formed by cells on the surface continuing to grow and divide. The cap of the mushroom however forms as planktonic cells in the medium attach to the already growing structure, essentially pasting themselves to the outside of the colony and its extracellular polymeric substance (EPS) consisting of polysaccharides, extracellular DNA and other components [49]. Within the biofilm's structure, channels are formed around the macrocolonies that allow for nutrient and waste transport, creating a complex structure. When the colonies reach a certain size, cells in the middle of the structure begin to leave until finally the structure collapses.

Molecular genetic assays and proteomic studies have shown that particular sets of genes and

proteins are involved in specific steps along this pathway. For reviews see O'Toole 2003 [72], Ghigo 2003 [31], Stanley and Lazazzera 2004 [94] and Prüß et al [76]. While there are different pathways for making a biofilm, biofilm formation seems to be regulated at five main steps: surface attachment, microcolony formation, microcolony growth, depth of the mature biofilm and detachment. In attachment, both stable cell-surface interactions and specific environmental conditions are important. In many Gram-negative bacteria, flagella or pili are required for sensing contact with a surface and initiating surface adhesion [72]. In some non-motile Gram-positive strains however, only protein and polysaccharide adhesins have been shown to be required [35].

Microcolony formation and growth occurs when a community of bacterial cells a few layers deep develops on a surface and EPS is produced. In this process there is a transition from reversible to irreversible attachment. Initial characterization of this process in *P. aeruginosa* revealed that SadB, a protein of unknown function, mediates this transition [14].

In the maturation of biofilm structures, thick layers of cells are encased in EPS matrix. The structures can be homogenous mats of cells or complex structures composed of pillars and water channels. Much of the molecular characterization of biofilms has been done in *P. aeruginosa* where mutants have been identified that affect the depth or structure of biofilms within a given species. Similarly, different environmental conditions can have an effect on biofilm structure morphology. Catabolite repression and the transcription factor RpoS affect biofilm depth. Both mechanisms are used to report nutrient levels and therefore indicates that biofilm maturation is potentially regulated in response to nutrient levels in the environment [94]. Another mechanism important in biofilm maturation is a chemical cell-cell communication mechanism called quorum sensing, discussed in more detail below. During the maturation phase of biofilm development, cells must be maintained in the structures. Rhamnolipid surfactant production is one component required for the maintenance of the pillar structures [23].

Because of the interest in eliminating biofilms in medical environments, attention has been paid to the process of cell detachment from a biofilm. It has been shown that this process is inducible by sudden carbon or oxygen limitation and that certain genetic pathways and cyclic dinucleotides are involved in this process [45, 105, 103].

These are some of the mechanisms in biofilm development that have been studied in more detail, but many proteomic and genomic studies have examined gene and protein expression at all stages of biofilm formation [86, 89, 88, 92, 118]. Progress continues in studying the role of some of these genes in biofilm development and maintenance.

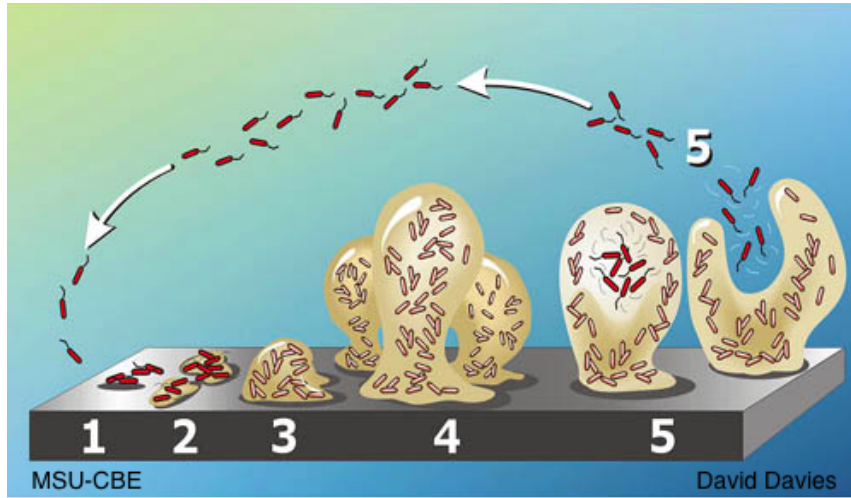


Figure 2.1: Stages of biofilm development.

2.3 Spatial organization of biofilm communities

While biofilm attachment, maturation and detachment have been well-studied, the metabolic states and organization of these states has been less well-characterized. In the complex structures that result from biofilm formation, each region has its own microenvironment due to diffusion and metabolism. Profiles of oxygen in aerobically grown biofilms show that oxygen is depleted approximately $30 \mu\text{m}$ into a *P. aeruginosa* biofilm structure [83]. Similarly, in *S. oneidensis* lactate does not diffuse through the entire biofilm structure [62].

In laboratory based single species biofilms, several studies have investigated spatial patterns of cellular growth activity and metabolism using a variety of techniques. For a review see Tolker-Nielsen and Molin 2000 [108].

Growth activity has been monitored in *Klebsiella pneumoniae*, using an acridine orange dye [115], and by tracking alkaline phosphatase activity under phosphate starvation conditions [43]. In both of these studies, growth activity was limited to the outer edges of the biofilm, in the regions at the nutrient-biofilm interface. Numerous studies using Syto9 and propidium iodide in the Live/Dead stain as well as other methods have concluded that these cells in the middle of the biofilm are dead, or not actively synthesizing proteins [42, 60, 110], but the accuracy of the Live/Dead stain as a reporter of cell viability has been questioned [8]. A more direct measure is to make use of the link between growth rate and ribosomal synthesis. Direct *in situ* measurements of rRNA were used initially to determine ribosomal content [74]. Sternberg et al developed a fluorescent reporter assay to track ribosome synthesis. Fusing an unstable green fluorescent protein (*gfp*(AAV)) to the

rrnB P1 promoter, which has been shown to correlate with ribosome synthesis and growth, growth activity could be tracked by monitoring green fluorescence levels [95]. Werner et al used this reporter in conjunction with an IPTG inducible green fluorescent protein (GFP) to track growth activity by ribosomal content as well as protein synthesis [116]. Additionally Werner et al tracked cells capable of elongation in a biofilm, treating colonies with carbenicillin to block cell division and then measuring individual cell length by transmission electron microscopy. Rani et al track growth activity and protein synthesis in Staphylococcal biofilms [82]. These studies demonstrate that cells display different amounts of growth activity correlated with the cell's location in the biofilm and the biofilm biomass. Growth activity was localized to the biofilm/bulk interface in both cases. It has been suggested that these profiles are determined by oxygen availability [119].

The use of these fluorescent reporters has greatly aided in the study of localization within biofilms. They have been used to track rhamnolipid synthesis [55] in *P. aeruginosa*, the virulence factor glucosyltransferases in *Streptococcus mutans* [121], multidrug efflux pumps [48] and other genes of interest [93]. These fluorescent protein reporters allow for real-time *in vivo* analysis of gene expression in a developing community and have the potential to elucidate the dynamics and distribution of gene expression within a developing biofilm. GFP requires oxygen to fold and fluoresce, but the lower limits required for folding, 0.1ppm dissolved oxygen, are likely to be present in biofilm conditions [36] and signals from GFP labelled cells have been shown to correlate with SYTO 60 nucleic acid staining [69].

These studies demonstrate that heterogeneity with regard to cellular activity and metabolism exists, and in particular, that biofilm communities show decreased growth activity near the center of the biofilm, where it is expected that cells are nutrient limited. Yet the specific localization of metabolic processes that occur in biofilms and how they might change over the course of biofilm development has remained largely unexplored. Questions remain as to whether growth inactive cells can decouple growth from metabolism so that they are still capable of generating energy for maintenance and responding to changes in environmental conditions.

2.4 The role of small molecules in biofilm development and maintenance

One mechanism that may be important in bacterial maintenance under these conditions is the generation of endogenous small molecules. Small molecule production has been show to occur under

conditions of nutrient-limitation and high cell-density, and these molecules are readily diffusible in biofilms [96]. Bacteria can use small molecules to control gene expression, as antibiotics, and as shuttles or redox active compounds to promote energy generation or iron acquisition. Because energy generation in low-nutrient regions of microbial communities is relatively unknown, the function of these small molecules is potentially of great importance for the ability of bacteria to sustain their metabolism [15].

2.4.1 Quorum sensing

One area of small molecule signaling that has received much recent attention, however, is that of quorum sensing. In many Gram-negative bacteria including *P. aeruginosa* and *Vibrio fisheri*, bacteria produce acyl-homoserine lactones that are sensed by other bacteria in a process known as quorum sensing [29]. In these species of bacteria, two sensing systems are in place, one that can recognize the AHLs of their own species and one that recognizes the signaling molecules of other organisms. The response of the bacteria is a threshold response, so that when the bacteria senses a specific concentration of its own species' AHL, it activates a genetic program in response [29]. In the case of *Vibrio fisheri*, this response is to generate light. In many other species however, this response is what activates biofilm formation and mutants in the genes that produce or sense the compound are unable to form biofilms. Through this system, bacteria are able to communicate information about the cell density in their environment. Recent evidence has also suggested that nutrient levels in the environment are another part of this sensing process, so that the bacteria are able to tune their threshold response based on the current nutritional environment [120].

While the generation and sensing of these compounds has received much study, the degradation of these compounds is not well understood. The degradation of AHL compounds may be as important a part of the signaling system as that of their production. AHLs in a biofilm may need to be degraded to activate programs responsible for dispersal from biofilms in the late stages of biofilm development. Another capability of AHLs may be important in community maintenance as well. Certain forms of AHLs may be able to be used as a carbon source, suggesting a role for AHLs in energy generation as well as in that of signaling. Understanding the lifecycle and potential uses of these compounds can help us understand all aspects of their roles in biofilm communities.

2.4.2 Redox active compounds

While quorum sensing has received much of the recent focus, small molecules may be essential in many other processes involved in community response and metabolic maintenance. Redox-active compounds are usually implicated primarily for their role in virulence. However, recent evidence is suggesting that these compounds may play other roles in redox homeostasis, iron-chelation and metabolic maintenance as well as acting as signals to regulate community wide responses. It has been shown that the phenazine pyocyanin, a redox-active compound produced by *P. aeruginosa* is used as an additional signaling factor in quorum sensing [26]. This same compound can be used to promote mineral reduction [40] or may be used to regulate redox state through NADH pools (Price-Whelan et al 2007, in press). The *P. aeruginosa* quinolone signal involved in quorum sensing also has an iron-chelating effect [13]. Because these small molecules are produced under conditions of low-nutrients and high cell-density, it is possible that they are playing an important role in biofilm physiology.

It is not clear how pervasive the production, degradation and response mechanisms of these molecules is however. In order to establish their role in metabolism and biofilm physiology, we must first determine how widespread these compounds are and the types of effects these compounds have on bacteria.

2.4.3 *Shewanella oneidensis* as a model organism for the study of metabolic organization in biofilms

Shewanella oneidensis MR-1 is a facultatively anaerobic Gram-negative bacterium with remarkable respiratory versatility found mainly in sediment environments [111]. Under anaerobic conditions, *S. oneidensis* can use many oxidized metals such as Mn(III), Mn(IV), Fe(III), Cr(VI), and U(VI) as well as thiosulfate, fumarate, sulfite, elemental sulfur, and nitrate as terminal electron acceptors. *S. oneidensis* can use lactate, succinate, pyruvate, and D-galactose as carbon sources [91, 106]. The bacterium is rod-shaped and non-spore forming. Individual cells are 2-3 μm long and 0.5 - 0.6 μm in diameter. The cells are motile with a single unsheathed polar flagella. Colonies are pinkish in color and circular with 1-4 mm diameters. *Shewanella oneidensis* can form biofilms under batch and flow conditions on a variety of surfaces [104, 111]. The genome of *S. oneidensis* has been sequenced and annotated, and it is relatively easy to manipulate genetically. [39]

As well as being able to utilize a variety of substrates for growth, *Shewanella oneidensis* can reduce electron acceptors, such as Fe(III) at a distance, raising the possibility that cells not directly

associated with an electron acceptor may still be able to generate energy from its reduction [57].

Because of its versatile respiratory capabilities, *S. oneidensis* is of interest in bioremediation processes [106] and in energy generation using fuel cells [9, 17, 84], and as such its response to various environmental conditions has been studied extensively. Genome-wide examinations of *S. oneidensis*'s response to acidic and alkaline pH [54], elevated salt conditions [59], ionizing radiation [77], UV radiation [78] and strong magnetic fields [30], as well as studies of growth on Cr(VI), Vanadium(V), and U(VI) have been conducted [7, 16]. Microarray and proteomic analyses have characterized the regulons under anaerobic and aerobic conditions, such that genes regulated under specific oxygen conditions have been determined [6, 5, 32].

Additionally, the central metabolic pathways of *S. oneidensis* under a variety of oxygen conditions have also been examined in the Keasling laboratory. Tracking cellular metabolites and the products of carbon metabolism, they were able to construct a metabolic pathway model to quantify the central metabolic flux distributions [100, 98, 99]. In these studies they also find that cells can continue to grow well at low dissolved oxygen levels [100].

Because of *S. oneidensis*'s versatile respiration, ability to form biofilms, well-characterized metabolism and response to different environmental conditions, as well as its potential to use redox-active compounds to promote energy generation, it is an ideal experimental system in which to explore domains of metabolism within a biofilm.

2.4.4 *Pseudomonas aeruginosa* as a model organism for the study of community response to endogenous small molecules

Pseudomonas aeruginosa is a Gram-negative bacterium measuring approximately 0.5 μm by 2.0 μm . It is an aerobic bacterium found commonly in water and soils, but is renowned as a opportunistic pathogen, causing infections in wounds, burns and those who are immunocompromised. *P. aeruginosa* infects the lungs of patients with cystic fibrosis, forming biofilm-like microcolonies encased in the thick mucous layer associated with the pathology of this disease. These infections caused by *P. aeruginosa* biofilms are extremely resistant to antibiotics.

Quorum sensing has been well-established for *P. aeruginosa* and is controlled in part by the lasI/R, rhlI/R, which synthesize and detect specific AHLs [46] and also by the psq system [63]. Also, because of the interest in *P. aeruginosa* biofilms in infection, the development and genetic pathways involved in biofilm production are the most well-characterized of any microbe.

P. aeruginosa produces several redox active small molecules that are used as antibiotics, signals

in co-ordinating community responses and potentially facilitating extracellular electron transfer [26, 40]. One class of these compounds, phenazines, are heterocyclic redox-active compounds that are produced endogenously [53]. They are excreted from cells in stationary phase and have antibiotic effects on other microbes and eukaryotes. While the effects of phenazines as antibiotics has received much attention, the primary function of phenazines in the producing organism is still unknown.

Because *P. aeruginosa* has been well-established as a model organism in biofilm development and quorum sensing and endogenously produces AHLs and phenazine compounds under low-nutrient and high-cell density conditions, it is an ideal organism with which to study the effects of small molecules on cell physiology and to elucidate what their role might be in metabolism and signaling in biofilm communities.

2.5 Summary

Bacterial biofilms are prevalent in the environment, but their resilience is not well understood. Due to diffusion, metabolism and microscale interactions, biofilm communities are spatially stratified such that cells in different regions of the biofilm experience different microenvironments. Within these microenvironments, activity levels and biochemical processes occur differentially according to the location of a cell in the biofilm and the biofilm structure's biomass. The heterogeneous nature of these communities is likely a key factor in the community's ability to survive in the face of challenging environmental conditions, yet the metabolic organization and dynamics within a biofilm community are not well-understood. In this dissertation, a study of the metabolic organization of biofilms and an exploration of possible roles for small molecules in maintaining energy generation within the community is presented.

Chapter 3

Spatiotmetabolic stratification of *Shewanella oneidensis* biofilms

This chapter includes sections from Teal, T.K., D. Lies, B. J. Wold, D. K. Newman. 2006. Spatiometabolic stratification of *Shewanella oneidensis* biofilms. Applied and Environmental Microbiology 72(11): 7324-30.

3.1 Abstract

Biofilms, or surface-attached microbial communities, are both ubiquitous and resilient in the environment. Although much is known about how biofilms form, develop, and detach, very little is understood about how these events are related to metabolism and its dynamics. It is commonly thought that large subpopulations of cells within biofilms are not actively producing proteins or generating energy and are therefore dead. An alternative hypothesis is that within the growth-inactive domains of biofilms, significant populations of living cells persist and retain the capacity to dynamically regulate their metabolism. To test this, we employed unstable fluorescent reporters to measure growth activity and protein synthesis *in vivo* over the course of biofilm development and created a quantitative routine to compare domains of activity in independently grown biofilms. Here we report that *Shewanella oneidensis* biofilm structures reproducibly stratify with respect to growth activity and metabolism as a function of size. Within domains of growth-inactive cells, genes typically up-regulated under anaerobic conditions are expressed well after growth has ceased. These findings reveal that, far from being dead, the majority of cells in mature *S. oneidensis* biofilms have actively turned-on metabolic programs appropriate to their local microenvironment and developmental stage.

3.2 Introduction

Many bacteria in the environment are thought to grow as surface-attached microbial communities, or biofilms, and it has been suggested that this biofilm lifestyle may account for the remarkable persistence of bacterial populations in the face of changing environmental conditions [24]. Biofilms are composed of many hundreds of cells, each of which experiences its own microenvironment due to strong chemical gradients that are established by metabolism and diffusion. Biofilm communities are therefore heterogeneous and spatially stratified, so that activity levels and biochemical processes occur differentially according to the location of a cell in the biofilm and the biofilm structures biomass [108]. Previous studies have investigated the spatial organization of microbial biofilm communities. In mixed species biofilms, using measurements of metabolites, fluorescent in situ hybridization, and community analysis by PCR, it has been shown that species stratification occurs [19, 37, 65, 71]. In laboratory based single species biofilms, several studies have investigated spatial patterns of cellular growth activity and metabolism using a variety of techniques [25, 44, 43, 55, 62, 70, 74, 95, 115, 116, 119, 121]. These studies demonstrate that heterogeneity with regard to cellular activity and metabolism exists, and in particular, that biofilm communities show decreased growth activity near the center of the biofilm, where it is expected that cells are nutrient limited. To our knowledge, however, no systematic studies have been done to characterize the specific metabolic processes that occur in biofilms and how they might change over the course of biofilm development. As a first step towards this end, we set out to create a system where we could quantitatively and reproducibly measure spatiometabolic patterning in biofilms. In particular we wanted to address the question of whether biofilm cells could decouple growth from metabolism. Numerous studies using the LIVE/DEAD stain and other methods have concluded that cells in the middle of the biofilm are dead, or not actively synthesizing proteins [42, 60, 110], but it is not clear how accurately these reporters reflect cell viability in a biofilm. To explore the spatiometabolic stratification of developing and mature biofilms, we selected *Shewanella oneidensis* strain MR-1, a biofilm-forming, facultative anaerobe with remarkable metabolic versatility. *S. oneidensis* can use oxygen and many other lower potential substrates, including metals, as electron acceptors in respiration, making it an attractive experimental system in which to explore domains of metabolism within a biofilm [39, 104, 105, 111].

3.3 Materials and Methods

3.3.0.1 Bacterial strains, plasmids and media.

Shewanella oneidensis strain MR-1 was grown planktonically using LML medium [pH 7.4, containing 0.2 g/L yeast extract, 0.1 g/L peptone, 2.5 g/L Na HEPES and 0.243 mL/L 60% lactate syrup (5 mM lactate)]. Planktonic cells were grown shaking at 250 rpm at 30°C. When required, antibiotics were added at final concentrations of 15 μ g/mL tetracycline or 50 μ g/mL kanamycin.

S. oneidensis MR-1 constitutively expressing the GFPmut3* (green) or ECFP (cyan) fluorescent protein were generated using mini-Tn7-KSGFP or mini-Tn7-KSCFP to insert the gfpmut3* or ecfp gene at the unique attTn7 site in the MR-1 genome, creating strains DKN308 and DKN309 respectively. (The mini-Tn7 system in Supplemental Methods [2, 18, 22, 33, 50, 68, 112]) To allow detection of growth activity in *S. oneidensis* the reporter system described by Sternberg et al. was used [95]. The NotI fragment of pSM1606 [95] containing the growth-rate regulated *E. coli rrnB* P1 promoter [3] fused to the *gfp*(AAV) gene encoding an unstable green fluorescent protein (GFP) was cloned into the highly stable broad host range plasmid pME6031 [38] to create the plasmid pTK4. GFP(AAV) is unstable because it has a specific C-terminal oligopeptide extension that makes it susceptible to relatively fast degradation by intracellular tail-specific proteases thereby enabling real-time expression imaging [1]. pTK4 was transferred by conjugation into the ECFP-expressing strain *S. oneidensis* DKN309, to yield strain DKN310. The *mtrB* reporter strain, DKN311, was made via homologous recombination. Primers were designed to amplify flanking 1kb regions up and downstream of the end of the *mtrB* gene from *S. oneidensis* MR-1 (upstream region primers 5 CGGGATCCGCAGGCCATAATACCCAAGTAGAAGAA and 3 AT-CAATCAACTAGTTCTAGAGCGATTAGAGTTGTAACTCATGCT; downstream region primers 5 GCAGCAGTTAACATGCTAGCGAACATTGCCTCATATGCTAAAAG and 3 ATAAGAAT-GCGGCCGCTGTTGAATTGAATCCCCTGTT) and insert *eyfp*(AAV) between them. *eyfp*(AAV) encodes an unstable yellow fluorescent protein and was constructed by amplifying *eyfp* from pMP4658 [10] using primers that included the AAV tail [1] to fuse the AAV to *eyfp*. Using NotI restriction sites, the upstream region, the sequence for *eyfp*(AAV) and the downstream region were inserted into the kanamycin-resistance suicide plasmid pSMV10, such that *eyfp*(AAV) was in between the upstream and downstream regions of the end of the *mtrB* gene. This plasmid was cloned into *E. coli* WM3064 [85] and mated with *S. oneidensis* MR-1, selecting for strains with kanamycin resistance. Such transconjugants were plated on LB/5% sucrose plates to select for secondary recombinants lacking the integrated plasmid, which encodes sucrose sensitivity. Colonies

from these plates were tested via PCR for the presence of the *eyfp*(AAV) gene. P_{lac} -ecfp from miniTn7(Gm)PA1/04/03 ecfp-a [52] was inserted into pME6031 using KpnI and MluI to create constitutively-expressing ecfp on plasmid, pTK5. This plasmid was introduced into the MR-1 *mtrB*-*yfp*(AAV) strain DKN311 by conjugation to create strain DKN312 that constitutively expresses ECFP and expresses EYFP(AAV) from the end of the *mtr* operon.

3.3.0.2 Plasmid stability determination.

To assay the stability of pTK4 and pTK5 in *S. oneidensis* MR-1 biofilms, *S. oneidensis* with pTK4 was grown for 5 days in 96 well polyvinyl chloride plates at 30°C in LML medium. As biofilm cells were attached to the walls of the well, the medium was exchanged every day to eliminate planktonic cells. After 5 days, the biofilm cells that were still attached to the well walls were removed and resuspended. Dilutions were plated on LB plates and incubated at 30°C overnight. 309 colonies from the plates were picked and each colony was streaked on LB and LB + tetracycline plates that were incubated at 30°C overnight. 308 of the 309 colonies grew on both plates, indicating that 99.7% of MR-1 cells were tetracycline resistant and therefore contained pTK4.

3.3.0.3 GFP expression and stability measurements.

Cells were grown overnight in LML medium and allowed to reach stationary phase. Cells were then diluted into fresh medium to an OD₆₀₀ of 0.0143 and grown aerobically for 20 hours with samples taken for growth and fluorescence measurements using a Bio-Tek Synergy HT. For measuring growth, optical density at an absorbance of 600nm was used. For green fluorescence, measurements were taken using a 485/20 excitation filter and a 528/20 emission filter.

3.3.0.4 Determination of respiration rates.

S. oneidensis overnight cultures were diluted into fresh LML medium and allowed to reach stationary phase. Cells were then transferred to a stoppered bottle where no oxygen could be introduced. Oxygen concentrations were measured over time using an oxygen microelectrode until concentrations reached zero. The slope of this data was calculated, and this was determined to be the oxygen consumption rate for the number of cells in the flask. Colony forming unit counts were done for each flask, and the slope value was divided by the number of cells in the flask to determine the oxygen consumption rate per cell.

3.3.0.5 Biofilm experiments.

A flow cell system was constructed such that biofilms could be grown under constant conditions and imaged over time. Flow cells have 4 channels machined from polyurethane with coverslips attached via epoxy. Each channel is 40.6 mm long, 11.4 mm wide and 0.203 mm deep. A 0.5 mM lactate LML medium [pH 7.4, 0.2 g/L yeast extract, 0.1 g/L peptone, 2.5 g/L Na HEPES and 0.043 mL 60% lactate syrup] is run through the flow cell system. The flow cell is inoculated with 300 μ L of a culture in exponential phase, at an OD₆₀₀ of approximately 0.075, using a sterile syringe. Flow is not started immediately in order to allow cells to attach to the surface. After 1 hour the flow is started at a rate of 4.1 μ /sec, 1.5 rpm on a Watson-Marlow peristaltic pump. The flow continues at this rate for the length of the experiment. Using this technique, biofilms were grown for up to 7 days. Confocal fluorescence microscopy was used to image bacterial biofilms grown in the flow cells. A Zeiss LSM 510 inverted microscope with a 63x Achroplan water immersion lens at the Caltech Beckman Institute Biological Imaging Center was used. Z-series images were acquired for multiple fields of view at multiple time points during the experiment. For imaging egfp or eyfp, the excitation was 488nm and the emission filter used was a BP500-550. For imaging ecfp the excitation was 420nm and the emission filter used was a BP465-485. Images were processed using the Imaris software.

3.3.0.6 LIVE/DEAD stain.

S. oneidensis biofilms were grown in flow cells. At an end time point, flow was stopped and 1.5 μ L of Propidium Iodide and 1.5 μ L of Syto 9 from the Molecular Probes BacLight LIVE/DEAD stain kit L7012, in 1 mL 0.5mm lactate LML, was injected into the tubing upstream of the biofilm. Flow was started briefly to deliver the stain to the biofilm. Flow was then stopped for 1 minute to allow staining to occur, and was resumed to wash away residual stain. Imaging was done using 488 nm excitation and the emission filter BP500-550 for the green fluorescence. Excitation was 543 nm and the emission filter was LP605 to image the red fluorescence.

3.3.0.7 *mtrB* expression with varying oxygen levels.

LB medium containing 20 mM lactate was prepared. 10 mL of media was added to 250 mL anaerobic Balch tubes. The tubes were stoppered and flushed with the appropriate oxygen concentration. 0%, 2% and 10% oxygen tanks consisted of the appropriate concentration of oxygen and the remainder nitrogen. Tubes containing 21% oxygen were flushed with filtered air. 20 mM fumarate was added to 0% oxygen cultures. Cells were grown overnight in aerobic cultures. Cells were then diluted 1:1000

into each tube to an OD₆₀₀ of 0.075 at each oxygen concentration in duplicate. Cells were allowed to grow for 2 hours or less to an OD₆₀₀ of 0.150. Cells were then collected and treated with Qiagen RNA protect, and the RNA was immediately extracted using the Qiagen RNAqueous Micro kit. The RNA was DNase treated using the Qiagen DNase I treatment and DNase inactivation protocol. To synthesize cDNA, reverse transcriptase PCR (RT-PCR) was done using the Applied Biosystems TaqMan kit in a 50 μ L reaction. To quantitate the cDNA, Quantitative RT-PCR was performed. Twenty-one base pair primers flanking a 100 base pair region for genes *mtrB*, *gfp*, *envZ* and *recA* were diluted to 5 pmol/ μ L. For each reaction, 1 μ L cDNA from the RT-PCR reaction, 6.5 μ L DEPC water, 10 μ L 2x SybrGreen mix and 2.5 μ L of a primer pair mix were added to one well of a 96 well QPCR plate. A no cDNA control was also run for each primer set. Q-RT-PCR analysis was done using an Applied Biosystems Gene Amp 7500 Sequence Detector machine. A fluorescence level of 0.5 on a log scale was selected as the threshold for comparison of cycle numbers. The genes *envZ* and *recA* were used for normalization.

3.3.0.8 Quantitative analysis of biofilm images.

Biofilms were imaged at multiple time points in multiple fields of view. For each image, the fluorescence intensity profile for the reporter was mapped through the center x-axis of the structure using NIH ImageJ. These fluorescence values were exported as a text file of x-coordinates and fluorescence intensity for each pixel. We wrote an analysis program to analyze and process this data. The brightest pixel was defined as 100% fluorescence and all fluorescence values were determined relative to that value. To automatically determine the edges of a structure, an edge detection algorithm was used where the region of greatest contrast between the empty space surrounding the biofilm structure and the fluorescence of the structure was defined to be the edge. Using the defined edges, the center could then be specified. Then, the intensity of each nine-pixel bin was determined in relationship to its distance from the center of the structure, and a plot of fluorescence intensity versus distance from the center of the structure was constructed automatically for each image. This analysis generated a profile of fluorescence for each image. Twelve biofilms from the growth reporter strain, DKN310 and eight from the anaerobic reporter strain, DKN312, representing images from all stages in biofilm development were analyzed in this way, determining the size of the structure and its fluorescence profile. Biofilms were binned into representative sizes, and the average fluorescence profile across all the structures of that size, with a minimum of six in each category, was calculated

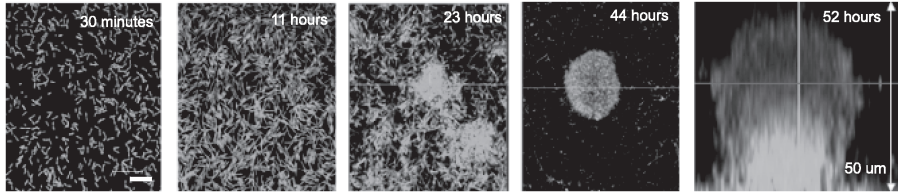


Figure 3.1: Time course of *S. oneidensis* biofilm development. Cells are expressing a constitutive GFP. The first four panels are x-y slices at the base of the developing biofilm structure. The final panel is a z-profile through the structure. Scale bar is 10 μm .

3.4 Results

3.4.0.9 Development of *S. oneidensis* biofilms

S. oneidensis was labeled with a constitutively expressing GFP from a lac basal promoter. Cells were grown in a flow cell system with a 0.5 mM lactate LML medium and imaged using confocal laser scanning microscopy. As shown in Figure 3.1, *S. oneidensis* first forms a monolayer; after 23 hours, the first structures become 3-dimensional mounds; at about 44 hours, these structures begin to become mushroom-like with a distinct stalk and cap. This basic mushroom morphology is then maintained until approximately 100 hours when the biofilms begin to dissolve at both cap and stalk. Although *S. oneidensis* forms single-layer biofilms under some conditions [105], in our flow cell system biofilms develop as mushroom-shaped structures very similar to those described for other bacteria, including *Pseudomonas aeruginosa*, *Pseudomonas fluorescens* and *Escherichia coli* [90].

3.4.0.10 LIVE/DEAD stain for *S. oneidensis* biofilms

To establish the live/dead patterns within a *S. oneidensis* biofilm, as typically reported by the Molecular Probes® LIVE/DEAD®BacLight stain, biofilms grown in the flow cell system were stained with the LIVE/DEAD® reagent at developmental time points (Figure 3.2). At early time points, or in structures with little biomass, the entire biofilm stains as live. As biofilms increase in biomass, cells throughout the structure stain dead, until structures reach their maximum biomass when almost all cells in the middle of the structure stain dead. These patterns match the live and dead profiles reported for similar biofilms [28, 60]. Yet some studies have seen a discrepancy between LIVE/DEAD® staining and other viability measures indicating that there may be a potential for bias with this method [79]. The LIVE/DEAD® stain uses two fluorescent nucleic acid stains, Syto9 and propidium iodide. Syto9 is used to quantify live cells because it can permeate cells under all conditions; propidium iodide is used to quantify dead cells because, as a highly charged molecule,

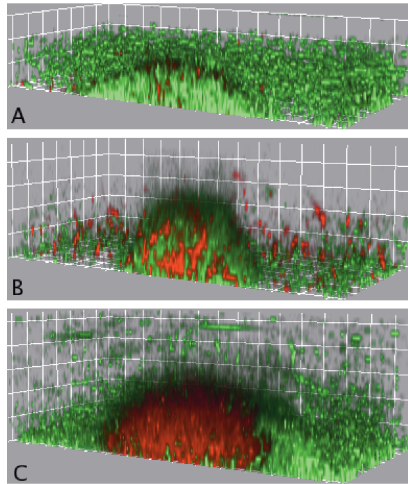


Figure 3.2: LIVE/DEAD staining in *S. oneidensis* biofilms. Green is the live stain, Syto9, and red is the dead stain, propidium iodide. Grid marks are 10 μm . (A) At 60 μm in diameter most cells continue to stain as live. (B) At \sim 80 μm in diameter cells throughout the biofilm start to stain dead. (C) At \sim 140 μm in diameter almost all cells in the middle of the biofilm are stained as dead.

it is unable to permeate cells with a strong electrochemical gradient across their membrane (i.e. the chemiosmotic potential). Although the LIVE/DEAD® stain typically correlates with growth assays in liquid or solid nutrient medium, as described in the Molecular Probes® manual, little is understood about how the membrane properties of cells in biofilms might change with time. Given this uncertainty, and that the LIVE/DEAD® stain is a terminal assay, we reasoned that an *in vivo* method for assessing growth might give a more accurate representation of the metabolic state of the biofilm.

3.4.0.11 Patterns of growth activity in biofilms using the *rrnB* P1 reporter

Strains of *S. oneidensis* MR-1 with *in vivo* fluorescent reporters of growth activity were constructed to spatially monitor cell growth *in situ* over the development and maturation of a biofilm. The growth reporter plasmid, pTK4, was made using the system designed by Sternberg et al. [95], in which GFP is expressed from the *E. coli rrnB* P1 ribosomal promoter, the activity of which correlates with ribosome production [3]. *S. oneidensis* MR-1 containing pTK4 fluoresces green with an unstable GFP, GFP(AAV), when cells are producing ribosomes, a process associated with growth and protein synthesis capacity. To determine if this reporter would function as a good indicator of growth state in *S. oneidensis* time course experiments were performed with well-characterized planktonic cultures. As seen in Figure 3.3, for both the constitutively green fluorescent strain, DKN308, and the strain containing the ribosomal green fluorescent reporter, DKN310, fluorescence increased with

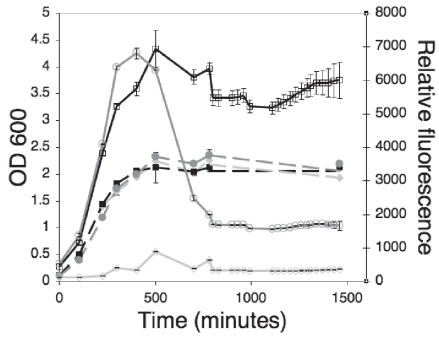


Figure 3.3: Fluorescence levels and absorbance at OD₆₀₀ for *S. oneidensis* MR-1 (diamonds), *S. oneidensis* DKN308 constitutively expressing GFP (squares), and *S. oneidensis* DKN310 expressing GFP-AAV from a ribosomal promoter, representing growth activity (circles). OD₆₀₀ is indicated by dashed lines, and fluorescence by solid lines. As cells grow through exponential phase, fluorescence levels increase, but when stationary phase is reached, fluorescence levels from the constitutively expressing GFP remain high whereas fluorescence from the growth active version decreases rapidly. Error bars represent standard deviations of triplicate cultures; in some cases the error is smaller than the size of the symbol.

OD₆₀₀ until the culture reached 1.2 x10⁸ cells/mL where the OD₆₀₀ plateaued. Fluorescence then stayed high in strain DKN308 but decreased in strain DKN310, reaching zero 240 minutes after the cell density stopped increasing. Green fluorescence from the ribosomal reporter increased during exponential phase, as expected for a marker of growth, and then decreased due to the combined effects of RNA downregulation and prompt protein turnover during stationary phase. These results verify that this GFP reporter is a sensitive, time-resolved indicator of growth activity in *S. oneidensis*.

To monitor growth activity relative to the entire developing biofilm over time, pTK4 was used as one part of a dual color fluorescent system imaged by confocal microscopy. The pTK4 plasmid was introduced into *S. oneidensis* DKN309, a strain of *S. oneidensis* that also expresses ECFP constitutively from a basal lac promoter. The resulting new strain, DKN310, fluoresces cyan at all times to mark cellularity and also fluoresces green to mark cells actively engaged in growth, as indicated by active synthesis of the ribosomal machinery. To learn if there is a defined developmental progression, and to ask what parameters (size, shape, age, etc.) correlate most directly with growth activity, *S. oneidensis* DKN310 biofilms were grown in flow cells for up to 100 hours. Individual biofilms were imaged longitudinally, at multiple time points and in multiple fields of view, using dual-channel fluorescence imaging of cyan and green on a Zeiss 510 confocal laser scanning microscope. A representative developmental course is shown in Figures 3.4A-E. Growth activity, indicated by pTK4 reporter fluorescence, was uniform throughout the biofilm at early stages in development, in

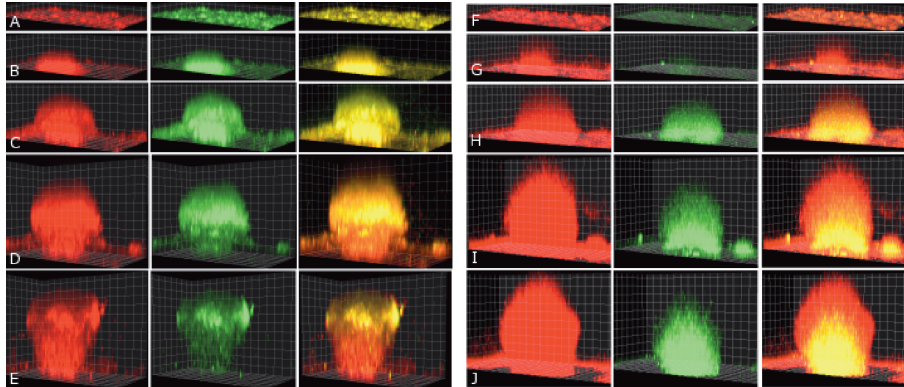


Figure 3.4: Development of a mushroom structure in a *S. oneidensis* biofilm with a ribosomal (growth) reporter (DKN310, panels A-E) and an anaerobic reporter *mtrB* (DKN312, panels F-J). Grid squares are $10 \mu\text{m} \times 10 \mu\text{m}$. In the first column cells are constitutively expressing ecfp and fluorescence from it is false colored red. In the second column of panels A-E, cells expressing the growth active GFP(AAV) appear as green. In the second column of panels F-J, cells expressing the *mtrB* reporter are green. The third column is an overlay of red and green channels. (A) 18 hours, height 8 μm (B) 28 hours, height 18 μm (C) 41 hours, height 52 μm (D) 65 hours, height 92 μm (E) 77 hours, height 112 μm . (F) 17 hours, height 8 μm (G) 29 hours, height 31 μm (H) 47 hours, height 58 μm (I) 71 hours, height 104 μm (J) 85 hours, height 118 μm

structures up to 60 μm in height that do not have a mushroom cap. When the structures develop a mushroom cap, structures can then get up to 120 μm in height and still be growth active in all regions of the biofilm. As structures get larger and reach their final mature state, up to 140 μm in height, growth activity in the cap is maintained, but growth activity in the stalk is only maintained in the outer approximately 25 μm .

3.4.0.12 Patterns of metabolism under anaerobic conditions in biofilms using the *mtrB* reporter

To determine if metabolism (i.e. protein synthesis and energy generation) might occur in regions where cells are not actively growing, a reporter that is expressed under these conditions was required. It is known that as biofilms increase in biomass, molecular oxygen (O_2) levels in the inner regions become more limited [83, 96], and these might correspond to domains where the *rrnB* P1 growth reporter is not active. To test whether this might be relevant for our system, we measured the O_2 consumption rate for stationary phase *S. oneidensis* cells in LML medium. Using this rate (5.53mg $\text{O}_2/\text{L}^*\text{s}$) and applying a biofilm diffusion model, as described by Stewart [96], we estimate that the concentration of O_2 required to sustain growth will be depleted approximately 30 μm into the biofilm. This is consistent with O_2 profiles measured in many other biofilm systems [19, 83, 96]. Therefore, if cells are still capable of actively metabolizing in regions of low growth activity, it is

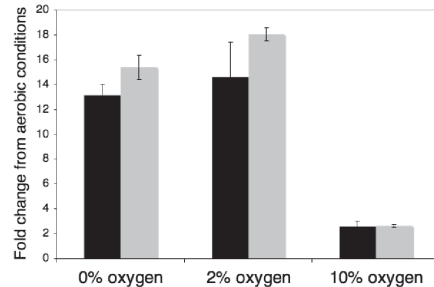


Figure 3.5: Fold change in expression, as measured by Q-RT-PCR, of *mtrB* and *eyfp* in *S. oneidensis* DKN312 relative to aerobic (21% O₂) conditions. Black bars represent *mtrB* and gray bars *eyfp*. *mtrB* and *eyfp* expression is upregulated under anaerobic and microaerobic conditions. Error bars represent the range of duplicate cultures.

expected that genes expressed under low O₂ conditions would most likely be upregulated in these regions. Previous work from our lab and those of others suggested that *mtrB* might be such a gene: *mtrB* is expressed under low O₂ conditions by Shewanella, and its product, an outer membrane β-barrel protein, facilitates electron transfer under anaerobic conditions [6, 57]. Therefore, a reporter construct for *mtrB* was made, and an unstable YFP, *eyfp*(AAV), was inserted into the chromosome after the *mtr* operon, creating strain DKN311. To establish whether YFP fluorescence from the *mtr* operon in DKN311 is an accurate indicator of metabolism under anaerobic conditions, DKN311 was grown under aerobic, microaerobic, and anaerobic conditions. Quantitative real-time PCR experiments conducted with different O₂ concentrations (0%, 2%, 10% and 21%, or air) showed that *mtrB* and *eyfp* expressed from the *mtr* operon were 12-fold upregulated only under 0% and 2% O₂ concentrations (Figure 3.5), validating that *eyfp*(AAV) expression in the *mtr* operon can be used as a marker of new metabolism in low oxygen domains. DKN312, the reporter strain used for imaging, was created by inserting the pTK5 plasmid that constitutively expresses ECFP from the lac promoter, into strain DKN311; DKN312 constitutively expresses ECFP and expresses EYFP only under anaerobic or microaerobic conditions. Because EYFP and ECFP have an absolute requirement for O₂ to fold properly, fluorescence of either color implies the presence of at least trace amounts of oxygen in the biofilm [36]. Biofilms of *S. oneidensis* DKN312 were grown exactly as described for the growth activity reporter strain, DKN310. Figures 3.4F-J show that *mtrB* is not expressed at early stages of biofilm development, consistent with full O₂ availability in structures less than 60 μm in diameter. *mtrB* expression only appeared in the interior spatial domains of biofilms at late developmental stages, in structures greater than 100 μm in diameter, when the interior cells were likely O₂-limited.

3.4.0.13 Quantitative analysis of expression patterns

To assess the reproducibility of these results across multiple individual biofilms and through replicate experiments, we developed a quantitative analysis system to map reporter expression profiles across multiple biofilms. Using this system a plot of fluorescence intensity versus distance from the center of the structure was constructed automatically for each image. For the different biofilm developmental stages, averages for the *S. oneidensis* DKN310, or growth activity, strain and the *S. oneidensis* DKN312, or *mtrB*, strain were calculated. The patterns of the reporters were remarkably consistent relative to structure size and shape. The most important factor in determining these patterns was not the time that the biofilm had developed, but its size, which is a far better and more consistent correlate of reporter gene domain of activity. This quantitative analysis also reveals that *mtrB* expression profiles are the inverse of those for the growth activity GFP marker (Figure 3.6).

3.5 Discussion

Although various single-species biofilms have been well studied with respect to what controls their physical development, far less attention has been paid to their metabolic dynamics. From the LIVE/DEAD® stains (Figure ??), it might be predicted that large sub-populations of cells within mature biofilms are not actively generating energy and are therefore dead. However, our *in vivo* metabolic activity reporter system does not support this interpretation. Although patterns of cell viability at early stages in biofilm development (diameter < 60 μm) correlate with the results from the LIVE/DEAD® stain, beginning in the middle developmental stages (60 μm < diameter < 140 μm), the patterns of metabolic activity diverge from the LIVE/DEAD® stain. Larger regions of growth activity (as measured by the *rrnB* P1 reporter) are observed, and subpopulations where metabolism decouples from growth (as measured by the *mtrB* reporter) also appear. In mature biofilms (diameter > 140 μm), although growth activity is restricted to the outer ~25 μm , strong fluorescent signatures of *mtrB* expression dominate the interior; this is in sharp contrast to what is seen in the LIVE/DEAD® stain, where all cells in the interior stain as dead. These patterns, of both growth activity and *mtrB* expression, are remarkably consistent and correlate specifically with the size of the biofilm structure. This demonstrates that growth-inactive regions of the biofilm are, nevertheless, metabolically active. At a minimum, they generate sufficient energy to synthesize recently induced new proteins. The involvement of the *mtr* operon further implies competence for key cellular metabolism including electron transport and anaerobic metabolism that is enabled

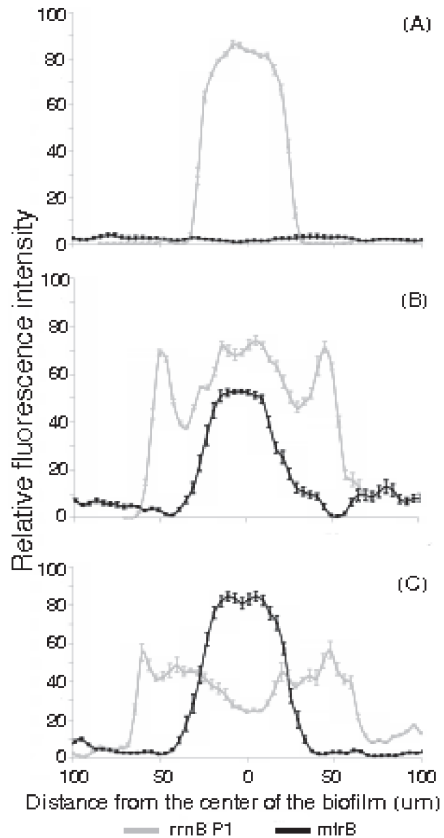


Figure 3.6: Quantitative analysis of patterns of growth activity and metabolism in *S. oneidensis* biofilms. Gray lines are strain DKN310 (*rrnB* P1) showing growth activity profiles and black lines are strain DKN312 showing *mtrB* expression. (A) Biofilm structures approximately 60 μm in diameter. (B) Structures approximately 110 μm in diameter. (C) Structures approximately 140 μm in diameter. Each line represents an average of a minimum of six different structures. Error bars are the standard deviation of the binned pixel intensity values across all the images included in the plot. In panels (B) and (C), local minima at the edge of the colonies are regions with no cells, thought to be EPS. Patterns of expression relative to the size of the biofilm structure are remarkably consistent across multiple structures, and *mtrB* continues to be expressed in regions where growth activity has decreased.

by mtr gene products. Thus, there appear to be major interior domains of biofilms where cells generate energy although they are not actively growing. The state of these interior cells may be akin to the stationary phase of planktonic cultures or might represent a biofilm-specific state of metabolism. What is strikingly clear from these time-resolved imaging studies is that the vast majority of cells in all regions of a biofilm are physiologically active, even though they are eventually running dramatically different programs of activity. In conclusion, we have observed remarkably reproducible spatiometabolic stratification in *S. oneidensis* biofilms. These findings are leading us to rethink previous interpretations of what it means to be a dead cell in a biofilm and has implications for understanding how cells in a biofilm react to antibiotics, toxins or other changes in environmental conditions. Cells that are maintained in a non-growing state, yet are still capable of synthesizing proteins, may be responding to introduced agents in unexpected ways and have the ability to act as a reservoir of survival. Indeed, in many natural systems where microorganisms exist at high cell densities, such as infections, microbial mats, as well as in engineered bioreactors, it is likely that a significant fraction of the population is not actively growing [24, 108]. A better understanding of what defines and controls the capabilities and activities of this growth-inactive state is not only essential for understanding basic aspects of biofilm biology, but is also extremely relevant for applications that aim to exploit the metabolic activity of biofilms for energy conversion and other purposes [41, 80].

3.6 Acknowledgements

We thank William Berelson for help with O₂ respiration measurements, Søren Molin for plasmids and the Caltech Biological Imaging Center for use of the facility. This work was supported by grants from the Office of Naval Research, Packard Foundation and Howard Hughes Medical Institute to D.K.N.

3.7 Supplemental methods

3.7.0.14 Mini-Tn7 Derivative Construction and Characterization.

Mini-Tn7 derivatives for constitutive expression of fluorescent proteins in *S. oneidensis* were constructed as follows. The EcoRI-XbaI mini-Tn7KmASm1 fragment from pBK-miniTn7-KmASm1 [50] was cloned into the EcoRI site of the small mobilizable R6K-based plasmid pUX66 (D. Lies and G. Roberts, unpublished), after the digested plasmid and insert fragment were treated with

Klenow DNA polymerase to generate blunt ends, to create plasmid pURR21. The NotI fragment from pBK-miniTn7-gfp3 [50] containing the *gfpmut3** gene expressed from the lac PA1/04/03 promoter derivative was cloned into the NotI site of pURR21 to generate the transposon mini-Tn7-KSGFP and the plasmid pURR25. Mini-Tn7-KSGFP contains the NotI fragment after the Λ cassette in the transposon while mini-Tn7gfp3 has the NotI fragment between the cassette and the kanamycin resistance cassette. An ECFP expression cassette was constructed by cloning the pURR25 NotI fragment onto a version of pOK12 [112] lacking SphI and HindIII sites and replacing the *gfpmut3** gene from this fragment with an *ecfp* gene amplified by PCR from pMP4641 [10] using ECFPN (5-GACCGCATGCTGAGCAAGGGCGAGGAGCTG-3) and ECFPC (5-GGTGAAGCTTACTTGTACAGCTCGCCATGCC-3) primers. This ECFP expression cassette was cloned as a NotI fragment into pURR21 to generate the transposon mini-Tn7-KSCFP and the plasmid pURR27. The plasmid pURR21 and its derivatives were constructed to provide mini-Tn7 and fluorescent protein gene delivery vehicles with a plasmid R6K-based origin of replication. We examined the utility of these plasmids in *S. oneidensis* using a donor strain containing pURR25 in comparison with the pMB1-based plasmid pBK-miniTn7-gfp2, which was previously used as a mini-Tn7 donor to produce GFPmut3* expression in *S. oneidensis* MR-1 [104]. The *E. coli* donor strain WM3064 [85] carrying either plasmid was mated with *S. oneidensis* MR-1 using a 1:5 donor:recipient ratio and incubated for 5h at 30°C on LB agar plates containing 300 μ M diaminopimelic acid, in the presence or absence of WM3064 containing the transposition helper plasmid pUX-BF13 [2]. In the absence of pUX-BF13, matings between WM3064(pBK-miniTn7-gfp2) and MR-1 yielded *S. oneidensis* transconjugants resistant to 15 μ g/ml gentamicin at frequencies of 10-5 per recipient. Plasmid extractions from 12 of these transconjugants all contained plasmid DNA of the same size as pBK-miniTn7-gfp2. Similar matings in the presence of pUX-BF13 yielded the same frequency of transconjugants and these transconjugants also contained plasmid DNA of the same size as pBK-miniTn7-gfp2. Matings performed with WM3064(pURR25) and *S. oneidensis* MR-1 in the absence of pUX-BF13 yielded transconjugants resistant to 50 μ g/ml kanamycin at frequencies of 10-9 per recipient. Matings between WM3064(pURR25), WM3064(pUX-BF13) and *S. oneidensis* MR-1 yielded kanamycin-resistant transconjugants at frequencies of 10-5 per recipient. No new plasmid DNA was detected in plasmid extractions from two transconjugants from matings lacking pUX-BF13 or from five transconjugants from matings in the presence of pUX-BF13. These results indicate that, unlike pURR25, pBK-miniTn7-gfp2 replicates in *S. oneidensis* MR-1 and cannot easily be used for delivery of mini-Tn7 derivatives at single copy into the genome of MR-1. We have

confirmed this observation with seven other derivatives of this group of mini-Tn7 delivery plasmids reported by [52] and have demonstrated that the plasmid pRK2013 is also maintained in *S. oneidensis* MR-1. Thus, contrary to a previous report [68] but consistent with a more recent report [33], we find that pMB1- and ColE1-based plasmids replicate in MR-1. Plasmid R6K-based derivatives such as those constructed here and reported elsewhere [18] are more useful vehicles for chromosomal delivery of mini-Tn7 derivatives. Tn7 inserts in most Gram-negative bacteria in a site- and orientation-specific manner downstream of the *glmS* gene [18, 22]. We analyzed 20 MR-1 transconjugants containing mini-Tn7-KSGFP by PCR using transposon-specific primers (Tn7aphAUp: GCCAGTT-TAGTCTGACCATCTC and Tn7catEndDown: TGTCGGCAGAATGCTTAATGA) and primers targeting *glmS* and the downstream gene *menB* from MR-1 (MR1glmSDown: CGCCACTGATT-TACACTATCCC and MR1menBUp: CGATCAAGACTTCTCAGCCTTC). Specific PCR products for all 20 transconjugants could be obtained with the primer pairs MR1glmSDown-Tn7catEndDown and Tn7aphAUp-MR1menBUp but not with other combinations of these primers. Only the MR1glmSDown-MR1menBUp primer pair yielded a specific PCR product from wild-type MR-1 DNA, which was absent in the transconjugants presumably because of the large size of the inserted transposon. These results indicate that Tn7 inserts between *glmS* and *menB* in *S. oneidensis* MR-1, oriented with the Tn7R end near *glmS* and the Tn7L end near *menB*. We sequenced the specific upstream and downstream PCR products from five of the mini-Tn7-KSGFP transconjugants to determine the specific insertion site for the transposon in MR-1. In all five of the transconjugants, mini-Tn7-KSGFP inserted following base pair (bp) 4951342 of the MR-1 genome sequence (NCBI accession number AE014299.1) and duplicated the six-bp sequence GCCAGT (bp 4951347-4951342 of the MR-1 genome). This sequence is part of an imperfect 42 bp inverted repeat presumably capable of forming a stem-and-loop structure and putatively serving as the rho-independent transcriptional terminator of *glmS*, which would be interrupted by insertion of the transposon.

Chapter 4

Metabolic dynamics and heterogeneity in *Shewanella oneidensis* biofilms

4.1 Abstract

Bacteria in biofilm communities are resilient to changes in environmental conditions and resistant to toxins and antibiotics. The communities are spatially stratified and metabolically heterogenous, suggesting that the communities may respond differentially to environmental changes. Some regions within the community are not growth-active, but are still persisting and are capable of generating energy for maintenance. To determine whether these growth-inactive regions are able to dynamically respond to nutrient changes and how growth-activity profiles might be affected by these changes, we modified the nutrient environments of mature *Shewanella oneidensis* biofilms and tracked *in vivo* expression of a growth activity reporter. Using a quantitative analysis, we determined regions of growth activity and how these profiles changed under different conditions. We found that cells previously growth-inactive could become active with the addition of an electron acceptor and that profiles of growth activity match those expected for the diffusion and reaction of the acceptor. However, the addition of an electron donor had little effect on biofilm metabolic profiles. These findings suggest that metabolic organization of *S. oneidensis* biofilms is dynamic and influenced primarily by the availability of an electron acceptor.

4.2 Introduction

Bacteria grow in the environment as surface-attached microbial communities that are heterogeneous and spatially stratified [24, 108]. It has been shown that while not all regions of the biofilm are actively growing, much of the community is still alive and capable of generating energy to persist [101]. Some studies have shown that growth activity profiles can be modified when media conditions are changed, but these studies have focused on early stages of biofilm development when the community may not have been as differentiated as in mature structures [95]. In mature biofilms studies have been conducted to trigger cell dispersal and in these cases a subset of the population responds and detaches from the community [105]. Often these changes in environmental conditions are very dramatic. It is not known however, how growth and metabolic profiles might be modified in response to changes in nutrient availability or what substrates might have an effect on growth profiles. Gaining an understanding of how biofilm growth and metabolic profiles are affected can give us insight into how biofilms live in the environments and how responsive or terminally differentiated they might be.

To explore whether growth activity patterns of mature biofilms are dynamically responsive to changes in nutrient availability and how these patterns might be affected by different nutrients and concentrations, we chose to work with *Shewanella oneidensis*. *S. oneidensis* can form biofilms, has versatile respiratory capabilities and its metabolism has been well-characterized, making it an ideal organism for investigating metabolic responsiveness and heterogeneity.

4.3 Material and Methods

4.3.1 Bacterial strains, plasmids and media.

Shewanella oneidensis strains were grown planktonically using LB (Sigma) or LML (0.2 g/L yeast extract, 0.1 g/L peptone, 2.5 g/L sodium HEPES, and 0.243 mL/L 60% lactate syrup (20mM), pH 8.0). When required tetracycline was added at the final concentration 15 µg/mL. For cultures grown with fumarate 20mM or 2mM Disodium fumaric acid was added to the basal media. For biofilm experiments LML with 0.5mM lactate was used.

S. oneidensis derivative DKN310 expressing an ECFP from a lac promoter and an unstable gfp (*gfpAAV*), from a ribosomal reporter, *rrnB* P1, were constructed as described [101]. The *lac-ecfp* fusion was inserted into the chromosome using a mini-Tn7 system. The *rrnB* P1-*gfpAAV* fusion was inserted into plasmid pME6031, creating plasmid pTK4. *S. oneidensis* strain DKN580 is strain

MR-1 with the pTK4 plasmid.

S. oneidensis DSP10 is a spontaneous rifampicin resistant mutant of MR-1, created by Doug Lies [102]. No differences in growth aerobically or anaerobically on any alternative electron acceptor have been observed between DSP10 and MR-1. A non-polar mutant in the fumarate reductase flavoprotein subunit precursor, SO_0970, was made by deleting a portion of the gene using the native PstI sites in the gene in *S. oneidensis* DSP10, creating strain NP-FC-1 [58]. This deletion was confirmed to be in frame by sequencing. Plasmid pTK4 was added to strains DSP10 and NP-FC-1 creating strains DSP10 pTK4 and NP-FC-1 pTK4. NP-FC-1 is unable to reduce fumarate, but could still grow on and reduce TMAO and thiosulfate under anaerobic conditions [58]. The pTK4 plasmid was added to DSP10 and NP-FC-1 creating strains *S. oneidensis* DSP10 pTK4 (DKN578) and *S. oneidensis* NP-FC-1 pTK4 (DKN579) respectively.

Anaerobic cultures were grown using LML media and adding 20mM fumarate as the electron acceptor. Media was prepared, dispensed into Balch tubes, stoppered and autoclaved. Immediately after autoclaving, media was flushed with mixed gas for 30 seconds.

4.3.2 Measurements of growth and fluorescence

Growth and fluorescence measurements were taken using a Bio-Tek Synergy HT. For measuring growth, optical density at an absorbance of 600nm was used. For green fluorescence, measurements were taken using a 485/20 excitation filter and a 528/20 emission filter.

4.3.3 Fermentor experiments

Cultures were grown in a New Brunswick Scientific BIOFLO 110 Fermentor/Bioreactor to supply oxygen at a constant rate and measure dissolved oxygen concentrations. Oxygen was supplied to the culture by attaching a standard air line, presumably containing 21% oxygen, to the fermentor and regulating the inflow pressure to 2 lpm. The fermentor was calibrated to measure oxygen values by thoroughly oxygenated the medium using the air inflow line and setting this value to 100%. or 1.0. As per the instructions for the fermentor, the dissolved oxygen sensor was disconnected from the machine and when the readout settled, this value was set to 0.0. Oxygen values were then recorded as the readout from the dissolved oxygen sensor. Samples were taken from the fermentor at various time points using the sampling port. Samples were measured for OD₆₀₀.

4.3.4 NADH and NAD⁺ measurements

Measurements of NADH and NAD⁺ were obtained as described [87]. Briefly, two 1mL aliquots of culture were collected in two separate ependoroph tubes and centrifuged at 14,000 for 1 minute. The supernatant was removed and one pellet was resuspended in 300 μ L of 0.2M NADH for the NADH measurement and the other pellet was resuspended in 300 μ L of 0.2M HCl for the NAD⁺ measurement. Samples are incubated at 50°C for 10 minutes and then incubated on ice for 20 minutes, or until they reached 0°. Then 150 μ L of 0.1M HCl (for the NADH sample) or 0.1M NaOH (for the NAD⁺ sample) is added to the lysate and vortexed. An additional 150 μ L of the same reagent is added to the lysate and vortexed. Samples are centrifuged for 3 minutes at 14,000 rpm. The supernatant is then extracted to a fresh tube and stored at -80°C. To measure NADH and NAD⁺ concentrations in the samples, a reagent mix of 8x H₂O, 1x 2.0M Bicine, 2x 100% EtOH, 1x 80mM EDTA, 2x 4.2 mM MTT and 4x 16.6 mM PES is prepared under anaerobic conditions. The reagent mix is allowed to warm up to 30°C. 90 μ L of the reagent mix is pipetted to wells of a 96 well plate. 5 μ L of the NADH or NAD⁺ sample is then added to the well, and the plate is kept anaerobic. On the benchtop 3mg Alcohol Dehydrogenase (ADH II) is added to 3 mL 0.1M Bicine and dispensed into a boat. The plate is transferred to the benchtop where 5 μ L ADHII mix is quickly added to each well. The plate is transferred to a Bio-Tek Synergy HT plate reader held at a temperature of 30°C, and kinetic measurements are taken at 570nm at intervals of 53 seconds for 20 minutes. Before each read the plate is shaken for 1 second at an intensity of 1. For each well the data is plotted and the slope of the line is determined. The slope of the line is what indicates how much NADH and NAD⁺ is in the sample. This data is also obtained for known concentrations of NADH and NAD⁺. Using the slopes of the lines from the NADH and NAD⁺ standard curves, the concentrations of NADH and NAD⁺ for each sample can be determined.

4.3.5 Growth activity response to the addition of fumarate

10 mL LB with 20mM lactate was added to 25 mL tubes. 4 tubes contained LB with 20mM lactate. 2 tubes contained LB with 20mM lactate and 100mM fumarate. *S. oneidensis* pTK4 was innoculated into the tubes to an OD₆₀₀ of 0.01. Cultures were grown shaking at 250rpm and 30°C and time points for OD₆₀₀ and green fluorescence were taken every 60 minutes for 720 minutes. At 420 minutes, when cells had entered stationary phase, the four cultures not containing fumarate were spun down at 7500rpm for 2 minutes. Cells from two samples were resuspended in the same media: LB with 20mM lactate. The two other samples were resuspended in LB with 20mM lactate

and 100mM fumarate, effectively spiking the culture with an addition of 100mM fumarate. Cultures continued to grow shaking at 30°C, and growth and fluorescence were measured every hour.

4.3.6 Growth activity of *S. oneidensis* DSP10 and *S. oneidensis* NP-FC-1 in aerobic and anaerobic conditions

Strains *S. oneidensis* DSP10 pTK4 and *S. oneidensis* NP-FC-1 pTK4 were grown aerobically and anaerobically. Aerobic cultures were grown in 3mL LML in 25mL tubes at 30°C shaking. Anaerobic cultures were grown at 30°C in Balch tubes in LML with 20mM fumarate. Cultures were grown for 1320 minutes. At each time point OD₆₀₀ and green fluorescence were measured.

4.3.7 Biofilm experiments

A flow cell system was constructed as described such that biofilms could be grown under constant conditions and imaged over time [101]. A 0.5 mM lactate LML medium [pH 8.0, 0.2 g/L yeast extract, 0.1 g/L peptone, 2.5 g/L Na HEPES and 0.043 mL 60% lactate syrup] was used as the basal media. For experiments with fumarate, 20mM or 2mM Disodium fumaric acid was added to the media. For experiments with increased lactate concentrations, 20mM lactate was added to the media. The flow cell is inoculated with 300 μ L of a culture in exponential phase, at an OD₆₀₀ of approximately 0.075, using a sterile syringe. Flow is not started immediately in order to allow cells to attach to the surface. After 1 hour the flow is started at a rate of 4.1 μ L/sec, 1.5 rpm on a Watson-Marlow peristaltic pump. The flow continues at this rate for the length of the experiment. Using this technique, biofilms were grown for up to 4 days. If media conditions were changed bottles of the original media were exchanged for new media, and the new media flowed through the system at the same rate. Confocal fluorescence microscopy was used to image bacterial biofilms grown in the flow cells. A Zeiss LSM 510 inverted microscope with a 40x C-Apochromat 1.2W corr water immersion lens at the Caltech Beckman Institute Biological Imaging Center was used. Z-series images were acquired for multiple fields of view at multiple time points during the experiment. For imaging EGFP or EYFP, the excitation was 488nm and the emission filter used was a BP500-550. For imaging ECFP the excitation was 420nm and the emission filter used was a BP465-485. Images were processed using the Imaris software.

4.3.8 Quantitative image analysis

Fluorescence profiles and colony sizes were quantitated as described [101]. To determine colony size an x-axis cross-section through the largest part of the colony was taken. An edge detection algorithm was used to determine the region of greatest contrast between the empty space around the colony and the colony. In this way, the edge of each side of the colony was found, and the distance between the two edges was taken to be the size of the colony.

4.4 Results

4.4.1 Growth and growth activity of *S. oneidensis* DSP10 and *S. oneidensis* NP-FC-1 in aerobic and anaerobic conditions

Shewanella oneidensis contains one gene required for fumarate reduction, SO_0970 [61, 109]. When a mutant is made in this gene, *S. oneidensis* can no longer grow on fumarate under anaerobic conditions. We tested the ability of our mutant strain, NP-FC-1 to grow aerobically and anaerobically on fumarate. Aerobically NP-FC-1 grew the same as wild-type DSP10 (Figure 4.1). To determine growth activity, we used the pTK4 plasmid, where GFP is expressed from the *E. coli rrnB* P1 ribosomal reporter, whose activity correlates with ribosome production. This growth activity, as measured by fluorescence, increased during exponential phase, but decreased during stationary phase, as expected since the cells are producing less ribosomes and less growth active. However, when grown in anaerobic conditions on fumarate strain NP-FC-1 is not able to grow, while strain DSP10 pTK4 can. The growth activity profile is shifted so that growth activity decreases later in stationary phase than under aerobic conditions, but growth activity still is high during exponential phase and drops off through stationary phase. Both DSP10 and NP-FC-1 behave as wild-type MR-1 when grown aerobically in both their growth curve and growth activity profiles, but NP-FC-1 is not able to grow anaerobically on fumarate as we expected.

4.4.2 Fermentor measurements of growth, dissolved oxygen and NADH/NAD⁺ ratios

To determine the correlation between growth state, oxygen concentration and NADH/NAD⁺ levels, cultures of *S. oneidensis* MR-1 were grown in a fermentor where dissolved oxygen levels could be monitored. LB medium was added to the fermentor at the beginning of the experiment and was not

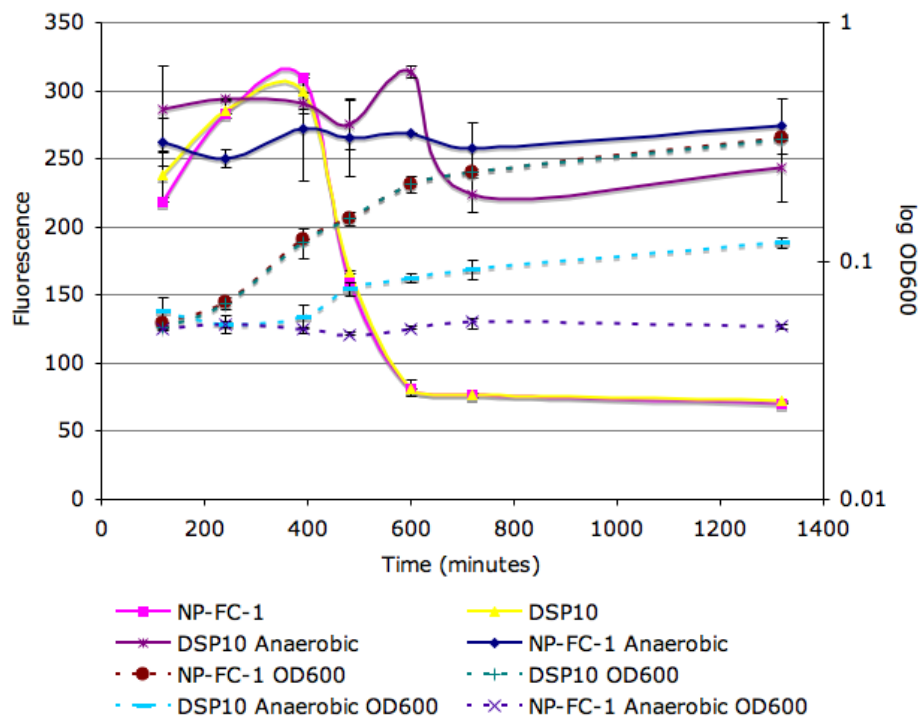


Figure 4.1: Fluorescence levels and $\log \text{OD}_{600}$ for *S. oneidensis* DSP10 pTK4 and *S. oneidensis* NP-FC-1 pTK4 grown aerobically and anaerobically on fumarate. $\log \text{OD}_{600}$ is indicated by dashed lines and fluorescence by solid lines.

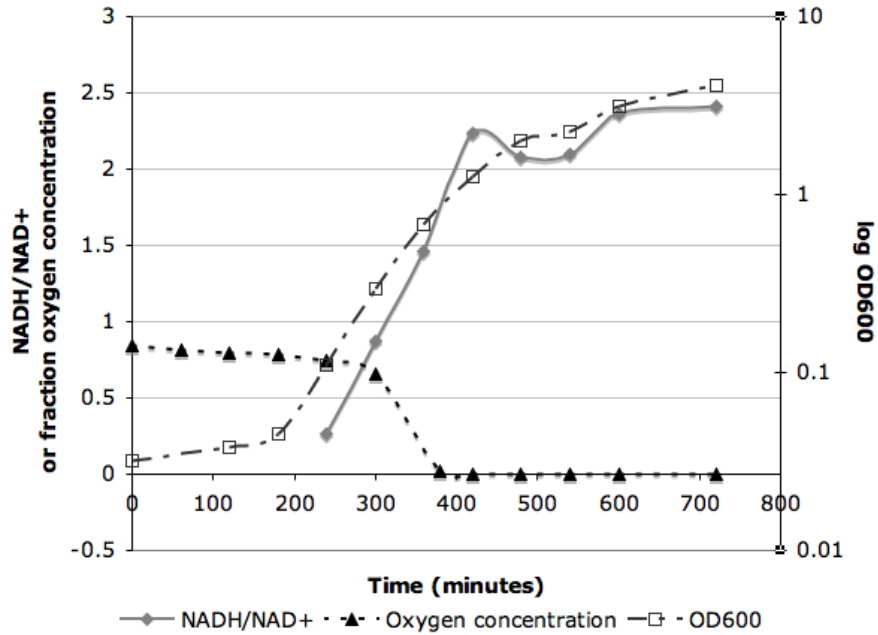


Figure 4.2: Representative curve of growth, dissolved oxygen concentration and NADH/NAD⁺ ratios for *S. oneidensis* MR-1 cultures grown in a chemostat. The solid gray line is NADH/NAD⁺ ratio. The dashed black line with the solid black triangles is dissolved oxygen concentration, where 1.0 represents the maximum concentration in air, 21% oxygen. The dashed black line with the open squares is growth as measured by OD₆₀₀. Oxygen concentrations decrease as cell density increases, and there is a brief drop in the NADH/NAD⁺ ratios during this transition in cell density and oxygen concentration.

exchanged. Air was added to the fermentor at a constant flow rate of 2 lpm and the culture was well-mixed. Oxygen levels stayed high through lag and early exponential phase, but as the cells entered exponential phase, dissolved oxygen concentrations decreased until they were being measured as zero in early stationary phase (Figure 4.2). A dissolved oxygen concentration of zero does not mean that there is no oxygen in the system, only that cells are consuming the oxygen as quickly as it enters the system. The decrease in oxygen concentrations and entrance into stationary phase also correlates with a brief drop in the NADH/NAD⁺ ratio. This brief decrease in the NADH/NAD⁺ ratio is observed in flask cultures as well (data not shown). This suggests that the cells may be switching systems utilized to keep NADH/NAD⁺ ratios, and the redox state, constant under electron acceptor limited or stationary phase conditions.

4.4.3 Growth activity response to the addition of fumarate

To determine if the addition of alternative electron acceptor could influence the growth activity of *S. oneidensis* MR-1, we grew MR-1 aerobically in media without fumarate, with fumarate and with

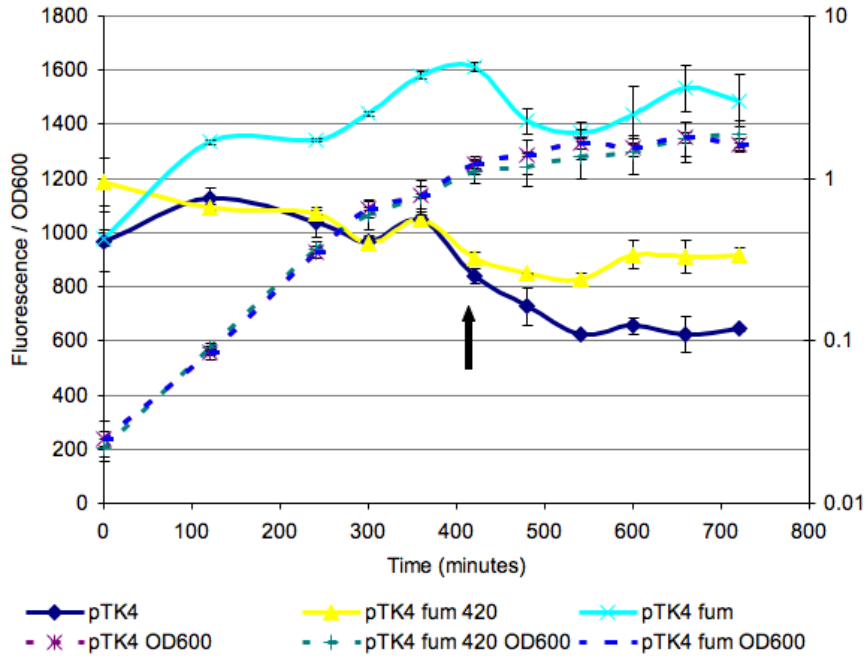


Figure 4.3: Fluorescence levels and OD_{600} for *S. oneidensis* MR-1 pTK4 grown aerobically with and without fumarate. OD_{600} is indicated by dashed lines and fluorescence by solid lines. pTK4 fum 420 cultures were switched to media containing fumarate at 420 minutes, indicated by the arrow on the graph. pTK4 fum cultures were grown in media containing fumarate through the whole experiment.

fumarate added in early stationary phase when cultures became oxygen limited. Cultures without fumarate were grown in LB plus 20mM lactate. Cultures with fumarate were grown in LB plus 20mM lactate and 100mM fumarate. From chemostat measurements where growth and dissolved oxygen concentrations were measured, we were able to determine that oxygen levels quickly dropped to zero when cells reached early stationary phase. Therefore, when cells reached early stationary phase and were limited for oxygen as an electron acceptor we switched the cells to media amended with 100mM fumarate. As seen in Figure 4.3 cells grown with fumarate through the whole experiment maintained a high growth activity even when cells were oxygen limited in stationary phase. In cultures where fumarate was added, growth activity stopped decreasing through stationary phase in contrast to cultures not amended with fumarate that continued to show decreased growth activity. This demonstrates that the addition of an alternative electron acceptor when cells are electron acceptor limited can influence the cells and allow them to be more growth active. Interestingly, the addition of fumarate did not change the amount of growth in the cultures. It may be that the addition of 100mM fumarate, as a less favorable electron acceptor than oxygen, is enough to affect ribosome synthesis, but cannot generate enough energy to appreciably affect cell number.

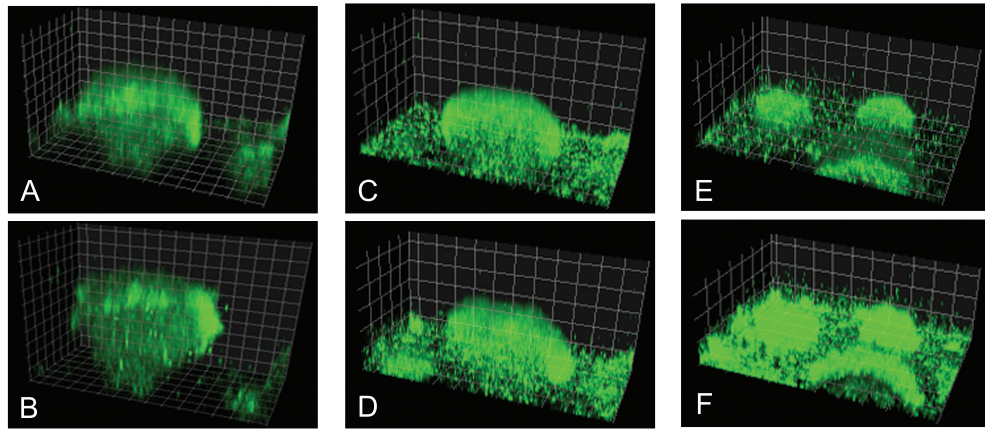


Figure 4.4: Representative images of *S. oneidensis* MR-1 pTK4 biofilms with no change in media (A and B), with the addition of 2mM fumarate (C and D) or with the addition of 20mM fumarate (E and F). Images A, C and F are the biofilms at 48 hours before a change in conditions. Images B, D and F are 56 hours, 6 hours after the media change. Green fluorescence is fluorescence from the ribosomal reporter pTK4 and indicates regions of growth activity. In panels A and B, no change in the media is made and there is a slight decrease in fluorescence intensity at 56 hours. In panels C and D, there is a slight increase in the intensity and region of fluorescence at 56 hours when the biofilm has been exposed to 2mM fumarate. In panels E and F there is a greater increase in the intensity and region of fluorescence after exposure to 20mM fumarate.

4.4.4 Biofilm growth activity profiles with the addition of fumarate or lactate.

Biofilms were grown for approximately 48 hours and imaged in multiple fields of view for each sample. At approximately 50 hours the media was switched to media amended with 2mM fumarate, 20mM fumarate, 20mM lactate or left the same. Biofilms were allowed to grow in this new media for approximately 6 hours and the same colonies were re-imaged. In biofilms where conditions were switched to media containing fumarate the regions of growth activity increased. The increase was more significant in the biofilms amended with 20mM fumarate than with 2mM fumarate (Figure 4.4.). In biofilms where 20mM lactate was added, there was no significant change in the growth activity profiles.

Quantifying the regions of growth activity for a minimum of 6 colonies under each condition, regions of growth activity increase from $30 \mu\text{m}$ in no fumarate biofilms to $37 \mu\text{m}$ in biofilms grown with 2mM fumarate and $46 \mu\text{m}$ in biofilms grown with 20mM fumarate. There was no significant change in the colony size under each condition, indicating that regions of growth activity were increasing and not that new cells were attaching to the structure.

Meshulam-Simon et al measured fumarate and succinate levels in *S. oneidensis* MR-1 cultures

grown anaerobically on pyruvate and fumarate [64]. While the electron donor is different than in our medium, a rate of fumarate respiration can be calculated from this data that should be comparable to reduction rates under our conditions. Calculating the rate through the linear sections of the curve, the rate of fumarate reduction is $60.8 \mu\text{mols/hour}$. Using this value, we can then calculate how far we would expect 20mM and 2mM fumarate to diffuse into the biofilm. Using the equation from Stewart 2003, we predict that 20mM fumarate will diffuse approximately $11 \mu\text{m}$ into the biofilm [96]. This value is made assuming that all cells are consuming fumarate. However, since the fumarate reduction requires proteins expressed only under oxygen-limiting conditions, it is likely that cells on the outer edges that are exposed to oxygen are not consuming fumarate. If we instead add the region where we predict oxygen to be available ($30 \mu\text{m}$) [101] and the region of predicted fumarate diffusion, we find that an electron acceptor should be available approximately $33 \mu\text{m}$ into the biofilm in the presence of 2mM fumarate and approximately $41 \mu\text{m}$ into the biofilm with 20mM fumarate. This matches well with our results where we observe that growth activity occurs $37 \mu\text{m}$ into the biofilm with 20mM fumarate and $46 \mu\text{m}$ into the biofilm with 2mM fumarate.

4.4.5 Profiles of growth activity in biofilms of the *S. oneidensis* fumarate reductase mutant, NP-FC-1

Biofilms of *S. oneidensis* NP-FC-1 develop the same as wild type *S. oneidensis* MR-1 using 0.5mM LML media. However, when *S. oneidensis* NP-FC-1 biofilms are switched to a media containing 20mM fumarate, the colony size decreases dramatically. Average colony size in biofilms with media with no fumarate are $110 \mu\text{m}$ and the average colony size in fumarate amended biofilms is $68 \mu\text{m}$ (Figure 4.5). Growth activity remains high in these smaller colonies, but it appears that cells are leaving the biofilms. This phenotype is similar to that seen when pH is decreased dramatically or high concentrations of DMSO are added to the media (data not shown). It is possible that without a functioning fumarate reductase, fumarate is not able to be metabolized by the cells and is having a toxic effect. This issue remains to be explored.

4.5 Discussion

Although hypotheses about biofilm resilience and the heterogeneous nature of biofilm communities would predict that regions within the biofilm are able to respond differentially to changes in nutrient conditions, it has been yet to be demonstrated conclusively. We have shown that when the availability

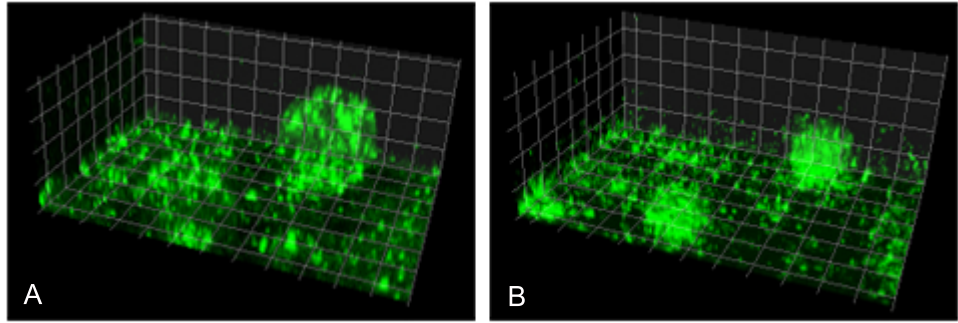


Figure 4.5: Representative images of the fumarate reductase mutant, *S. oneidensis* NP-FC-1 pTK4, biofilms before and after the addition of 20mM fumarate to the media. Panel A is 48 hours and panel B is at 56 hours, 6 hours after the addition of fumarate. Green fluorescence is fluorescence from the ribosomal reporter pTK4 and indicates regions of growth activity. After the addition of fumarate, colonies of *S. oneidensis* NP-FC-1 pTK4 maintain their growth activity, but significantly decrease in size.

of the electron acceptor, fumarate, is increased, growth activity profiles expand. In particular, regions that were not growth active and were instead in a more dormant metabolic state, responded to the electron acceptor availability and were activated.

These regions of growth activity correspond with predictions for fumarate diffusion into a biofilm if different regions or different cells were primarily using one electron acceptor. Since the fumarate reductase of *S. oneidensis* is only upregulated under microaerobic or anaerobic conditions, cells sensing and respiring on higher levels of oxygen are not likely to be able to respire on fumarate as well, validating this prediction. If individual cells are primarily using one electron acceptor, it indicates the the biofilm community is metabolically differentiated, giving credence to the idea that metabolic heterogeneity may be contributing to the persistence of biofilms.

S. oneidensis is able to use fumarate as a part of its citric acid cycle. In order to differentiate the effects of fumarate as an electron acceptor versus its potential role in the the electron donor pathway, we determined the response of the biofilm community to the addition of an electron donor, lactate. When lactate was added there was no significant effect on colony morphology or growth activity profiles. This result is interesting, since we might predict that given the low concentration of electron donor in the basal media, 0.5mM lactate, the cells would be electron donor limited. While electron acceptor concentrations are low, at the biofilm-bulk interface at least, oxygen should be readily available. However, these low lactate conditions are required for biofilm formation [104], and it may be that under these conditions the bacteria utilize another carbon source such as EPS components, extracellular DNA or endogenously produced compounds. It may also be that under biofilm conditions, the requirements for electron donor are extremely low or that the primary limiting

resource is the electron acceptor.

When a strain is not able to reduce fumarate for growth, in the presence of increased fumarate concentrations, biofilm colonies get smaller while maintaining high growth activity. We expected to see only that growth activity profiles would not be affected by the addition of an electron acceptor that the bacteria could not utilize. Instead this dispersal suggests that fumarate has some toxic effects on *S. oneidensis* when it is unable to reduce it, or that the redox balance may somehow be skewed. While many studies have characterized *S. oneidensis* growth and molecular mechanisms of fumarate respiration under anaerobic conditions, to our knowledge no one has investigated the potential effects of fumarate on a fumarate reductase mutant. Since the fumarate reductase is required for growth on fumarate, it is potentially difficult to decouple an inability to grow with a toxic effect. It may also be that this phenotype is unique to cells grown in biofilm conditions, where the bacteria may be particularly sensitive to changes in redox balance.

In this paper, we have shown that the metabolic organization of a *S. oneidensis* biofilm community is dynamic and responsive to changes in electron acceptor availability. The response of biofilm communities to antibiotics and other exogenous compounds has received much focus, but a better knowledge of how bacteria in biofilms can respond to changes in nutrient availability and redox balance is important for the understanding of how bacteria live in biofilms and are so resilient in the environment.

Chapter 5

Conclusion

5.1 Summary

In this thesis, I set out to explore the spatial organization and dynamics of metabolic states within bacterial biofilms and to further investigate what types of processes and compounds might be important for maintaining populations of cells in these environments. Molecular methods, *in vivo* gene expression analyses, confocal microscopy and quantitative image analysis were used to determine profiles of growth and gene expression in *Shewanella oneidensis* and *Pseudomonas aeruginosa* biofilms. Bioinformatic analyses were conducted to determine the ubiquity of an endogenous small molecule sensing mechanism and elucidate the types of systems that are affected. With the work presented here, the questions posed in Chapter 1 can now be revisited.

5.1.1 What is the spatial and temporal stratification of growth and metabolic states within a biofilm? In particular, can cells decouple metabolism from growth?

We demonstrated that remarkably reproducible spatiometabolic stratification occurs in *S. oneidensis* biofilms with growth activity localized to the outer regions of the biofilm in a pattern that correlates with oxygen availability. Within domains of growth-inactive cells, genes typically upregulated under anaerobic conditions are expressed well after growth has ceased, showing that cells in nutrient-limited regions, previously thought to be dead, are instead maintained in a non-growing state, where they are capable of generating energy and synthesizing proteins. Regions of growth activity and anaerobically induced gene expression are inversely correlated, definitively demonstrating that cells within biofilms can decouple metabolism and energy generation from growth.

5.1.2 Does nutrient availability affect growth and metabolic stratification dynamically?

Since subpopulations of cells in a biofilm are growth-inactive but still alive, we investigated whether *S. oneidensis* biofilms are able to respond to changes in nutrient conditions and how those changes affect growth-activity patterns. Bacteria in growth-inactive regions are able to respond to nutrient changes and their growth activity profiles match that of predictions for nutrient diffusion into the biofilm. Electron acceptor availability appears to affect growth activity profiles more significantly than electron donor concentrations. Nutrient availability has predictable effects on metabolic organization in biofilms and the community is able to dynamically respond to nutrient changes in the environment.

5.1.3 How are small molecules used differently within different regions of a biofilm?

Given that biofilm populations are metabolically stratified and can activate metabolic programs appropriate to their local microenvironment and developmental stage, we wondered whether endogenously produced small molecules might be influencing local environments or be differentially produced or degraded within the community. *P. aeruginosa* endogenously produces several small molecules. We studied one such molecule, acyl-homoserine lacone (AHL), which is involved in quorum sensing. We observed and quantified the degradation patterns in *P. aeruginosa* biofilms and determined that AHL degradation occurs in the middle of biofilm communities. In this study we also established that AHLs can be used as a substrate for growth. Whether it is being used as a nutrient or to affect the AHL signaling pathway, AHL degradation does not appear to be important in the biofilm/bulk interface, but occurs preferentially in the middle of biofilm colonies demonstrating that the role of small molecules varies within different regions of the community.

5.1.4 Might redox-active small molecule production and sensing be a ubiquitous process that could be utilized for metabolism under biofilm conditions?

Finally, since small molecules have differential effects on subpopulations of the biofilms, it is possible that small molecules or secondary metabolites may be important in these nutrient-limited domains where maintenance energy generation is not well understood. It must first be determined if small

molecules can elicit maintenance type processes. We used a bioinformatics analysis to determine the regulation patterns of the SoxR system and discovered that in bacterial organisms outside of the enterics, SoxR regulates transport and oxidoreductase genes and not the superoxide stress response as the *E. coli* paradigm would suggest. Results from the literature and our experiments in *Streptomyces coelicolor* confirm these predictions. These results suggest that the response to endogenously produced small molecules is ubiquitous across many types of organisms, and that genes in the response regulon are those that may be important in bacterial energy maintenance. Since these endogenous small molecules are produced primarily under biofilm-like conditions, they may play a primary role in the maintenance of biofilm communities.

5.2 Future directions

The work presented here definitively demonstrates that biofilm communities are stratified in terms of growth activity, metabolism and their response to endogenously produced small molecules, and that this stratification is dynamic and can be modified in response to changes in environmental conditions. However these studies only begin to elucidate the true heterogeneity and diversity of metabolisms and energy generating processes that are fundamental to biofilm growth and maintenance.

Studies of biofilm communities are inherently community based. Any protein or genetic analysis of a biofilm encompasses many distinct populations in many different growth states. While single-cell *in vivo* microscope studies allow a researcher to tease apart individual contributions or responses within the community, conducting these studies on a large scale is not realistic. However, having established a reporter construct that is expressed preferentially in the middle of a biofilm community may be useful in other methods of analysis. One way of assaying broader gene expression profiles within a subset of the community, that we have often discussed, would be to use these single-cell reporters to define particular sub-populations and then to use these reporters in sorting criteria, and a given sub-population can be extracted, so that microarray or proteomic analyses can be conducted on this population alone. By understanding the genes and proteins that are up or down regulated within a given region of the biofilm, we may be able to determine what processes are important for their maintenance. This data could also provide a starting point for creating mutants that could be essential in this maintenance phase of biofilm development. Certain technical challenges exist, including finding and developing appropriate reporter constructs and maintaining the RNA and protein pools during the sorting and extraction processes, but these are issues that can be addressed. In particular the environmental microbiology community has begun to explore the use of

fluorescence in situ hybridization (FISH) in extracting subsets of communities and while the studies are typically more focused on DNA analysis, some of the same techniques might be employed. It is surprising with so much focus on biofilm development and detachment and the effects of antibiotics on biofilm viability that more research hasn't been done on the basic metabolic properties of cells within the community. Taking this sub-population level approach would produce significant insight into metabolic processes in unexplored sub-domains of the biofilm. Additionally, a data set such as this might provide a good starting point for further research and invigorate the study of metabolism and maintenance essential for the cells in biofilm communities.

Another interesting direction for future research is that of the role of redox-active small molecules in biofilm metabolism and maintenance. Many of these compounds do act as antibiotics, so they have been primarily studied for their role in virulence. However, this virulence effect is potentially not enough to explain why bacteria would use their limited energy resources to produce these molecules only to fend off some competitors or host response that often isn't present. In the Newman lab, we began to explore alternate roles for these compounds and have already shown that these redox-active small molecules have multiple and broad effects. Since these molecules are upregulated under biofilm type conditions, easily diffusible and redox-active, it seems an interesting route of investigation to assay their role in biofilms. Studies of the effects of phenazines on biofilms and colony morphology in *P. aeruginosa* have already begun in the lab in more detail. And previous studies have investigated the role of redox active compounds in iron reduction at a distance. Using the growth reporter assay it would be interesting to see how these compounds can affect growth-activity profiles. Also combining the approach described above with the introduction of different compounds or mutants in endogenous compound production could elucidate the differential regulation and sensing mechanisms for these compounds in different regions of the biofilm.

These studies focus on the elucidation of metabolism in single-species biofilm systems, but similar questions remain to be explored in multi-species systems where bacteria compete for resources or exist in a syntrophic relationship. In these systems it is possible to see a more apparent spatial stratification within the system and to determine the effects of small molecule production across species. As bacteria in environment mainly exist in multi-species communities, small molecules may have a different role in these interactions and it would be interesting to conduct various competition experiments with for instance *P. aeruginosa* phenazine mutant strains and wild type strains against other species of bacteria that may or may not produce their own redox compounds.

Obtaining a more complete understanding of the growth states and metabolism of bacterial

biofilms, composed of different species and under different conditions, will aid in our understanding the lifecycle of bacteria and help us to understand what effects these communities have on the environment and human health. It will be easier to combat or foster biofilm communities when we understand the mechanisms involved in maintaining them.

Appendix A

Development of *Shewanella oneidensis* biofilms

A.1 Abstract

A method for growing and imaging *Shewanella oneidensis* biofilms in a flow cell system is presented. This work is an elaboration of the previously published work in Teal et al, 2006 [101].

A.2 Introduction

Over the last decade it has been recognized that many bacteria grow preferentially as surface-attached microbial communities, or biofilms. Bacteria attach to a surface and go through a developmental-like pathway that leads to a structure composed of hundreds of cells and the extracellular matrix that the cells produce [24]. Because of this structural configuration, individual cells within a community experience their own microenvironment due to gradients established by diffusion of nutrients and metabolism. Biofilm communities are therefore heterogeneous and spatially stratified, so that each cell's growth state and metabolism is affected by its location in the biofilm and the structure's biomass [108].

To explore the spatiometabolic stratification of developing and mature biofilms, we selected *Shewanella oneidensis* strain MR-1, a biofilm-forming, facultative anaerobe with remarkable metabolic versatility. *S. oneidensis* can use oxygen and many other lower potential substrates, including metals, as electron acceptors in respiration, making it an attractive experimental system in which to explore domains of metabolism within a biofilm [111, 39, 104].

Here we present a method for growing *Shewanella oneidensis* biofilms in a flow cell system that can be used to track biofilm development under controlled conditions.



Figure A.1: Setup of biofilm once flow-through system on the biofilm cart.

A.3 Methods

A.3.1 Setup of flow cell system

To monitor biofilms over time, it is important to be able to image in a non-destructive way. For this purpose a once-through flow cell system was constructed as described [66]. A Watson-Marlow type pump, an MPL PumpPro, is used to flow media from a flask containing sterile media to a bubble trap to a flow cell device where biofilms are grown and can be imaged, to an effluent container as shown in Figure A.3.1.

To set up the system, Masterflex platinum cured silicone tubing, size 14 (Fisher Scientific #96410-14), is used to connect the media flask to the flow pump and between the bubble traps, flow cells and effluent. The tubing used through the flow pump is Cole Parmer 2-stop silicone tubing, 1.65mm (Cole-Parmer #07616-38). The bubble traps are PGC Scientific 3-cylinder bubble traps (PGC Scientific #82-106). Bubble traps are used to trap air bubbles that may have been introduced at the start of the system so they do not go through the flow cell. Flow cells were designed and manufactured at the California Institute of Technology. Flow cells have 4 channels machined from polyurethane with number 1 coverslips attached via epoxy. Each channel is 40.6 mm long, 11.4 mm wide and 0.203 mm deep. The coverslip is etched in a large grid pattern with a diamond pen, as a guide to localizing regions within the flow cell during microscopy.

Before starting the biofilm experiment, all tubing is autoclaved. Flow cells and bubble traps cannot be autoclaved, so they are bleached after each use as described below. Using sterile tubing and bleached flow cells and bubble traps, the setup is assembled. For each lane one line of tubing goes into the media and through the pump where it is connected to a bubble trap, then the flow cell

and finally into an effluent container. To rinse and sterilize the system, sterile water is run through the system for a minimum of one hour at a rate of 6.0 rpm on the MPL Pump Pro. The water is then emptied out of the system and the inflow is switched to media. The system, including the bubble traps are filled with media.

Media flow is stopped and 300 μ L of culture is injected into the tubing just upstream of the flow cell chamber using a 1cc insulin syringe U-100 28G $\frac{1}{2}$ (Becton Dickinson #309309). The flow is kept off for 1 hour to allow the cells to attach to the surface. The flow is then started at a rate of 1.5 rpm (4.1 μ L/sec). This flow rate is kept for the duration of the experiment.

When the experiment is finished 5% bleach is run through the system for a minimum of 2 hours. Initially a rate of 12.0 - 20.0 rpms is used to flush the biofilms from the system, but after approximately 30 minutes, a slower flow rate of 6.0 rpms is used. After bleaching, the system is rinsed with non-sterile water. The system is then disassembled and re-sterilized.

A.3.2 Media

For *Shewanella oneidensis* biofilms a .5mM lactate LML medium is used. The medium contains 0.2 g/L yeast extract, 0.1 g/L peptone, 2.5 g/L Na HEPES and 0.043 mL 60% lactate syrup and is at pH 8.0. If alternative electron acceptors are used, they are added to this medium base.

A.3.3 Cultures

Cultures of *S. oneidensis* MR-1 are grown in LB to stationary phase. The cells are then subcultured 1:1000 into 5mM lactate LML media and grown shaking at 30°C for approximately 3 hours into early exponential phase at an OD₆₀₀ of approximately 0.075. This early exponential phase culture is used to inoculate the flow cells.

A.3.4 Imaging

Biofilms in flow cells are imaged at the Caltech Beckman Institute Biological Imaging Center using a Zeiss LSM 510 inverted Confocal Laser Scanning Microscope with a 63x or 40x C-Apochromat 1.2W corr water immersion lens and an Argon laser line. Using the Zeiss LSM 510 software, Z-series images are acquired for multiple fields of view at multiple time points during the experiment.

For imaging EGFP or EYFP, the excitation is 488nm and the emission filter used is a BP500-550. For imaging ECFP the excitation is 420nm and the emission filter used is a BP465-485, consistent

with the EGFP, EYFP and ECFP excitation and emission spectra as seen in Figure A.2. Biofilms can be imaged in bright field using the ChD setting in the Zeiss LSM software.

A.3.5 Image processing

Images are processed using Zeiss LSM software or Imaris. Orthogonal views are obtained by using the orthogonal view setting in the LSM software and selecting an X, Y and Z plane of interest, usually through the middle of a biofilm colony. 3-D reconstructions were made using the Volume setting in the Imaris software. To visualize the middle of a colony, a cutting plane was used to virtually cut a colony in half, so that the inside of the colony could be viewed.

A.3.6 Quantitative image analysis

To determine a profile of fluorescence through a biofilm structure, quantitative measurements are made for biofilm images. For each image, the fluorescence intensity profile is mapped through the center x-axis of a biofilm structure using NIH ImageJ. These fluorescence values are exported as a text file of x-coordinates and fluorescence intensity for each pixel. An analysis program written in Python `image-recenter.py` is used to analyze and process this data. The program takes as input a text file with two columns - position and pixel - and a cutoff value that defines the low intensity cutoff. The brightest pixel is defined as 100% fluorescence and all fluorescence values are determined relative to that value. To automatically determine the edges of a structure, an edge detection algorithm is used where the region of greatest contrast between the empty space surrounding the biofilm structure and the fluorescence of the structure is defined to be the edge. Using the defined edges, the center is specified. Then, the intensity of each nine-pixel bin is determined in relationship to its distance from the center of the structure. The output is in two files. One file contains the colony size, calculated by the distance between the left and right edges, and the cutoff threshold used. Another file is the average position of the nine-pixel bin as a function of the distance from the center of the colony and the average intensity for that bin. Using this output, a plot of fluorescence intensity versus distance from the center of the structure can be constructed for each image. Biofilms of the same type are binned into representative sizes, and using the script `avg-error-files.py`, the average fluorescence profile and standard deviations across all the structures of that size are calculated. `avg-error-files.py` takes as input a list of files generated from `image-recenter.py` and generates as output: position, as a distance from the center of the colony, and the average and standard deviation of the fluorescence intensity at that position. This output is used to generate

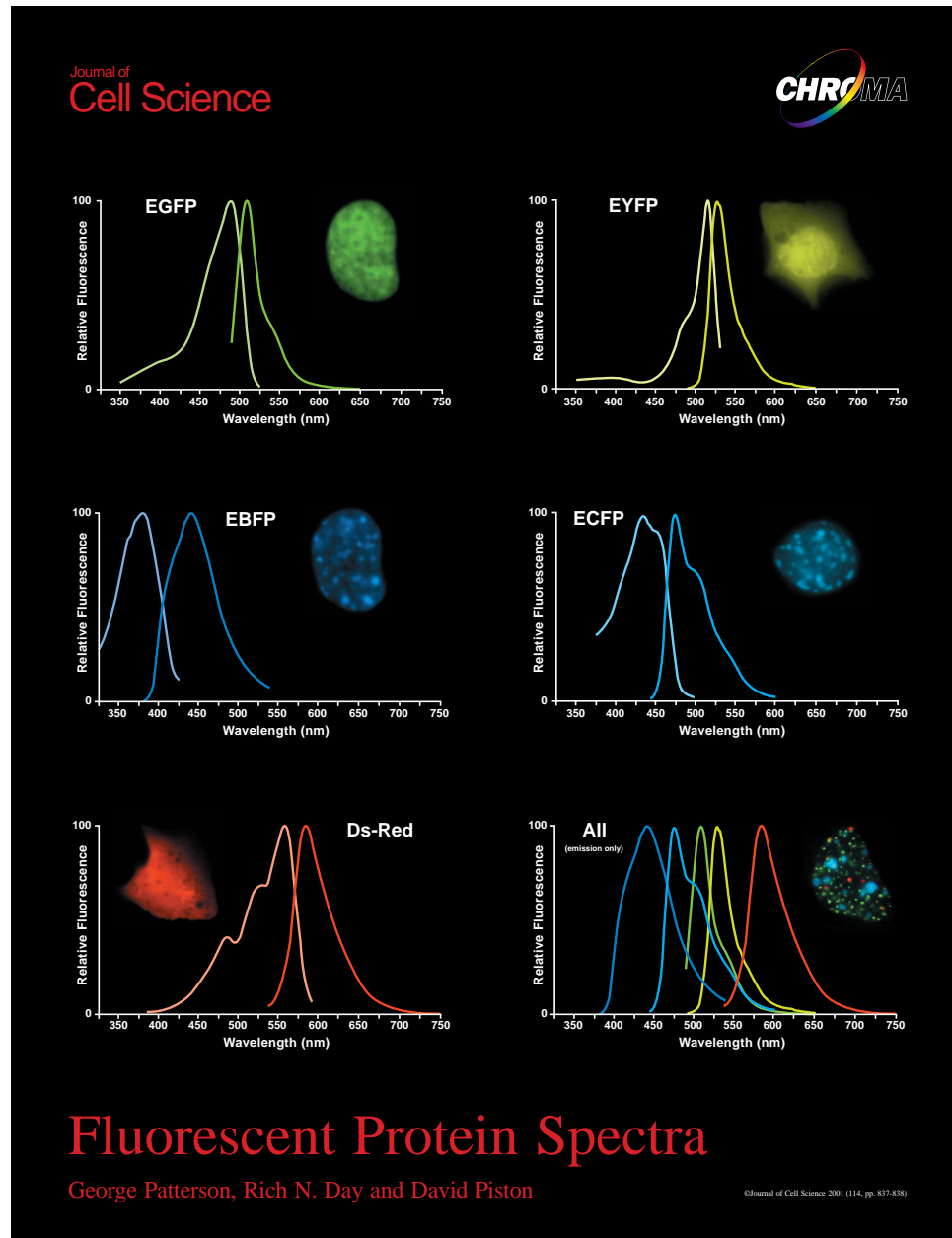


Figure A.2: Excitation and emission spectra for the enhanced fluorescent proteins. From Patterson, Day and Piston [73].

a plot of fluorescence intensity versus the distance from the center of the structure for all biofilm structures of a given size. Scripts are available at <http://idyll.org/~tracyt/qbiofilm/>.

Appendix B

Supplemental tables for Chapter 6

B.1 Pyscangen table

Table B.1 is the output of `pyscangen.py` for the soxbox position weight matrix (PWM) described in Chapter 6. For each genome containing a SoxR protein, the number of sites found at or below each threshold is shown along with the percentage of those sites found in intergenic regions versus the percentage found in genes. If the PWM is finding true binding sites, it is expected that there will be more sites found in intergenic regions than within genes.

Table B.2 is the output of `pyscangenes.py` for the soxbox PWM described in Chapter 6. For each genome containing a SoxR protein, the soxbox sites found and the operons adjacent to them are listed.

Table B.1: The number of sites found in intergenic regions and within genes for thresholds 1.0 - 13.0 in each genome containing SoxR.

Acidovorax avenae subsp. citrulli AAC00-1, complete genome			
Threshold	Total sites found	Percent in genes	Percent intergenic
1.00	0	0%	0%
2.00	0	0%	0%
3.00	0	0%	0%
4.00	0	0%	0%
5.00	1	0%	100%
6.00	1	0%	100%
7.00	1	0%	100%
8.00	1	0%	100%
9.00	2	0%	100%
10.00	3	0%	100%
11.00	3	0%	100%
12.00	3	0%	100%
13.00	4	0%	100%

Acidobacteria bacterium Ellin345, complete genome

Cutoff	Total sites found	Percent in genes	Percent intergenic
1.00	0	0%	0%
2.00	1	0%	100%
3.00	1	0%	100%
4.00	1	0%	100%
5.00	1	0%	100%
6.00	1	0%	100%
7.00	1	0%	100%
8.00	1	0%	100%
9.00	1	0%	100%
10.00	1	0%	100%
11.00	1	0%	100%
12.00	1	0%	100%
13.00	2	0%	100%

Acidovorax avenae subsp. citrulli AAC00-1, complete genome

Cutoff	Total sites found	Percent in genes	Percent intergenic
1.00	0	0%	0%
2.00	0	0%	0%
3.00	0	0%	0%
4.00	0	0%	0%
5.00	1	0%	100%
6.00	1	0%	100%
7.00	1	0%	100%
8.00	1	0%	100%
9.00	2	0%	100%
10.00	3	0%	100%
11.00	3	0%	100%
12.00	3	0%	100%
13.00	4	0%	100%

Acinetobacter sp. ADP1, complete genome

Cutoff	Total sites found	Percent in genes	Percent intergenic
1.00	0	0%	0%
2.00	1	0%	100%
3.00	1	0%	100%
4.00	1	0%	100%
5.00	1	0%	100%
6.00	1	0%	100%
7.00	1	0%	100%
8.00	1	0%	100%
9.00	1	0%	100%
10.00	1	0%	100%
11.00	2	50%	50%
12.00	7	57%	43%
13.00	18	72%	28%

Aeromonas hydrophila subsp. hydrophila ATCC 7966, complete genome

Cutoff	Total sites found	Percent in genes	Percent intergenic
1.00	0	0%	0%
2.00	0	0%	0%
3.00	0	0%	0%
4.00	0	0%	0%
5.00	1	0%	100%
6.00	1	0%	100%
7.00	1	0%	100%
8.00	1	0%	100%
9.00	1	0%	100%
10.00	1	0%	100%
11.00	1	0%	100%
12.00	1	0%	100%
13.00	3	33%	67%

Agrobacterium tumefaciens str. C58 chromosome circular, complete sequence

Cutoff	Total sites found	Percent in genes	Percent intergenic
1.00	0	0%	0%
2.00	0	0%	0%
3.00	0	0%	0%
4.00	0	0%	0%
5.00	0	0%	0%
6.00	0	0%	0%
7.00	1	0%	100%
8.00	1	0%	100%
9.00	1	0%	100%
10.00	1	0%	100%
11.00	2	50%	50%
12.00	2	50%	50%
13.00	2	50%	50%

Agrobacterium tumefaciens str. C58 chromosome linear, complete sequence

Cutoff	Total sites found	Percent in genes	Percent intergenic
1.00	0	0%	0%
2.00	0	0%	0%
3.00	0	0%	0%
4.00	0	0%	0%
5.00	0	0%	0%
6.00	1	0%	100%
7.00	2	0%	100%
8.00	2	0%	100%
9.00	2	0%	100%
10.00	2	0%	100%
11.00	3	0%	100%
12.00	5	0%	100%
13.00	8	13%	88%

Arthrobacter aurescens TC1, complete genome

Cutoff	Total sites found	Percent in genes	Percent intergenic
1.00	0	0%	0%
2.00	0	0%	0%
3.00	0	0%	0%
4.00	0	0%	0%
5.00	0	0%	0%
6.00	1	0%	100%
7.00	1	0%	100%
8.00	2	50%	50%
9.00	2	50%	50%
10.00	2	50%	50%
11.00	2	50%	50%
12.00	2	50%	50%
13.00	5	60%	40%

Bdellovibrio bacteriovorus HD100, complete genome

Cutoff	Total sites found	Percent in genes	Percent intergenic
1.00	0	0%	0%
2.00	1	0%	100%
3.00	1	0%	100%
4.00	1	0%	100%
5.00	1	0%	100%
6.00	1	0%	100%
7.00	1	0%	100%
8.00	1	0%	100%
9.00	2	0%	100%
10.00	2	0%	100%
11.00	2	0%	100%
12.00	5	40%	60%
13.00	9	56%	44%

Bordetella bronchiseptica RB50, complete genome

Cutoff	Total sites found	Percent in genes	Percent intergenic
1.00	0	0%	0%
2.00	0	0%	0%
3.00	0	0%	0%
4.00	0	0%	0%
5.00	0	0%	0%
6.00	0	0%	0%
7.00	1	0%	100%
8.00	1	0%	100%
9.00	1	0%	100%
10.00	1	0%	100%
11.00	1	0%	100%
12.00	2	0%	100%
13.00	3	33%	67%

Bordetella parapertussis 12822, complete genome

Cutoff	Total sites found	Percent in genes	Percent intergenic
1.00	0	0%	0%
2.00	0	0%	0%
3.00	0	0%	0%
4.00	0	0%	0%
5.00	0	0%	0%
6.00	0	0%	0%
7.00	0	0%	0%
8.00	0	0%	0%
9.00	1	0%	100%
10.00	1	0%	100%
11.00	1	0%	100%
12.00	2	0%	100%
13.00	3	33%	67%

Bordetella pertussis Tohama I, complete genome

Cutoff	Total sites found	Percent in genes	Percent intergenic
1.00	0	0%	0%
2.00	0	0%	0%
3.00	0	0%	0%
4.00	0	0%	0%
5.00	0	0%	0%
6.00	0	0%	0%
7.00	1	0%	100%
8.00	1	0%	100%
9.00	1	0%	100%
10.00	1	0%	100%
11.00	1	0%	100%
12.00	1	0%	100%
13.00	2	50%	50%

Burkholderia sp. 383 chromosome 3, complete sequence

Cutoff	Total sites found	Percent in genes	Percent intergenic
1.00	0	0%	0%
2.00	0	0%	0%
3.00	0	0%	0%
4.00	0	0%	0%
5.00	0	0%	0%
6.00	0	0%	0%
7.00	0	0%	0%
8.00	0	0%	0%
9.00	0	0%	0%
10.00	0	0%	0%
11.00	0	0%	0%
12.00	0	0%	0%
13.00	1	0%	100%

Burkholderia sp. 383 chromosome 1, complete sequence

Cutoff	Total sites found	Percent in genes	Percent intergenic
1.00	0	0%	0%
2.00	0	0%	0%
3.00	0	0%	0%
4.00	0	0%	0%
5.00	0	0%	0%
6.00	0	0%	0%
7.00	0	0%	0%
8.00	0	0%	0%
9.00	0	0%	0%
10.00	0	0%	0%
11.00	0	0%	0%
12.00	1	100%	0%
13.00	1	100%	0%

Burkholderia sp. 383 chromosome 2, complete sequence

Cutoff	Total sites found	Percent in genes	Percent intergenic
1.00	0	0%	0%
2.00	0	0%	0%
3.00	0	0%	0%
4.00	1	0%	100%
5.00	1	0%	100%
6.00	1	0%	100%
7.00	1	0%	100%
8.00	2	0%	100%
9.00	2	0%	100%
10.00	3	0%	100%
11.00	4	0%	100%
12.00	4	0%	100%
13.00	4	0%	100%

Chromobacterium violaceum ATCC 12472, complete genome

Cutoff	Total sites found	Percent in genes	Percent intergenic
1.00	0	0%	0%
2.00	0	0%	0%
3.00	0	0%	0%
4.00	0	0%	0%
5.00	1	0%	100%
6.00	2	0%	100%
7.00	2	0%	100%
8.00	2	0%	100%
9.00	2	0%	100%
10.00	2	0%	100%
11.00	2	0%	100%
12.00	3	0%	100%
13.00	3	0%	100%

Erythrobacter litoralis HTCC2594, complete genome

Cutoff	Total sites found	Percent in genes	Percent intergenic
1.00	0	0%	0%
2.00	0	0%	0%
3.00	0	0%	0%
4.00	1	100%	0%
5.00	1	100%	0%
6.00	1	100%	0%
7.00	1	100%	0%
8.00	1	100%	0%
9.00	1	100%	0%
10.00	1	100%	0%
11.00	1	100%	0%
12.00	1	100%	0%
13.00	1	100%	0%

Escherichia coli CFT073, complete genome

Cutoff	Total sites found	Percent in genes	Percent intergenic
1.00	0	0%	0%
2.00	0	0%	0%
3.00	1	0%	100%
4.00	1	0%	100%
5.00	1	0%	100%
6.00	1	0%	100%
7.00	1	0%	100%
8.00	1	0%	100%
9.00	1	0%	100%
10.00	1	0%	100%
11.00	3	67%	33%
12.00	4	75%	25%
13.00	6	67%	33%

Escherichia coli K12, complete genome

Cutoff	Total sites found	Percent in genes	Percent intergenic
1.00	0	0%	0%
2.00	0	0%	0%
3.00	1	0%	100%
4.00	1	0%	100%
5.00	1	0%	100%
6.00	1	0%	100%
7.00	1	0%	100%
8.00	1	0%	100%
9.00	1	0%	100%
10.00	1	0%	100%
11.00	2	50%	50%
12.00	2	50%	50%
13.00	4	50%	50%

Frankia alni ACN14a, complete genome

Cutoff	Total sites found	Percent in genes	Percent intergenic
1.00	0	0%	0%
2.00	0	0%	0%
3.00	0	0%	0%
4.00	0	0%	0%
5.00	0	0%	0%
6.00	0	0%	0%
7.00	0	0%	0%
8.00	0	0%	0%
9.00	0	0%	0%
10.00	0	0%	0%
11.00	0	0%	0%
12.00	3	67%	33%
13.00	4	50%	50%

Frankia sp. CcI3, complete genome

Cutoff	Total sites found	Percent in genes	Percent intergenic
1.00	0	0%	0%
2.00	0	0%	0%
3.00	0	0%	0%
4.00	0	0%	0%
5.00	0	0%	0%
6.00	0	0%	0%
7.00	0	0%	0%
8.00	1	0%	100%
9.00	1	0%	100%
10.00	2	0%	100%
11.00	3	0%	100%
12.00	4	0%	100%
13.00	5	0%	100%

Hahella chejuensis KCTC 2396, complete genome

Cutoff	Total sites found	Percent in genes	Percent intergenic
1.00	0	0%	0%
2.00	1	0%	100%
3.00	1	0%	100%
4.00	1	0%	100%
5.00	1	0%	100%
6.00	2	0%	100%
7.00	2	0%	100%
8.00	2	0%	100%
9.00	2	0%	100%
10.00	4	0%	100%
11.00	4	0%	100%
12.00	5	20%	80%
13.00	8	25%	75%

Hyphomonas neptunium ATCC 15444, complete genome

Cutoff	Total sites found	Percent in genes	Percent intergenic
1.00	0	0%	0%
2.00	0	0%	0%
3.00	0	0%	0%
4.00	0	0%	0%
5.00	0	0%	0%
6.00	1	0%	100%
7.00	1	0%	100%
8.00	1	0%	100%
9.00	1	0%	100%
10.00	1	0%	100%
11.00	1	0%	100%
12.00	1	0%	100%
13.00	1	0%	100%

Maricaulis maris MCS10, complete genome

Cutoff	Total sites found	Percent in genes	Percent intergenic
1.00	0	0%	0%
2.00	0	0%	0%
3.00	0	0%	0%
4.00	0	0%	0%
5.00	0	0%	0%
6.00	0	0%	0%
7.00	0	0%	0%
8.00	0	0%	0%
9.00	0	0%	0%
10.00	1	0%	100%
11.00	1	0%	100%
12.00	1	0%	100%
13.00	1	0%	100%

Mesorhizobium loti MAFF303099, complete genome

Cutoff	Total sites found	Percent in genes	Percent intergenic
1.00	0	0%	0%
2.00	0	0%	0%
3.00	0	0%	0%
4.00	1	0%	100%
5.00	2	0%	100%
6.00	2	0%	100%
7.00	2	0%	100%
8.00	2	0%	100%
9.00	3	0%	100%
10.00	3	0%	100%
11.00	3	0%	100%
12.00	3	0%	100%
13.00	3	0%	100%

Mycobacterium vanbaalenii PYR-1, complete genome

Cutoff	Total sites found	Percent in genes	Percent intergenic
1.00	0	0%	0%
2.00	0	0%	0%
3.00	0	0%	0%
4.00	0	0%	0%
5.00	0	0%	0%
6.00	0	0%	0%
7.00	0	0%	0%
8.00	0	0%	0%
9.00	0	0%	0%
10.00	2	0%	100%
11.00	4	0%	100%
12.00	4	0%	100%
13.00	6	0%	100%

Mycobacterium sp. JLS, complete genome

Cutoff	Total sites found	Percent in genes	Percent intergenic
1.00	0	0%	0%
2.00	0	0%	0%
3.00	0	0%	0%
4.00	0	0%	0%
5.00	0	0%	0%
6.00	0	0%	0%
7.00	1	0%	100%
8.00	1	0%	100%
9.00	2	0%	100%
10.00	4	0%	100%
11.00	4	0%	100%
12.00	4	0%	100%
13.00	4	0%	100%

Mycobacterium sp. KMS, complete genome

Cutoff	Total sites found	Percent in genes	Percent intergenic
1.00	0	0%	0%
2.00	0	0%	0%
3.00	0	0%	0%
4.00	0	0%	0%
5.00	0	0%	0%
6.00	0	0%	0%
7.00	1	0%	100%
8.00	1	0%	100%
9.00	2	0%	100%
10.00	4	0%	100%
11.00	4	0%	100%
12.00	5	0%	100%
13.00	5	0%	100%

Mycobacterium sp. MCS, complete genome

Cutoff	Total sites found	Percent in genes	Percent intergenic
1.00	0	0%	0%
2.00	0	0%	0%
3.00	0	0%	0%
4.00	0	0%	0%
5.00	0	0%	0%
6.00	0	0%	0%
7.00	1	0%	100%
8.00	1	0%	100%
9.00	2	0%	100%
10.00	4	0%	100%
11.00	4	0%	100%
12.00	5	0%	100%
13.00	5	0%	100%

Mycobacterium smegmatis str. MC2 155, complete genome

Cutoff	Total sites found	Percent in genes	Percent intergenic
1.00	0	0%	0%
2.00	0	0%	0%
3.00	0	0%	0%
4.00	0	0%	0%
5.00	0	0%	0%
6.00	0	0%	0%
7.00	0	0%	0%
8.00	1	0%	100%
9.00	3	0%	100%
10.00	4	0%	100%
11.00	4	0%	100%
12.00	4	0%	100%
13.00	9	0%	100%

Nocardia farcinica IFM 10152, complete genome

Cutoff	Total sites found	Percent in genes	Percent intergenic
1.00	0	0%	0%
2.00	0	0%	0%
3.00	0	0%	0%
4.00	0	0%	0%
5.00	1	0%	100%
6.00	1	0%	100%
7.00	1	0%	100%
8.00	1	0%	100%
9.00	3	0%	100%
10.00	5	0%	100%
11.00	7	0%	100%
12.00	9	0%	100%
13.00	9	0%	100%

Novosphingobium aromaticivorans DSM 12444, complete genome

Cutoff	Total sites found	Percent in genes	Percent intergenic
1.00	0	0%	0%
2.00	0	0%	0%
3.00	0	0%	0%
4.00	0	0%	0%
5.00	1	0%	100%
6.00	1	0%	100%
7.00	1	0%	100%
8.00	1	0%	100%
9.00	1	0%	100%
10.00	1	0%	100%
11.00	1	0%	100%
12.00	2	50%	50%
13.00	3	67%	33%

Photobacterium profundum SS9 chromosome 1, complete sequence

Cutoff	Total sites found	Percent in genes	Percent intergenic
1.00	0	0%	0%
2.00	0	0%	0%
3.00	0	0%	0%
4.00	0	0%	0%
5.00	0	0%	0%
6.00	0	0%	0%
7.00	0	0%	0%
8.00	0	0%	0%
9.00	0	0%	0%
10.00	0	0%	0%
11.00	1	0%	100%
12.00	3	67%	33%
13.00	4	75%	25%

Photobacterium profundum SS9 chromosome 2, complete sequence

Cutoff	Total sites found	Percent in genes	Percent intergenic
1.00	0	0%	0%
2.00	0	0%	0%
3.00	0	0%	0%
4.00	0	0%	0%
5.00	0	0%	0%
6.00	0	0%	0%
7.00	1	0%	100%
8.00	1	0%	100%
9.00	1	0%	100%
10.00	1	0%	100%
11.00	2	0%	100%
12.00	3	0%	100%
13.00	9	33%	67%

Polaromonas sp. JS666, complete genome

Cutoff	Total sites found	Percent in genes	Percent intergenic
1.00	0	0%	0%
2.00	0	0%	0%
3.00	1	0%	100%
4.00	1	0%	100%
5.00	1	0%	100%
6.00	1	0%	100%
7.00	1	0%	100%
8.00	1	0%	100%
9.00	1	0%	100%
10.00	1	0%	100%
11.00	1	0%	100%
12.00	1	0%	100%
13.00	2	50%	50%

Pseudomonas aeruginosa PAO1, complete genome

Cutoff	Total sites found	Percent in genes	Percent intergenic
1.00	0	0%	0%
2.00	2	0%	100%
3.00	3	0%	100%
4.00	3	0%	100%
5.00	3	0%	100%
6.00	3	0%	100%
7.00	3	0%	100%
8.00	3	0%	100%
9.00	4	0%	100%
10.00	4	0%	100%
11.00	4	0%	100%
12.00	4	0%	100%
13.00	5	0%	100%

Pseudomonas entomophila L48, complete genome

Cutoff	Total sites found	Percent in genes	Percent intergenic
1.00	0	0%	0%
2.00	0	0%	0%
3.00	0	0%	0%
4.00	0	0%	0%
5.00	0	0%	0%
6.00	0	0%	0%
7.00	1	0%	100%
8.00	1	0%	100%
9.00	1	0%	100%
10.00	1	0%	100%
11.00	3	0%	100%
12.00	3	0%	100%
13.00	4	0%	100%

Pseudomonas fluorescens Pf-5, complete genome

Cutoff	Total sites found	Percent in genes	Percent intergenic
1.00	0	0%	0%
2.00	0	0%	0%
3.00	0	0%	0%
4.00	0	0%	0%
5.00	0	0%	0%
6.00	0	0%	0%
7.00	0	0%	0%
8.00	1	0%	100%
9.00	1	0%	100%
10.00	1	0%	100%
11.00	1	0%	100%
12.00	1	0%	100%
13.00	3	33%	67%

Pseudomonas fluorescens PfO-1, complete genome

Cutoff	Total sites found	Percent in genes	Percent intergenic
1.00	0	0%	0%
2.00	0	0%	0%
3.00	0	0%	0%
4.00	0	0%	0%
5.00	1	0%	100%
6.00	1	0%	100%
7.00	1	0%	100%
8.00	1	0%	100%
9.00	1	0%	100%
10.00	1	0%	100%
11.00	1	0%	100%
12.00	3	67%	33%
13.00	7	57%	43%

Pseudomonas putida KT2440, complete genome

Cutoff	Total sites found	Percent in genes	Percent intergenic
1.00	0	0%	0%
2.00	0	0%	0%
3.00	1	100%	0%
4.00	1	100%	0%
5.00	2	50%	50%
6.00	2	50%	50%
7.00	3	33%	67%
8.00	3	33%	67%
9.00	4	25%	75%
10.00	5	20%	80%
11.00	5	20%	80%
12.00	7	14%	86%
13.00	7	14%	86%

Ralstonia eutropha H16 chromosome 1, complete sequence

Cutoff	Total sites found	Percent in genes	Percent intergenic
1.00	0	0%	0%
2.00	0	0%	0%
3.00	0	0%	0%
4.00	0	0%	0%
5.00	0	0%	0%
6.00	0	0%	0%
7.00	0	0%	0%
8.00	0	0%	0%
9.00	1	0%	100%
10.00	1	0%	100%
11.00	1	0%	100%
12.00	1	0%	100%
13.00	1	0%	100%

Ralstonia eutropha H16 chromosome 2, complete sequence

Cutoff	Total sites found	Percent in genes	Percent intergenic
1.00	0	0%	0%
2.00	0	0%	0%
3.00	0	0%	0%
4.00	1	0%	100%
5.00	1	0%	100%
6.00	1	0%	100%
7.00	1	0%	100%
8.00	1	0%	100%
9.00	1	0%	100%
10.00	1	0%	100%
11.00	1	0%	100%
12.00	1	0%	100%
13.00	1	0%	100%

Ralstonia metallidurans CH34 chromosome 1, complete sequence

Cutoff	Total sites found	Percent in genes	Percent intergenic
1.00	0	0%	0%
2.00	0	0%	0%
3.00	0	0%	0%
4.00	0	0%	0%
5.00	0	0%	0%
6.00	0	0%	0%
7.00	0	0%	0%
8.00	0	0%	0%
9.00	0	0%	0%
10.00	0	0%	0%
11.00	0	0%	0%
12.00	0	0%	0%
13.00	0	0%	0%

Ralstonia metallidurans CH34 chromosome 2, complete sequence

Cutoff	Total sites found	Percent in genes	Percent intergenic
1.00	0	0%	0%
2.00	0	0%	0%
3.00	0	0%	0%
4.00	0	0%	0%
5.00	0	0%	0%
6.00	1	0%	100%
7.00	1	0%	100%
8.00	1	0%	100%
9.00	1	0%	100%
10.00	1	0%	100%
11.00	1	0%	100%
12.00	1	0%	100%
13.00	2	50%	50%

Rhizobium etli CFN 42, complete genome

Cutoff	Total sites found	Percent in genes	Percent intergenic
1.00	0	0%	0%
2.00	0	0%	0%
3.00	0	0%	0%
4.00	0	0%	0%
5.00	0	0%	0%
6.00	0	0%	0%
7.00	1	0%	100%
8.00	2	0%	100%
9.00	2	0%	100%
10.00	2	0%	100%
11.00	2	0%	100%
12.00	3	0%	100%
13.00	5	0%	100%

Rhizobium leguminosarum bv. viciae 3841, complete genome

Cutoff	Total sites found	Percent in genes	Percent intergenic
1.00	0	0%	0%
2.00	0	0%	0%
3.00	0	0%	0%
4.00	1	100%	0%
5.00	2	100%	0%
6.00	2	100%	0%
7.00	2	100%	0%
8.00	2	100%	0%
9.00	3	100%	0%
10.00	3	100%	0%
11.00	4	100%	0%
12.00	4	100%	0%
13.00	4	100%	0%

Rhodococcus sp. RHA1, complete genome

Cutoff	Total sites found	Percent in genes	Percent intergenic
1.00	0	0%	0%
2.00	0	0%	0%
3.00	0	0%	0%
4.00	0	0%	0%
5.00	0	0%	0%
6.00	0	0%	0%
7.00	0	0%	0%
8.00	0	0%	0%
9.00	2	50%	50%
10.00	4	25%	75%
11.00	4	25%	75%
12.00	4	25%	75%
13.00	6	17%	83%

Rhodopseudomonas palustris BisB5, complete genome

Cutoff	Total sites found	Percent in genes	Percent intergenic
1.00	0	0%	0%
2.00	0	0%	0%
3.00	0	0%	0%
4.00	0	0%	0%
5.00	0	0%	0%
6.00	1	0%	100%
7.00	1	0%	100%
8.00	1	0%	100%
9.00	1	0%	100%
10.00	1	0%	100%
11.00	1	0%	100%
12.00	1	0%	100%
13.00	1	0%	100%

Saccharopolyspora erythraea NRRL 2338, complete genome

Cutoff	Total sites found	Percent in genes	Percent intergenic
1.00	0	0%	0%
2.00	0	0%	0%
3.00	0	0%	0%
4.00	0	0%	0%
5.00	0	0%	0%
6.00	0	0%	0%
7.00	0	0%	0%
8.00	2	0%	100%
9.00	3	0%	100%
10.00	3	0%	100%
11.00	3	0%	100%
12.00	6	0%	100%
13.00	7	0%	100%

Salmonella enterica subsp. enterica serovar Typhi str. CT18, complete genome

Cutoff	Total sites found	Percent in genes	Percent intergenic
1.00	0	0%	0%
2.00	0	0%	0%
3.00	1	0%	100%
4.00	1	0%	100%
5.00	1	0%	100%
6.00	1	0%	100%
7.00	1	0%	100%
8.00	1	0%	100%
9.00	1	0%	100%
10.00	1	0%	100%
11.00	1	0%	100%
12.00	1	0%	100%
13.00	5	20%	80%

Salmonella typhimurium LT2, complete genome

Cutoff	Total sites found	Percent in genes	Percent intergenic
1.00	0	0%	0%
2.00	0	0%	0%
3.00	1	0%	100%
4.00	1	0%	100%
5.00	1	0%	100%
6.00	1	0%	100%
7.00	1	0%	100%
8.00	1	0%	100%
9.00	1	0%	100%
10.00	1	0%	100%
11.00	1	0%	100%
12.00	1	0%	100%
13.00	6	17%	83%

Shewanella frigidimarina NCIMB 400, complete genome

Cutoff	Total sites found	Percent in genes	Percent intergenic
1.00	0	0%	0%
2.00	0	0%	0%
3.00	1	0%	100%
4.00	1	0%	100%
5.00	1	0%	100%
6.00	1	0%	100%
7.00	1	0%	100%
8.00	1	0%	100%
9.00	1	0%	100%
10.00	2	50%	50%
11.00	4	50%	50%
12.00	6	50%	50%
13.00	25	68%	32%

Shewanella denitrificans OS217, complete genome

Cutoff	Total sites found	Percent in genes	Percent intergenic
1.00	0	0%	0%
2.00	1	0%	100%
3.00	2	0%	100%
4.00	2	0%	100%
5.00	2	0%	100%
6.00	2	0%	100%
7.00	2	0%	100%
8.00	2	0%	100%
9.00	2	0%	100%
10.00	5	40%	60%
11.00	8	38%	63%
12.00	11	45%	55%
13.00	23	65%	35%

Shigella flexneri 2a str. 2457T, complete genome

Cutoff	Total sites found	Percent in genes	Percent intergenic
1.00	0	0%	0%
2.00	0	0%	0%
3.00	1	0%	100%
4.00	1	0%	100%
5.00	1	0%	100%
6.00	1	0%	100%
7.00	1	0%	100%
8.00	1	0%	100%
9.00	1	0%	100%
10.00	2	50%	50%
11.00	2	50%	50%
12.00	2	50%	50%
13.00	4	50%	50%

Shigella flexneri 2a str. 301, complete genome

Cutoff	Total sites found	Percent in genes	Percent intergenic
1.00	0	0%	0%
2.00	0	0%	0%
3.00	1	0%	100%
4.00	1	0%	100%
5.00	1	0%	100%
6.00	1	0%	100%
7.00	1	0%	100%
8.00	1	0%	100%
9.00	1	0%	100%
10.00	2	50%	50%
11.00	2	50%	50%
12.00	2	50%	50%
13.00	4	50%	50%

Shigella flexneri 5 str. 8401, complete genome

Cutoff	Total sites found	Percent in genes	Percent intergenic
1.00	0	0%	0%
2.00	0	0%	0%
3.00	1	0%	100%
4.00	1	0%	100%
5.00	1	0%	100%
6.00	1	0%	100%
7.00	1	0%	100%
8.00	1	0%	100%
9.00	1	0%	100%
10.00	2	50%	50%
11.00	2	50%	50%
12.00	2	50%	50%
13.00	4	50%	50%

Shigella sonnei Ss046, complete genome

Cutoff	Total sites found	Percent in genes	Percent intergenic
1.00	0	0%	0%
2.00	0	0%	0%
3.00	1	0%	100%
4.00	1	0%	100%
5.00	1	0%	100%
6.00	1	0%	100%
7.00	1	0%	100%
8.00	1	0%	100%
9.00	1	0%	100%
10.00	1	0%	100%
11.00	2	50%	50%
12.00	2	50%	50%
13.00	4	50%	50%

Silicibacter pomeroyi DSS-3, complete genome

Cutoff	Total sites found	Percent in genes	Percent intergenic
1.00	0	0%	0%
2.00	0	0%	0%
3.00	0	0%	0%
4.00	0	0%	0%
5.00	0	0%	0%
6.00	1	0%	100%
7.00	1	0%	100%
8.00	1	0%	100%
9.00	2	0%	100%
10.00	2	0%	100%
11.00	2	0%	100%
12.00	3	0%	100%
13.00	3	0%	100%

Sinorhizobium meliloti 1021, complete genome

Cutoff	Total sites found	Percent in genes	Percent intergenic
1.00	0	0%	0%
2.00	0	0%	0%
3.00	0	0%	0%
4.00	0	0%	0%
5.00	0	0%	0%
6.00	0	0%	0%
7.00	1	0%	100%
8.00	1	0%	100%
9.00	2	0%	100%
10.00	2	0%	100%
11.00	2	0%	100%
12.00	2	0%	100%
13.00	3	0%	100%

Sphingopyxis alaskensis RB2256, complete genome

Cutoff	Total sites found	Percent in genes	Percent intergenic
1.00	0	0%	0%
2.00	0	0%	0%
3.00	0	0%	0%
4.00	0	0%	0%
5.00	0	0%	0%
6.00	0	0%	0%
7.00	0	0%	0%
8.00	1	0%	100%
9.00	1	0%	100%
10.00	1	0%	100%
11.00	1	0%	100%
12.00	1	0%	100%
13.00	2	0%	100%

Streptomyces avermitilis MA-4680, complete genome

Cutoff	Total sites found	Percent in genes	Percent intergenic
1.00	0	0%	0%
2.00	0	0%	0%
3.00	0	0%	0%
4.00	0	0%	0%
5.00	0	0%	0%
6.00	2	0%	100%
7.00	4	0%	100%
8.00	5	0%	100%
9.00	5	0%	100%
10.00	5	0%	100%
11.00	6	0%	100%
12.00	6	0%	100%
13.00	8	0%	100%

Streptomyces coelicolor A3(2), complete genome

Cutoff	Total sites found	Percent in genes	Percent intergenic
1.00	0	0%	0%
2.00	0	0%	0%
3.00	0	0%	0%
4.00	0	0%	0%
5.00	0	0%	0%
6.00	1	0%	100%
7.00	1	0%	100%
8.00	1	0%	100%
9.00	3	0%	100%
10.00	3	0%	100%
11.00	5	20%	80%
12.00	6	17%	83%
13.00	7	14%	86%

Thermobifida fusca YX, complete genome

Cutoff	Total sites found	Percent in genes	Percent intergenic
1.00	0	0%	0%
2.00	0	0%	0%
3.00	0	0%	0%
4.00	1	0%	100%
5.00	1	0%	100%
6.00	1	0%	100%
7.00	2	0%	100%
8.00	2	0%	100%
9.00	3	0%	100%
10.00	3	0%	100%
11.00	3	0%	100%
12.00	3	0%	100%
13.00	5	0%	100%

Thermococcus kodakarensis KOD1, complete genome

Cutoff	Total sites found	Percent in genes	Percent intergenic
1.00	0	0%	0%
2.00	0	0%	0%
3.00	0	0%	0%
4.00	0	0%	0%
5.00	0	0%	0%
6.00	0	0%	0%
7.00	0	0%	0%
8.00	0	0%	0%
9.00	0	0%	0%
10.00	0	0%	0%
11.00	0	0%	0%
12.00	0	0%	0%
13.00	3	100%	0%

Vibrio cholerae O1 biovar eltor str. N16961 chromosome I, complete sequence

Cutoff	Total sites found	Percent in genes	Percent intergenic
1.00	0	0%	0%
2.00	0	0%	0%
3.00	0	0%	0%
4.00	0	0%	0%
5.00	0	0%	0%
6.00	0	0%	0%
7.00	0	0%	0%
8.00	0	0%	0%
9.00	0	0%	0%
10.00	1	100%	0%
11.00	1	100%	0%
12.00	2	100%	0%
13.00	3	67%	33%

Vibrio cholerae O1 biovar eltor str. N16961 chromosome II, complete sequence

Cutoff	Total sites found	Percent in genes	Percent intergenic
1.00	0	0%	0%
2.00	0	0%	0%
3.00	1	0%	100%
4.00	1	0%	100%
5.00	1	0%	100%
6.00	1	0%	100%
7.00	1	0%	100%
8.00	1	0%	100%
9.00	1	0%	100%
10.00	1	0%	100%
11.00	1	0%	100%
12.00	2	0%	100%
13.00	6	67%	33%

Vibrio parahaemolyticus RIMD 2210633 chromosome II, complete sequence

Cutoff	Total sites found	Percent in genes	Percent intergenic
1.00	0	0%	0%
2.00	0	0%	0%
3.00	0	0%	0%
4.00	0	0%	0%
5.00	1	0%	100%
6.00	4	0%	100%
7.00	4	0%	100%
8.00	5	0%	100%
9.00	5	0%	100%
10.00	5	0%	100%
11.00	5	0%	100%
12.00	7	14%	86%
13.00	15	13%	87%

Vibrio vulnificus CMCP6 chromosome I, complete sequence

Cutoff	Total sites found	Percent in genes	Percent intergenic
1.00	0	0%	0%
2.00	0	0%	0%
3.00	0	0%	0%
4.00	0	0%	0%
5.00	0	0%	0%
6.00	0	0%	0%
7.00	0	0%	0%
8.00	0	0%	0%
9.00	0	0%	0%
10.00	0	0%	0%
11.00	1	0%	100%
12.00	3	33%	67%
13.00	6	50%	50%

Vibrio vulnificus CMCP6 chromosome II, complete sequence

Cutoff	Total sites found	Percent in genes	Percent intergenic
1.00	0	0%	0%
2.00	1	0%	100%
3.00	2	0%	100%
4.00	3	0%	100%
5.00	3	0%	100%
6.00	3	0%	100%
7.00	3	0%	100%
8.00	3	0%	100%
9.00	3	0%	100%
10.00	3	0%	100%
11.00	3	0%	100%
12.00	3	0%	100%
13.00	4	25%	75%

Vibrio vulnificus YJ016 chromosome I, complete sequence

Cutoff	Total sites found	Percent in genes	Percent intergenic
1.00	0	0%	0%
2.00	0	0%	0%
3.00	0	0%	0%
4.00	0	0%	0%
5.00	0	0%	0%
6.00	0	0%	0%
7.00	0	0%	0%
8.00	0	0%	0%
9.00	0	0%	0%
10.00	0	0%	0%
11.00	0	0%	0%
12.00	2	50%	50%
13.00	4	75%	25%

Vibrio vulnificus YJ016 chromosome II, complete sequence

Cutoff	Total sites found	Percent in genes	Percent intergenic
1.00	0	0%	0%
2.00	1	0%	100%
3.00	2	0%	100%
4.00	3	0%	100%
5.00	3	0%	100%
6.00	3	0%	100%
7.00	3	0%	100%
8.00	3	0%	100%
9.00	3	0%	100%
10.00	3	0%	100%
11.00	3	0%	100%
12.00	3	0%	100%
13.00	4	25%	75%

Xanthomonas campestris pv. *campestris* str. 8004, complete genome

Cutoff	Total sites found	Percent in genes	Percent intergenic
1.00	0	0%	0%
2.00	0	0%	0%
3.00	0	0%	0%
4.00	0	0%	0%
5.00	0	0%	0%
6.00	0	0%	0%
7.00	0	0%	0%
8.00	0	0%	0%
9.00	1	0%	100%
10.00	1	0%	100%
11.00	2	0%	100%
12.00	2	0%	100%
13.00	3	0%	100%

Xanthomonas campestris pv. *campestris* str. ATCC 33913, complete genome

Cutoff	Total sites found	Percent in genes	Percent intergenic
1.00	0	0%	0%
2.00	0	0%	0%
3.00	0	0%	0%
4.00	0	0%	0%
5.00	0	0%	0%
6.00	0	0%	0%
7.00	0	0%	0%
8.00	0	0%	0%
9.00	1	0%	100%
10.00	1	0%	100%
11.00	2	0%	100%
12.00	2	0%	100%
13.00	3	0%	100%

Xanthomonas campestris pv. vesicatoria str. 85-10, complete genome

Cutoff	Total sites found	Percent in genes	Percent intergenic
1.00	0	0%	0%
2.00	0	0%	0%
3.00	0	0%	0%
4.00	0	0%	0%
5.00	0	0%	0%
6.00	1	0%	100%
7.00	1	0%	100%
8.00	1	0%	100%
9.00	1	0%	100%
10.00	1	0%	100%
11.00	2	50%	50%
12.00	3	67%	33%
13.00	5	40%	60%

Xanthomonas axonopodis pv. citri str. 306, complete genome

Cutoff	Total sites found	Percent in genes	Percent intergenic
1.00	0	0%	0%
2.00	0	0%	0%
3.00	0	0%	0%
4.00	0	0%	0%
5.00	0	0%	0%
6.00	1	0%	100%
7.00	1	0%	100%
8.00	1	0%	100%
9.00	2	0%	100%
10.00	2	0%	100%
11.00	2	0%	100%
12.00	2	0%	100%
13.00	2	0%	100%

Xanthomonas oryzae pv. oryzae MAFF 311018, complete genome

Cutoff	Total sites found	Percent in genes	Percent intergenic
1.00	0	0%	0%
2.00	0	0%	0%
3.00	0	0%	0%
4.00	0	0%	0%
5.00	0	0%	0%
6.00	0	0%	0%
7.00	0	0%	0%
8.00	0	0%	0%
9.00	0	0%	0%
10.00	1	0%	100%
11.00	1	0%	100%
12.00	2	0%	100%
13.00	2	0%	100%

B.2 Pyscangenes table

Table B.2: The soxbox sites found in genomes containing SoxR. Column 1 is the site energy of the site. Column 2 is the sequence of the site. Column 3 is the operon position, whether the named operon is to the left or the right of the soxbox site. Column 4 is the distance from the soxbox site to the start of the operon. Column 5 are the genes contained in the adjacent operon.

Acidovorax avenae subsp. citrulli AAC00-1, complete genome

Site Energy	Sequence	Operon pos	Distance to start	Genes in operon
4.90	TTGACCTCAAGTTAGTTGAGGTTCC	left	-62	Aave_2275
		right	-90	Aave_2276
8.12	TTGACCTCAACAATGGTTGAGGTTTG	left	-214	Aave_1362
9.29	TTGACTTCAAGTGGACTTGAAGTCGT	left	-71	Aave_2578
		right	-62	Aave_2579

Acidobacteria bacterium Ellin345, complete genome

Site Energy	Sequence	Operon pos	Distance to start	Genes in operon
1.61	TTGACCTCAAGTTACTTGAGGTTTT	left	-14	Acid345_3972
		right	-97	Acid345_3973-Acid345_3974

Acidovorax avenae subsp. citrulli AAC00-1, complete genome

Site Energy	Sequence	Operon pos	Distance to start	Genes in operon
4.90	TTGACCTCAAGTTAGTTGAGGTTCC	left	-62	Aave_2275
		right	-90	Aave_2276
8.12	TTGACCTCAACAATGGTTGAGGTTTG	left	-214	Aave_1362
9.29	TTGACTTCAAGTGGACTTGAAGTCGT	left	-71	Aave_2578
		right	-62	Aave_2579

Acinetobacter sp. ADP1, complete genome

Site Energy	Sequence	Operon pos	Distance to start	Genes in operon
1.54	TTGACCTCAAGTTAACTTGAGCTTG	left	-4	soxR (ACIAD3082)
		right	-42	ACIAD3083-ACIAD3084

Aeromonas hydrophila subsp. hydrophila ATCC 7966, complete genome

Site Energy	Sequence	Operon pos	Distance to start	Genes in operon
4.88	TTGACCTCAAGTTAGCTTAACTTGC	left	-8	soxR (AHA_2710)
		right	-90	AHA_2711

Agrobacterium tumefaciens str. C58 chromosome circular, complete sequence

Site Energy	Sequence	Operon pos	Distance to start	Genes in operon
6.29	TTGACCTCAACTATGGTTGAGGAATT	left	-33	Atu2361

Agrobacterium tumefaciens str. C58 chromosome linear, complete sequence

Site Energy	Sequence	Operon pos	Distance to start	Genes in operon
5.95	TTGACCTCAACTATAGTTGAGGAATT	left	-68	soxR (Atu3915)
6.67	TCGACCTCAACTCAAGTTGAGGTTGT	left	-108	Atu4895

Agrobacterium tumefaciens str. C58 chromosome linear, complete sequence

Site Energy	Sequence	Operon pos	Distance to start	Genes in operon
5.95	TTGACCTCAACTATAGTTGAGGAATT	left	-68	soxR (Atu3915)
6.67	TCGACCTCAACTCAAGTTGAGGTTGT	left	-108	Atu4895

Arthrobacter aurescens TC1, complete genome

Site Energy	Sequence	Operon pos	Distance to start	Genes in operon
5.78	TTGACCTCAACTTAAGTTGAGGTCCT	left right	-64 -160	AAur_0213 ureA (AAur_0214)- ureB (AAur_0215)- ureC (AAur_0216)- ureE (AAur_0217)

Bdellovibrio bacteriovorus HD100, complete genome

Site Energy	Sequence	Operon pos	Distance to start	Genes in operon
1.10	TTGACCTCAAGTTAACTTGAGGTTGT	left right	-7 -113	soxR (Bd1002) Bd1003
8.34	TTTACATCAACTTAACTCGAGTTTC	left right	-67 -98	Bd1662 Bd1663

Bordetella bronchiseptica RB50, complete genome

Site Energy	Sequence	Operon pos	Distance to start	Genes in operon
6.63	TTGACCTCAAGCTAGCTTGAGGGTCC	left	-90	BB4154

Bordetella parapertussis 12822, complete genome

Site Energy	Sequence	Operon pos	Distance to start	Genes in operon
8.93	TTGACCTCAAGCTCGTTGAGGGTCC	left	-89	BPP3708

Bordetella pertussis Tohama I, complete genome

Site Energy	Sequence	Operon pos	Distance to start	Genes in operon
6.63	TTGACCTCAAGCTAGCTTGAGGGTCC	left	-141	BP2837

Burkholderia sp. 383 chromosome 3, complete sequence

Site Energy	Sequence	Operon pos	Distance to start	Genes in operon
-------------	----------	------------	-------------------	-----------------

Burkholderia sp. 383 chromosome 1, complete sequence

Site Energy	Sequence	Operon pos	Distance to start	Genes in operon
-------------	----------	------------	-------------------	-----------------

Burkholderia sp. 383 chromosome 2, complete sequence

Site Energy	Sequence	Operon pos	Distance to start	Genes in operon
3.99	TTGACCTCAAGTGAAC TTGAAGTTGC	left	-2	Bcep18194_B1905
		right	-164	Bcep18194_B1906
7.14	TTGACTTGAAGTTAAC TTCAACTTTT	left	-19	Bcep18194_B1003
		right	-87	Bcep18194_B1004- Bcep18194_B1005- Bcep18194_B1006
9.80	TTGACCTCAAGCCGGCTTGAAGCAGC	left	-42	Bcep18194_B1876
		right	-185	Bcep18194_B1877- Bcep18194_B1878

Burkholderia cenocepacia AU 1054 chromosome 1, complete sequence

Site Energy	Sequence	Operon pos	Distance to start	Genes in operon
-------------	----------	------------	-------------------	-----------------

Burkholderia cenocepacia AU 1054 chromosome 2, complete sequence

Site Energy	Sequence	Operon pos	Distance to start	Genes in operon
3.99	TTGACCTCAAGTGAAC TTGAAGTTGC	left	-2	Bcen_4236
		right	-164	Bcen_4237
7.14	TTGACTTGAAGTTAAC TTCAACTTTT	left	-18	Bcen_3620
		right	-87	Bcen_3621

Burkholderia cenocepacia AU 1054 chromosome 3, complete sequence

Site Energy	Sequence	Operon pos	Distance to start	Genes in operon
-------------	----------	------------	-------------------	-----------------

Burkholderia cenocepacia HI2424 chromosome 1, complete sequence

Site Energy	Sequence	Operon pos	Distance to start	Genes in operon
-------------	----------	------------	-------------------	-----------------

Burkholderia cenocepacia HI2424 chromosome 2, complete sequence

Site Energy	Sequence	Operon pos	Distance to start	Genes in operon
3.99	TTGACCTCAAGTGAACTTGAAGTTGC	left	-112	Bcen2424_4129
		right	-54	Bcen2424_4130
7.14	TTGACTTGAAGTTAACTTCAACTTTT	left	-35	Bcen2424_4746-
		right	-70	Bcen2424_4747

Burkholderia cenocepacia HI2424 chromosome 3, complete sequence

Site Energy	Sequence	Operon pos	Distance to start	Genes in operon
-------------	----------	------------	-------------------	-----------------

Burkholderia cenocepacia HI2424 plasmid 1, complete sequence

Site Energy	Sequence	Operon pos	Distance to start	Genes in operon
-------------	----------	------------	-------------------	-----------------

Chromobacterium violaceum ATCC 12472, complete genome

Site Energy	Sequence	Operon pos	Distance to start	Genes in operon
4.25	TTGACTTCAAGTTAACTTGAACCTTG	left	-7	soxR (CV2793)
		right	-87	CV2794- CV2795
5.06	TTGACTTCAAGTTAACTTAACTTTC	left	-87	ebrB (CV3243)

Erythrobacter litoralis HTCC2594, complete genome

Site Energy	Sequence	Operon pos	Distance to start	Genes in operon
3.23	TTGACCTCAAGTCAGCTTGAGGTTGC	left	-27	ELI_02950
		right	-142	ELI_02955

Escherichia coli CFT073, complete genome

Site Energy	Sequence	Operon pos	Distance to start	Genes in operon
2.14	TTTACCTCAAGTTAACTTGAGGAATT	left	-52	soxS (c5053)
		right	-59	soxR (c5054)

Escherichia coli K12, complete genome

Site Energy	Sequence	Operon pos	Distance to start	Genes in operon
2.14	TTTACCTCAAGTTAACTTGAGGAATT	left	-52	soxS (b4062)
		right	-59	soxR (b4063)

Frankia alni ACN14a, complete genome

Site Energy	Sequence	Operon pos	Distance to start	Genes in operon
-------------	----------	------------	-------------------	-----------------

Frankia sp. CcI3, complete genome

Site Energy	Sequence	Operon pos	Distance to start	Genes in operon
9.44	TTGACTTCAATCATGGTTGAGGTTTT	left	-113	Francci3_1887

Hahella chejuensis KCTC 2396, complete genome

Site Energy	Sequence	Operon pos	Distance to start	Genes in operon
1.67	TTGACCTAAAGTTAACGTTGAGGTTTT	left	-10	soxR (HCH_01441)
		right	-96	HCH_01442
5.63	TTGACCTCAAGTCGACTTGAGCTTGT	left	-6	HCH_01327
		right	-140	HCH_01328
9.44	TTGACCTAAAGCTGACTTTAACATTGC	left	-7	HCH_01117
		right	-98	HCH_01118

Hyphomonas neptunium ATCC 15444, complete genome

Site Energy	Sequence	Operon pos	Distance to start	Genes in operon
5.92	TTGATCTAAAGTGAACCTTGAGATTGT	left	-43	HNE_3425
		right	-64	soxR (HNE_3426)

Maricaulis maris MCS10, complete genome

Site Energy	Sequence	Operon pos	Distance to start	Genes in operon
9.33	TTGACCTCAACCAAGGTTAACGAAATT	left	-3	Mmar10_0144
		right	-103	Mmar10_0145

Mesorhizobium loti MAFF303099, complete genome

Site Energy	Sequence	Operon pos	Distance to start	Genes in operon
3.74	TTGACCTCAACTTAAGTTGAGATTGT	left	-104	mlr7819
4.58	TTGACCTCAAGTTATGTTGAGCTTGT	left	-66	mlr2720
8.86	TTGACCTCAAGTCGGCTTGAACTCGT	left	-9	mll5378
		right	-100	mlr5379

Mycobacterium vanbaalenii PYR-1, complete genome

Site Energy	Sequence	Operon pos	Distance to start	Genes in operon
9.98	TTGACCTGAACAATAGTTGAGGTTGC	left	-125	Mvan_5552
		right	-64	Mvan_5553

Mycobacterium sp. JLS, complete genome

Site Energy	Sequence	Operon pos	Distance to start	Genes in operon
6.91	TTGACCTGAACCTTGAGGTCTT	left	-13	Mjls_1491
		right	-108	Mjls_1492
8.71	TTGACCTGAACCTTGAGGTCTGG	left	-32	Mjls_2737
		right	-64	Mjls_2738
9.40	TTGACCTGAAGTTCTGTTGAGGTACG	left	-15	Mjls_1552
		right	-63	Mjls_1553
9.94	TTGACCTCACCTTGTGAGGTTCT	left	-11	Mjls_4828
		right	-89	Mjls_4829

Mycobacterium sp. KMS, complete genome

Site Energy	Sequence	Operon pos	Distance to start	Genes in operon
6.91	TTGACCTGAACCTTGAGGTCTT	left	-13	Mkms_1515
		right	-180	Mkms_1516
8.71	TTGACCTGAACCTTGAGGTCTGG	left	-32	Mkms_2751
		right	-64	Mkms_2752
9.40	TTGACCTGAAGTTCTGTTGAGGTACG	left	-15	Mkms_1606
		right	-63	Mkms_1607
9.94	TTGACCTCACCTTGTGAGGTTCT	left	-11	Mkms_4533
		right	-90	Mkms_4534

Mycobacterium sp. MCS, complete genome

Site Energy	Sequence	Operon pos	Distance to start	Genes in operon
6.91	TTGACCTGAACCTTGAGGTCTT	left	-13	Mmcs_1493
		right	-180	Mmcs_1494
8.71	TTGACCTGAACCTTGAGGTCTGG	left	-32	Mmcs_2707
		right	-64	Mmcs_2708
9.40	TTGACCTGAAGTTCTGTTGAGGTACG	left	-15	Mmcs_1582
		right	-102	Mmcs_1583
9.94	TTGACCTCACCTTGTGAGGTTCT	left	-11	Mmcs_4446
		right	-90	Mmcs_4447

Mycobacterium smegmatis str. MC2 155, complete genome

Site Energy	Sequence	Operon pos	Distance to start	Genes in operon
7.79	TTCACCTGAAGTAAGGTTAGGTGTC	left	-20	arcA (MSMEG_5448)
		right	-58	soxR (MSMEG_5450)
8.44	TTGACCTCATCATTGGTTGAGGTTT	left right	-11 -130	MSMEG_5661 prA (MSMEG_5662)- MSMEG_5663
8.71	TTGACCTAACCTCACTTGAGGTGCC	left	-171	MSMEG_0572-
				MSMEG_0571- MSMEG_0570- MSMEG_0569- MSMEG_0568- MSMEG_0567- MSMEG_0566- MSMEG_0565- MSMEG_0564 MSMEG_0574
9.34	TTGACCTAACTTCGTTGAGGTCTT	left	-63	MSMEG_5819- MSMEG_5820

Nocardia farcinica IFM 10152, complete genome

Site Energy	Sequence	Operon pos	Distance to start	Genes in operon
4.94	TTGACTTCAAGTGAAC TTGAAATTT	left	-66	nfa33330
		right	-76	nfa33340
8.71	TTGACCTAACATTGGTTGAGGAAGC	left	-54	nfa29630- nfa29620
9.04	TTGACCTCGAGCGAGGTCGAGGTTGT	left	-117	nfa21820
		right	-58	nfa21830
9.31	TTGCCCTGAACTTGGTTGAGGTCTT	left right	-29 -100	nfa56070 nfa56080

Novosphingobium aromaticivorans DSM 12444, complete genome

Site Energy	Sequence	Operon pos	Distance to start	Genes in operon
4.72	TTGATCTCAAGCTAAC TTGAGGTTGC	left	-49	Saro_0953-
		right	-128	Saro_0952 Saro_0954

Photobacterium profundum SS9 chromosome 1, complete sequence

Site Energy	Sequence	Operon pos	Distance to start	Genes in operon

Photobacterium profundum SS9 chromosome 2, complete sequence

Site Energy	Sequence	Operon pos	Distance to start	Genes in operon
6.16	TTGACCTCAAGTTAACCTGAGGCACT	left right	-23 -91	PBPRB1505 PBPRB1506

Polaromonas sp. JS666, complete genome

Site Energy	Sequence	Operon pos	Distance to start	Genes in operon
2.71	TTGACCTCAACTTACTTGAGGTTT	left right	-10 -112	Bpro_1373 Bpro_1374

Pseudomonas aeruginosa PAO1, complete genome

Site Energy	Sequence	Operon pos	Distance to start	Genes in operon
1.10	TTGACCTCAACTTAACTTGAGGTTT	left	-154	mexG (PA4205)-mexH (PA4206)-mexI (PA4207)-opmD (PA4208)
1.95	TTGACCTCAAGTTTGCTTGAGGTTT	left right	-7 -96	PA2273 PA2274
2.42	TTTACCTCAAGTTAACTTGAGCTATC	left	-60	PA3718
8.78	TTGACCTCAAGTCGACTTGAAGTGGA	left right	-53 -56	PA5115 PA5116

Pseudomonas entomophila L48, complete genome

Site Energy	Sequence	Operon pos	Distance to start	Genes in operon
6.68	TTGACCTTGAGTTAACCTGGAGGTTT	left right	-48 -63	PSEEN3529 soxR (PSEEN3530)

Pseudomonas fluorescens Pf-5, complete genome

Site Energy	Sequence	Operon pos	Distance to start	Genes in operon
7.78	TTGACCTTGACTTAACTAGAGGTTT	left right	-55 -79	PFL_4159 soxR (PFL_4160)

Pseudomonas fluorescens PfO-1, complete genome

Site Energy	Sequence	Operon pos	Distance to start	Genes in operon
4.89	TTTACCTCTAGTTAACTCGAGGTTT	left right	-50 -66	Pfl_3919 Pfl_3920

Pseudomonas putida KT2440, complete genome

Site Energy	Sequence	Operon pos	Distance to start	Genes in operon
4.92	TCGACCTAAAGTTAACGGAGCTTT	left	-6	soxR (PP_2060)
6.80	TTGACCTCGAGTTAACGTCAAGGTTT	left	-288	PP_2505
		right	-55	PP_2506
8.88	TTGACCTTGACTTACTTGAGGTCTT	left	-100	PP_2235
9.18	TTGACCTCGAGTTAACTAAGGTCCG	left	-37	PP_3522
		right	-147	PP_3523

Ralstonia eutropha H16 chromosome 1, complete sequence

Site Energy	Sequence	Operon pos	Distance to start	Genes in operon
8.24	TTGACCTCAAGTCGACTTGAACTGGC	left	-45	h16_A0054 (H16_A0054)-
		right	-55	h16_A0053 (H16_A0053) h16_A0055 (H16_A0055)

Ralstonia eutropha H16 chromosome 2, complete sequence

Site Energy	Sequence	Operon pos	Distance to start	Genes in operon
3.92	TTGACCTCAATTAGGTTGAGGTTG	left	-50	h16_B2318 (H16_B2318)
		right	-71	h16_B2319 (H16_B2319)

Ralstonia metallidurans CH34 chromosome 1, complete sequence

Site Energy	Sequence	Operon pos	Distance to start	Genes in operon
-------------	----------	------------	-------------------	-----------------

Ralstonia metallidurans CH34 chromosome 2, complete sequence

Site Energy	Sequence	Operon pos	Distance to start	Genes in operon
5.63	TTGACCTCAAGCGTGCTTGAGGTTG	left	-63	Rmet_4538
		right	-85	Rmet_4539

Rhizobium etli CFN 42, complete genome

Site Energy	Sequence	Operon pos	Distance to start	Genes in operon
6.80	TTGACCTCAATATTAGTTGAGGTTT	left	-6	soxR (RHE_CH03863)
		right	-606	RHE_CH03864- RHE_CH03865
7.56	TTGACCTCAACCATAAGTTGAGGAATT	left	-399	RHE_CH02960
		right	-89	RHE_CH02961

Rhizobium leguminosarum bv. viciae 3841, complete genome

Site Energy	Sequence	Operon pos	Distance to start	Genes in operon
3.56	TTGACCTCAGGTTAACTTGAGGAATT	left	-92	RL3412
4.60	TTGACCTCAAGATTAGTTGAGGTTT	left	-6	RL4397
		right	-103	RL4398
8.62	TTGACCTCAAGTGGGTTGGGGTTGC	left	-24	arcB (RL3003)

Rhodococcus sp. RHA1, complete genome

Site Energy	Sequence	Operon pos	Distance to start	Genes in operon
8.52	TTGACCTCGAGTAACGTTGAGGTTCT	left	-57	RHA1_ro06043
9.39	TTGACATGAAGTGGACTCGAGGTTTC	left	-3	RHA1_ro00215-
		right	-171	RHA1_ro00214 RHA1_ro00216
9.98	TTGACCTGAACGCAACTCGACGTTT	left	-11	RHA1_ro04736

Rhodopseudomonas palustris BisB5, complete genome

Site Energy	Sequence	Operon pos	Distance to start	Genes in operon
5.71	TTGACCTCAACTAAGGTTGAGGTTCT	left	-73	RPD_3140-
		right	-58	RPD_3139 RPD_3141

Saccharopolyspora erythraea NRRL 2338, complete genome

Site Energy	Sequence	Operon pos	Distance to start	Genes in operon
7.72	TTGACCTCCAGCCAACTCGAAGTTTC	left	-11	SACE_5763-
		right	-98	SACE_5762 soxR (SACE_5764)
7.80	TTGACCTCGACCTTGCTTGAGCTTT	left	-44	SACE_4991
		right	-95	SACE_4992
8.19	TTGACCTGGAGTCAACTCGAAGTTTC	left	-206	SACE_1156
		right	-146	SACE_1157

Salmonella enterica subsp. enterica serovar Typhi str. CT18, complete genome

Site Energy	Sequence	Operon pos	Distance to start	Genes in operon
2.14	TTTACCTCAAGTTAACTTGAGGAATT	left	-53	soxS (STY4463)
		right	-59	soxR (STY4464)

Salmonella typhimurium LT2, complete genome

Site Energy	Sequence	Operon pos	Distance to start	Genes in operon
2.14	TTTACCTCAAGTTAACTTGAGGAATT	left right	-53 -59	soxS (STM4265) soxR (STM4266)

Shewanella frigidimarina NCIMB 400, complete genome

Site Energy	Sequence	Operon pos	Distance to start	Genes in operon
2.60	TTTACCTCAAGTTAGCTTAGGTATT	left right	-41 -86	Sfri_1565 Sfri_1566

Shewanella denitrificans OS217, complete genome

Site Energy	Sequence	Operon pos	Distance to start	Genes in operon
1.18	TTGACCTCAAGTTAGCTTGAGCTTT	left right	-38 -271	Sden_0647 Sden_0648
2.59	TTTACCTCAAGCTAACTTGAGGTTTT	left right	-33 -145	Sden_2124 Sden_2125
9.31	TGAACCTCAACTTAACCTTAGCTTTA	left	-89	Sden_0935

Shigella dysenteriae Sd197, complete genome

Site Energy	Sequence	Operon pos	Distance to start	Genes in operon
2.14	TTTACCTCAAGTTAACTTGAGGAATT	left right	-7 -104	soxR (SDY_4504) soxS (SDY_4505)

Shigella flexneri 2a str. 2457T, complete genome

Site Energy	Sequence	Operon pos	Distance to start	Genes in operon
2.14	TTTACCTCAAGTTAACTTGAGGAATT	left right	-52 -59	soxS (S3589) soxR (S3590)

Shigella flexneri 2a str. 301, complete genome

Site Energy	Sequence	Operon pos	Distance to start	Genes in operon
2.14	TTTACCTCAAGTTAACTTGAGGAATT	left right	-52 -59	soxS (SF4122) soxR (SF4123)

Shigella flexneri 5 str. 8401, complete genome

Site Energy	Sequence	Operon pos	Distance to start	Genes in operon
2.14	TTTACCTCAAGTTAACTTGAGGAATT	left	-7	soxR (SFV_4149)
		right	-104	soxS (SFV_4150)

Shigella sonnei Ss046, complete genome

Site Energy	Sequence	Operon pos	Distance to start	Genes in operon
2.14	TTTACCTCAAGTTAACTTGAGGAATT	left	-52	soxS (SSON_4242)
		right	-349	SSON_4243

Silicibacter sp. TM1040, complete genome

Site Energy	Sequence	Operon pos	Distance to start	Genes in operon
5.48	TTGATCTAAAGTGAGCTTGAGGAATT	left	-96	TM1040_1862-
		right	-122	TM1040_1861- TM1040_1860- TM1040_1859 TM1040_1863
8.24	TTGACCTCAAGTTGACTTGAATTTCGT	left	-2	TM1040_2614
		right	-91	TM1040_2615

Silicibacter pomeroyi DSS-3, complete genome

Site Energy	Sequence	Operon pos	Distance to start	Genes in operon
5.12	TTGACCTAAAGTTAGGTTAGAAATT	left	-38	SPO0313
		right	-72	soxR (SPO0314)
8.64	TTGACCTCAAGTTGACTTGAATTCCGC	left	-2	SPO3734
		right	-91	SPO3735

Sinorhizobium meliloti 1021, complete genome

Site Energy	Sequence	Operon pos	Distance to start	Genes in operon
6.98	TTGACCTCAACTATAAGTTGAGGTTCT	left	-44	SMc00183
		right	-60	SMc00182
8.01	TTGACCTCAAGTACGGTTGAGGTCGC	left	-88	SMc03095

Sphingopyxis alaskensis RB2256, complete genome

Site Energy	Sequence	Operon pos	Distance to start	Genes in operon
7.65	TTGACCTCCACTGCACTTGAGCTTC	left	-37	Sala_2373

Streptomyces avermitilis MA-4680, complete genome

Site Energy	Sequence	Operon pos	Distance to start	Genes in operon
5.53	TTGACCTGAAGTTGGTTGAGGTTGC	left	-637	gbsA1 (SAV1622)
		right	-64	SAV1623
6.45	TTGACCTCAAGATTGCTTGAGGTTCT	left	-253	SAV7217
		right	-64	SAV7218
7.73	TTGACCTCAAGATTGGTTGAGGTACC	left	-328	SAV5664
		right	-82	SAV5665

Streptomyces coelicolor A3(2), complete genome

Site Energy	Sequence	Operon pos	Distance to start	Genes in operon
5.78	TTGACCTCAAGCAAACCTTGAGGTACC	left	-57	SCO2478
		right	-178	SCO2479
8.53	TTGACCTCAAGCAGGCTTGAGGTCGT	left	-45	SCO4266
		right	-169	SCO7007
8.75	TTGACCTCAAGGTTGGTCGAGGTTCT	left	-70	SCO7008

Thermobifida fusca YX, complete genome

Site Energy	Sequence	Operon pos	Distance to start	Genes in operon
3.74	TTGACCTCAACTTGGTTGAGGTTTT	left	-278	Tfu_1696-
		right	-133	Tfu_1695 Tfu_1697
6.65	TTGACCTCAACCTAACCTGAGATTTG	left	-27	Tfu_0408
		right	-141	Tfu_0409
8.94	TGGATCTCACCTTAGGTTGAGGTTTC	left	-431	Tfu_1567

Thermococcus kodakarensis KOD1, complete genome

Site Energy	Sequence	Operon pos	Distance to start	Genes in operon
-------------	----------	------------	-------------------	-----------------

Vibrio cholerae O1 biovar eltor str. N16961 chromosome I, complete sequence

Site Energy	Sequence	Operon pos	Distance to start	Genes in operon
-------------	----------	------------	-------------------	-----------------

Vibrio cholerae O1 biovar eltor str. N16961 chromosome II, complete sequence

Site Energy	Sequence	Operon pos	Distance to start	Genes in operon
2.14	TTTACCTAAAGTTAACCTGAGGTATT	left	-115	VCA0084
		right	-89	VCA0085

Vibrio parahaemolyticus RIMD 2210633 chromosome II, complete sequence

Site Energy	Sequence	Operon pos	Distance to start	Genes in operon
4.79	TTTACCTCAAGTTACTTGAGGTTCT	left	-89	VPA0335
5.08	TTGACCTAACCAAACCTTGAGGTTTT	left	-99	VPA1738
5.48	TTTACCTCGATTTAACTTGAGGTTTT	left	-96	VPA1685
5.59	TTTACCTAAACCTAGCTTGAGGTTCT	left	-163	VPA0390
		right	-98	VPA0391

Vibrio vulnificus CMCP6 chromosome I, complete sequence

Site Energy	Sequence	Operon pos	Distance to start	Genes in operon
-------------	----------	------------	-------------------	-----------------

Vibrio vulnificus CMCP6 chromosome II, complete sequence

Site Energy	Sequence	Operon pos	Distance to start	Genes in operon
1.16	TTGACCTCAAGTTAACTTGAGGAATT	left	-109	VV2_1129
2.52	TTTACCTCAAGTTAAGTTGAGCTTT	left	-57	VV2_0936
		right	-97	VV2_0937
3.18	TTTACCTCAATTTAACTTGAGGTTTT	left	-35	VV2_0607
		right	-230	VV2_0608

Vibrio vulnificus YJ016 chromosome I, complete sequence

Site Energy	Sequence	Operon pos	Distance to start	Genes in operon
-------------	----------	------------	-------------------	-----------------

Vibrio vulnificus YJ016 chromosome II, complete sequence

Site Energy	Sequence	Operon pos	Distance to start	Genes in operon
1.16	TTGACCTCAAGTTAACTTGAGGAATT	left	-110	VVA1655- VVA1656
2.52	TTTACCTCAAGTTAAGTTGAGCTTT	left	-57	VVA1425
		right	-79	VVA1426
3.18	TTTACCTCAATTTAACTTGAGGTTTT	left	-35	VVA1158
		right	-230	VVA1159

Xanthomonas campestris pv. campestris str. 8004, complete genome

Site Energy	Sequence	Operon pos	Distance to start	Genes in operon
8.71	TTGACCTCACCTTGAGGCAGG	left	-166	XC_1279
		right	-56	XC_1280

Xanthomonas campestris pv. campestris str. ATCC 33913, complete genome

Site Energy	Sequence	Operon pos	Distance to start	Genes in operon
8.71	TTGACCTAACCTTGTTGAGGCAGG	left	-4	soxR (XCC2831)
		right	-729	XCC2832

Xanthomonas campestris pv. vesicatoria str. 85-10, complete genome

Site Energy	Sequence	Operon pos	Distance to start	Genes in operon
5.49	TTGACCTCAACTTAGGTTGAGGCAGG	left	-4	soxR (XCV3149)
		right	-121	XCV3150

Xanthomonas axonopodis pv. citri str. 306, complete genome

Site Energy	Sequence	Operon pos	Distance to start	Genes in operon
5.49	TTGACCTCAACTTAGGTTGAGGCAGG	left	-4	soxR (XAC3000)
		right	-121	ptr (XAC3001)
8.02	TTGACCTCAACTGCGTTGAGGTCGT	left	-31	XAC0314
		right	-278	XAC0315

Xanthomonas oryzae pv. oryzae MAFF 311018, complete genome

Site Energy	Sequence	Operon pos	Distance to start	Genes in operon
9.07	TTGACCTCAACTCAGGTTAAGGCAGG	left	-70	XOO1154 (XOO_1154)
		right	-56	XOO1155 (XOO_1155)

Bibliography

- [1] J. B. Andersen, C. Sternberg, L. K. Poulsen, S. P. Bjorn, M. Givskov, and S. Molin. New unstable variants of green fluorescent protein for studies of transient gene expression in bacteria. *Appl Environ Microbiol*, 64(6):2240–6, Jun 1998.
- [2] Y. Bao, D. P. Lies, H. Fu, and G. P. Roberts. An improved Tn7-based system for the single-copy insertion of cloned genes into chromosomes of gram-negative bacteria. *Gene*, 109(1):167–8, Dec 1991.
- [3] M. S. Bartlett and R. L. Gourse. Growth rate-dependent control of the rrnB P1 core promoter in *Escherichia coli*. *J Bacteriol*, 176(17):5560–4, Sep 1994. (eng) (hard copy only).
- [4] B. L. Bassler. How bacteria talk to each other: regulation of gene expression by quorum sensing. *Curr Opin Microbiol*, 2(6):582–7, Dec 1999.
- [5] A. S. Beliaev, D. M. Klingeman, J. A. Klappenbach, L. Wu, M. F. Romine, J. M. Tiedje, K. H. Nealson, J. K. Fredrickson, and J. Zhou. Global transcriptome analysis of *Shewanella oneidensis* MR-1 exposed to different terminal electron acceptors. *J Bacteriol*, 187(20):7138–45, Oct 2005.
- [6] A. S. Beliaev, D. K. Thompson, T. Khare, H. Lim, C. C. Brandt, G. Li, A. E. Murray, J. F. Heidelberg, C. S. Giometti, 3. r. d. Yates J, K. H. Nealson, J. M. Tiedje, and J. Zhou. Gene and protein expression profiles of *Shewanella oneidensis* during anaerobic growth with different electron acceptors. *OMICS*, 6(1):39–60, 2002.
- [7] R. Bencheikh-Latmani, S. M. Williams, L. Haucke, C. S. Criddle, L. Wu, J. Zhou, and B. M. Tebo. Global transcriptional profiling of *Shewanella oneidensis* MR-1 during Cr(VI) and U(VI) reduction. *Appl Environ Microbiol*, 71(11):7453–60, Nov 2005.

- [8] M. Berney, F. Hammes, F. Bosshard, H. U. Weilenmann, and T. Egli. Assessment and Interpretation of Bacterial Viability by Using the LIVE/DEAD BacLight Kit in Combination with Flow Cytometry. *Appl Environ Microbiol*, 73(10):3283–90, May 2007.
- [9] J. C. Biffinger, J. Pietron, R. Ray, B. Little, and B. R. Ringeisen. A biofilm enhanced miniature microbial fuel cell using *Shewanella oneidensis* DSP10 and oxygen reduction cathodes. *Biosens Bioelectron*, 22(8):1672–9, Mar 2007.
- [10] G. V. Bloemberg, A. H. Wijfjes, G. E. Lamers, N. Stuurman, and B. J. Lugtenberg. Simultaneous imaging of *Pseudomonas fluorescens* WCS365 populations expressing three different autofluorescent proteins in the rhizosphere: new perspectives for studying microbial communities. *Mol Plant Microbe Interact*, 13(11):1170–6, Nov 2000.
- [11] B. R. Boles, M. Thoendel, and P. K. Singh. Self-generated diversity produces insurance effects in biofilm communities. *Proc Natl Acad Sci U S A*, Nov 2004.
- [12] R. C. Boucher. Airway surface dehydration in cystic fibrosis: pathogenesis and therapy. *Annu Rev Med*, 58:157–70, 2007.
- [13] F. Bredenbruch, R. Geffers, M. Nimtz, J. Buer, and S. Haussler. The *Pseudomonas aeruginosa* quinolone signal (PQS) has an iron-chelating activity. *Environ Microbiol*, 8(8):1318–29, Aug 2006.
- [14] N. C. Caiazza and G. A. O'Toole. SadB is required for the transition from reversible to irreversible attachment during biofilm formation by *Pseudomonas aeruginosa* PA14. *J Bacteriol*, 186(14):4476–85, Jul 2004.
- [15] A. Camilli and B. L. Bassler. Bacterial small-molecule signaling pathways. *Science*, 311(5764):1113–6, Feb 2006.
- [16] W. Carpentier, K. Sandra, I. De Smet, A. Brige, L. De Smet, and J. Van Beeumen. Microbial reduction and precipitation of vanadium by *Shewanella oneidensis*. *Appl Environ Microbiol*, 69(6):3636–9, Jun 2003.
- [17] E. J. Cho and A. D. Ellington. Optimization of the biological component of a bioelectrochemical cell. *Bioelectrochemistry*, 70(1):165–72, Jan 2007.

- [18] K. H. Choi, J. B. Gaynor, K. G. White, C. Lopez, C. M. Bosio, R. R. Karkhoff-Schweizer, and H. P. Schweizer. A Tn7-based broad-range bacterial cloning and expression system. *Nat Methods*, 2(6):443–8, Jun 2005.
- [19] A. C. Cole, M. J. Semmens, and T. M. LaPara. Stratification of activity and bacterial community structure in biofilms grown on membranes transferring oxygen. *Appl Environ Microbiol*, 70(4):1982–9, Apr 2004.
- [20] J. W. Costerton. Cystic fibrosis pathogenesis and the role of biofilms in persistent infection. *Trends Microbiol*, 9(2):50–2, Feb 2001.
- [21] J. W. Costerton, L. Montanaro, and C. R. Arciola. Biofilm in implant infections: its production and regulation. *Int J Artif Organs*, 28(11):1062–8, Nov 2005.
- [22] N. L. Craig. Tn7: a target site-specific transposon. *Mol Microbiol*, 5(11):2569–73, Nov 1991.
- [23] M. E. Davey, N. C. Caiazza, and G. A. O'Toole. Rhamnolipid surfactant production affects biofilm architecture in *Pseudomonas aeruginosa* PAO1. *J Bacteriol*, 185(3):1027–36, Feb 2003.
- [24] M. E. Davey and G. A. O'toole. Microbial biofilms: from ecology to molecular genetics. *Microbiol Mol Biol Rev*, 64(4):847–67, Dec 2000.
- [25] D. G. Davies and G. G. Geesey. Regulation of the alginic biosynthesis gene algC in *Pseudomonas aeruginosa* during biofilm development in continuous culture. *Appl Environ Microbiol*, 61(3):860–7, Mar 1995.
- [26] L. E. Dietrich, A. Price-Whelan, A. Petersen, M. Whiteley, and D. K. Newman. The phenazine pyocyanin is a terminal signalling factor in the quorum sensing network of *Pseudomonas aeruginosa*. *Mol Microbiol*, 61(5):1308–21, Sep 2006.
- [27] A. S. Engel, M. L. Porter, L. A. Stern, S. Quinlan, and P. C. Bennett. Bacterial diversity and ecosystem function of filamentous microbial mats from aphotic (cave) sulfidic springs dominated by chemolithoautotrophic *Epsilonproteobacteria*. *FEMS Microbiol Ecol*, 51(1):31–53, Dec 2004.
- [28] A. Finelli, C. V. Gallant, K. Jarvi, and L. L. Burrows. Use of In-Biofilm Expression Technology To Identify Genes Involved in *Pseudomonas aeruginosa* Biofilm Development. *J Bacteriol*, 185(9):2700–10, May 2003.

- [29] W. C. Fuqua, S. C. Winans, and E. P. Greenberg. Quorum sensing in bacteria: the LuxR-LuxI family of cell density-responsive transcriptional regulators. *J Bacteriol*, 176(2):269–75, Jan 1994.
- [30] W. Gao, Y. Liu, J. Zhou, and H. Pan. Effects of a strong static magnetic field on bacterium *Shewanella oneidensis*: an assessment by using whole genome microarray. *Bioelectromagnetics*, 26(7):558–63, Oct 2005.
- [31] J. M. Ghigo. Are there biofilm-specific physiological pathways beyond a reasonable doubt? *Res Microbiol*, 154(1):1–8, Jan 2003.
- [32] C. S. Giometti, T. Khare, S. L. Tollaksen, A. Tsapin, W. Zhu, 3. r. d. Yates JR, and K. H. Nealson. Analysis of the *Shewanella oneidensis* proteome by two-dimensional gel electrophoresis under nondenaturing conditions. *Proteomics*, 3(5):777–85, May 2003.
- [33] J. L. Groh, Q. Luo, J. D. Ballard, and L. R. Krumholz. A method adapting microarray technology for signature-tagged mutagenesis of *Desulfovibrio desulfuricans* G20 and *Shewanella oneidensis* MR-1 in anaerobic sediment survival experiments. *Appl Environ Microbiol*, 71(11):7064–74, Nov 2005.
- [34] J. P. Grotzinger and A. H. Knoll. Stromatolites in Precambrian carbonates: evolutionary mileposts or environmental dipsticks? *Annu Rev Earth Planet Sci*, 27:313–58, 1999.
- [35] L. Hall-Stoodley and P. Stoodley. Developmental regulation of microbial biofilms. *Curr Opin Biotechnol*, 13(3):228–33, Jun 2002.
- [36] M. C. Hansen, J. r. Palmer RJ, C. Udsen, D. C. White, and S. Molin. Assessment of GFP fluorescence in cells of *Streptococcus gordonii* under conditions of low pH and low oxygen concentration. *Microbiology*, 147(Pt 5):1383–91, May 2001.
- [37] H. J. Harmsen, H. M. Kengen, A. D. Akkermans, A. J. Stams, and W. M. de Vos. Detection and localization of syntrophic propionate-oxidizing bacteria in granular sludge by in situ hybridization using 16S rRNA-based oligonucleotide probes. *Appl Environ Microbiol*, 62(5):1656–63, May 1996.
- [38] S. Heeb, Y. Itoh, T. Nishijyo, U. Schnider, C. Keel, J. Wade, U. Walsh, F. O’Gara, and D. Haas. Small, stable shuttle vectors based on the minimal pVS1 replicon for use in gram-negative, plant-associated bacteria. *Mol Plant Microbe Interact*, 13(2):232–7, Feb 2000.

- [39] J. F. Heidelberg, I. T. Paulsen, K. E. Nelson, E. J. Gaidos, W. C. Nelson, T. D. Read, J. A. Eisen, R. Seshadri, N. Ward, B. Methe, R. A. Clayton, T. Meyer, A. Tsapin, J. Scott, M. Beanan, L. Brinkac, S. Daugherty, R. T. DeBoy, R. J. Dodson, A. S. Durkin, D. H. Haft, J. F. Kolonay, R. Madupu, J. D. Peterson, L. A. Umayam, O. White, A. M. Wolf, J. Vamathevan, J. Weidman, M. Impraim, K. Lee, K. Berry, C. Lee, J. Mueller, H. Khouri, J. Gill, T. R. Utterback, L. A. McDonald, T. V. Feldblyum, H. O. Smith, J. C. Venter, K. H. Nealson, and C. M. Fraser. Genome sequence of the dissimilatory metal ion-reducing bacterium *Shewanella oneidensis*. *Nat Biotechnol*, Oct 2002.
- [40] M. E. Hernandez, A. Kappler, and D. K. Newman. Phenazines and Other Redox-Active Antibiotics Promote Microbial Mineral Reduction. *Appl Environ Microbiol*, 70(2):921–928, Feb 2004.
- [41] D. E. Holmes, D. R. Bond, R. A. O’Neil, C. E. Reimers, L. R. Tender, and D. R. Lovley. Microbial communities associated with electrodes harvesting electricity from a variety of aquatic sediments. *Microb Ecol*, 48(2):178–90, Aug 2004.
- [42] C. K. Hope, D. Clements, and M. Wilson. Determining the spatial distribution of viable and nonviable bacteria in hydrated microcosm dental plaques by viability profiling. *J Appl Microbiol*, 93(3):448–55, 2002.
- [43] C. T. Huang, K. D. Xu, G. A. McFeters, and P. S. Stewart. Spatial patterns of alkaline phosphatase expression within bacterial colonies and biofilms in response to phosphate starvation. *Appl Environ Microbiol*, 64(4):1526–31, Apr 1998.
- [44] C. T. Huang, F. P. Yu, G. A. McFeters, and P. S. Stewart. Nonuniform spatial patterns of respiratory activity within biofilms during disinfection. *Appl Environ Microbiol*, 61(6):2252–6, Jun 1995.
- [45] S. M. Hunt, E. M. Werner, B. Huang, M. A. Hamilton, and P. S. Stewart. Hypothesis for the role of nutrient starvation in biofilm detachment. *Appl Environ Microbiol*, 70(12):7418–25, Dec 2004.
- [46] M. Juhas, L. Eberl, and B. Tummler. Quorum sensing: the power of cooperation in the world of *Pseudomonas*. *Environ Microbiol*, 7(4):459–71, Apr 2005.
- [47] S. T. Kelley, U. Theisen, L. T. Angenent, A. St Amand, and N. R. Pace. Molecular analysis of shower curtain biofilm microbes. *Appl Environ Microbiol*, 70(7):4187–92, Jul 2004.

- [48] T. R. De Kievit, M. D. Parkins, R. J. Gillis, R. Srikumar, H. Ceri, K. Poole, B. H. Iglewski, and D. G. Storey. Multidrug efflux pumps: expression patterns and contribution to antibiotic resistance in *Pseudomonas aeruginosa* biofilms. *Antimicrob Agents Chemother*, 45(6):1761–70, Jun 2001.
- [49] M. Klausen, A. Aaes-Jorgensen, S. Molin, and T. Tolker-Nielsen. Involvement of bacterial migration in the development of complex multicellular structures in *Pseudomonas aeruginosa* biofilms. *Mol Microbiol*, 50(1):61–8, Oct 2003.
- [50] B. Koch, L. E. Jensen, and O. Nybroe. A panel of Tn7-based vectors for insertion of the gfp marker gene or for delivery of cloned DNA into Gram-negative bacteria at a neutral chromosomal site. *J Microbiol Methods*, 45(3):187–95, Jul 2001. (eng) (hard copy only).
- [51] P. E. Kolenbrander. Oral microbial communities: biofilms, interactions, and genetic systems. *Annu Rev Microbiol*, 54:413–37, 2000.
- [52] L. Lambertsen, C. Sternberg, and S. Molin. Mini-Tn7 transposons for site-specific tagging of bacteria with fluorescent proteins. *Environ Microbiol*, 6(7):726–32, Jul 2004.
- [53] J. B. Laursen and J. Nielsen. Phenazine natural products: biosynthesis, synthetic analogues, and biological activity. *Chem Rev*, 104(3):1663–86, Mar 2004.
- [54] A. B. Leaphart, D. K. Thompson, K. Huang, E. Alm, X. F. Wan, A. Arkin, S. D. Brown, L. Wu, T. Yan, X. Liu, G. S. Wickham, and J. Zhou. Transcriptome profiling of *Shewanella oneidensis* gene expression following exposure to acidic and alkaline pH. *J Bacteriol*, 188(4):1633–42, Feb 2006.
- [55] Y. Lequette and E. P. Greenberg. Timing and Localization of Rhamnolipid Synthesis Gene Expression in *Pseudomonas aeruginosa* Biofilms. *J Bacteriol*, 187(1):37–44, Jan 2005.
- [56] K. Lewis. Persister cells, dormancy and infectious disease. *Nat Rev Microbiol*, 5(1):48–56, Jan 2007.
- [57] D. P. Lies, M. E. Hernandez, A. Kappler, R. E. Mielke, J. A. Gralnick, and D. K. Newman. *Shewanella oneidensis* MR-1 Uses Overlapping Pathways for Iron Reduction at a Distance and by Direct Contact under Conditions Relevant for Biofilms. *Appl Environ Microbiol*, 71(8):4414–26, Aug 2005.
- [58] J. Liu. . PhD thesis, University of Wisconsin, 2003.

- [59] Y. Liu, W. Gao, Y. Wang, L. Wu, X. Liu, T. Yan, E. Alm, A. Arkin, D. K. Thompson, M. W. Fields, and J. Zhou. Transcriptome Analysis of *Shewanella oneidensis* MR-1 in Response to Elevated Salt Conditions. *J Bacteriol*, 187(7):2501–7, Apr 2005.
- [60] T. F. Mah, B. Pitts, B. Pellock, G. C. Walker, P. S. Stewart, and G. A. O'Toole. A genetic basis for *Pseudomonas aeruginosa* biofilm antibiotic resistance. *Nature*, 426(6964):306–10, Nov 2003.
- [61] T. M. Maier, J. M. Myers, and C. R. Myers. Identification of the gene encoding the sole physiological fumarate reductase in *Shewanella oneidensis* MR-1. *J Basic Microbiol*, 43(4):312–27, 2003.
- [62] P. D. Majors, J. S. McLean, G. E. Pinchuk, J. K. Fredrickson, Y. A. Gorby, K. R. Minard, and R. A. Wind. NMR methods for in situ biofilm metabolism studies. *J Microbiol Methods*, Jun 2005.
- [63] S. L. McKnight, B. H. Iglewski, and E. C. Pesci. The *Pseudomonas* quinolone signal regulates rhl quorum sensing in *Pseudomonas aeruginosa*. *J Bacteriol*, 182(10):2702–8, May 2000.
- [64] G. Meshulam-Simon, S. Behrens, A. D. Choo, and A. M. Spormann. Hydrogen metabolism in *Shewanella oneidensis* MR-1. *Appl Environ Microbiol*, 73(4):1153–65, Feb 2007.
- [65] D. Minz, J. L. Flax, S. J. Green, G. Muyzer, Y. Cohen, M. Wagner, B. E. Rittmann, and D. A. Stahl. Diversity of sulfate-reducing bacteria in oxic and anoxic regions of a microbial mat characterized by comparative analysis of dissimilatory sulfite reductase genes. *Appl Environ Microbiol*, 65(10):4666–71, Oct 1999.
- [66] S. Moller, C. Sternberg, J. B. Andersen, B. B. Christensen, J. L. Ramos, M. Givskov, and S. Molin. In situ gene expression in mixed-culture biofilms: evidence of metabolic interactions between community members. *Appl Environ Microbiol*, 64(2):721–32, Feb 1998.
- [67] T. S. Murray, M. Egan, and B. I. Kazmierczak. *Pseudomonas aeruginosa* chronic colonization in cystic fibrosis patients. *Curr Opin Pediatr*, 19(1):83–8, Feb 2007.
- [68] C. R. Myers and J. M. Myers. Replication of plasmids with the p15A origin in *Shewanella putrefaciens* MR-1. *Lett Appl Microbiol*, 24(3):221–5, Mar 1997.

- [69] Y. V. Nancharaiah, V. P. Venugopalan, S. Wuertz, P. A. Wilderer, and M. Hausner. Compatibility of the green fluorescent protein and a general nucleic acid stain for quantitative description of a *Pseudomonas putida* biofilm. *J Microbiol Methods*, 60(2):179–87, Feb 2005.
- [70] A. T. Nielsen, T. Tolker-Nielsen, K. B. Barken, and S. Molin. Role of commensal relationships on the spatial structure of a surface-attached microbial consortium. *Environ Microbiol*, 2(1):59–68, Feb 2000.
- [71] S. Okabe, T. Itoh, H. Satoh, and Y. Watanabe. Analyses of spatial distributions of sulfate-reducing bacteria and their activity in aerobic wastewater biofilms. *Appl Environ Microbiol*, 65(11):5107–16, Nov 1999.
- [72] G. A. O'Toole. To build a biofilm. *J Bacteriol*, 185(9):2687–9, May 2003.
- [73] G. Patterson, R. N. Day, and D. Piston. Fluorescent protein spectra. *J Cell Sci*, 114(Pt 5):837–8, Mar 2001.
- [74] L. K. Poulsen, G. Ballard, and D. A. Stahl. Use of rRNA fluorescence in situ hybridization for measuring the activity of single cells in young and established biofilms. *Appl Environ Microbiol*, 59(5):1354–60, May 1993.
- [75] L. A. Pratt and R. Kolter. Genetic analyses of bacterial biofilm formation. *Curr Opin Microbiol*, 2(6):598–603, Dec 1999.
- [76] B. M. Pruss, C. Besemann, A. Denton, and A. J. Wolfe. A complex transcription network controls the early stages of biofilm development by *Escherichia coli*. *J Bacteriol*, 188(11):3731–9, Jun 2006.
- [77] X. Qiu, M. J. Daly, A. Vasilenko, M. V. Omelchenko, E. K. Gaidamakova, L. Wu, J. Zhou, G. W. Sundin, and J. M. Tiedje. Transcriptome analysis applied to survival of *Shewanella oneidensis* MR-1 exposed to ionizing radiation. *J Bacteriol*, 188(3):1199–204, Feb 2006.
- [78] X. Qiu, G. W. Sundin, B. Chai, and J. M. Tiedje. Survival of *Shewanella oneidensis* MR-1 after UV Radiation Exposure. *Appl Environ Microbiol*, 70(11):6435–6443, 11 2004.
- [79] J. r. Renye JA, P. J. Piggot, L. Daneo-Moore, and B. A. Buttarro. Persistence of *Streptococcus mutans* in stationary-phase batch cultures and biofilms. *Appl Environ Microbiol*, 70(10):6181–7, Oct 2004.

- [80] K. Rabaey, N. Boon, S. D. Siciliano, M. Verhaege, and W. Verstraete. Biofuel cells select for microbial consortia that self-mediate electron transfer. *Appl Environ Microbiol*, 70(9):5373–82, Sep 2004.
- [81] R. J. Ram, N. C. Verberkmoes, M. P. Thelen, G. W. Tyson, B. J. Baker, R. C. Blake II, M. Shah, R. L. Hettich, and J. F. Banfield. Community Proteomics of a Natural Microbial Biofilm. *Science*, May 2005.
- [82] S. A. Rani, B. Pitts, H. Beyenal, R. A. Veluchamy, Z. Lewandowski, W. M. Davison, K. Buckingham-Meyer, and P. S. Stewart. Spatial Patterns of DNA Replication, Protein Synthesis and Oxygen Concentration within Bacterial Biofilms Reveal Diverse Physiological States. *J Bacteriol*, Mar 2007.
- [83] K. Rasmussen and Z. Lewandowski. Microelectrode measurements of local mass transport rates in heterogeneous biofilms. *Biotechnol Bioeng*, 59(3):302–9, Aug 1998.
- [84] B. R. Ringeisen, E. Henderson, P. K. Wu, J. Pietron, R. Ray, B. Little, J. C. Biffinger, and J. M. Jones-Meehan. High power density from a miniature microbial fuel cell using *Shewanella oneidensis* DSP10. *Environ Sci Technol*, 40(8):2629–34, Apr 2006.
- [85] C. W. Saltikov, A. Cifuentes, K. Venkateswaran, and D. K. Newman. The ars Detoxification System Is Advantageous but Not Required for As(V) Respiration by the Genetically Tractable *Shewanella* Species Strain ANA-3. *Appl Environ Microbiol*, 69(5):2800–9, May 2003.
- [86] B. Sampathkumar, S. Napper, C. D. Carrillo, P. Willson, E. Taboada, J. H. Nash, A. A. Potter, L. A. Babiuk, and B. J. Allan. Transcriptional and translational expression patterns associated with immobilized growth of *Campylobacter jejuni*. *Microbiology*, 152(Pt 2):567–77, Feb 2006.
- [87] K. Y. San, G. N. Bennett, S. J. Berrios-Rivera, R. V. Vadali, Y. T. Yang, E. Horton, F. B. Rudolph, B. Sariyar, and K. Blackwood. Metabolic engineering through cofactor manipulation and its effects on metabolic flux redistribution in *Escherichia coli*. *Metab Eng*, 4(2):182–92, Apr 2002.
- [88] K. Sauer. The genomics and proteomics of biofilm formation. *Genome Biol*, 4(6):219, 2003.
- [89] K. Sauer and A. K. Camper. Characterization of Phenotypic Changes in *Pseudomonas putida* in Response to Surface-Associated Growth. *J Bacteriol*, 183(22):6579–89, Nov 2001.

- [90] K. Sauer, A. K. Camper, G. D. Ehrlich, J. W. Costerton, and D. G. Davies. *Pseudomonas aeruginosa* displays multiple phenotypes during development as a biofilm. *J Bacteriol*, 184(4):1140–54, Feb 2002.
- [91] J. H. Scott and K. H. Nealson. A biochemical study of the intermediary carbon metabolism of *Shewanella putrefaciens*. *J Bacteriol*, 176(11):3408–11, Jun 1994.
- [92] Christopher J Southey-Pillig, David G Davies, and Karin Sauer. Characterization of Temporal Protein Production in *Pseudomonas aeruginosa* Biofilms. *J Bacteriol*, 187(23):8114–8126, Dec 2005.
- [93] C. M. Southward and M. G. Surette. The dynamic microbe: green fluorescent protein brings bacteria to light. *Mol Microbiol*, 45(5):1191–6, Sep 2002.
- [94] N. R. Stanley and B. A. Lazazzera. Environmental signals and regulatory pathways that influence biofilm formation. *Mol Microbiol*, 52(4):917–24, May 2004.
- [95] C. Sternberg, B. B. Christensen, T. Johansen, A. Toftgaard Nielsen, J. B. Andersen, M. Givskov, and S. Molin. Distribution of bacterial growth activity in flow-chamber biofilms. *Appl Environ Microbiol*, 65(9):4108–17, Sep 1999.
- [96] P. S. Stewart. Diffusion in biofilms. *J Bacteriol*, 185(5):1485–91, Mar 2003.
- [97] P. Stoodley, D. G. Davies, and J. W. Costerton. Biofilms as Complex Differentiated Communities. *Annu Rev Microbiol*, Apr 2002.
- [98] Y. J. Tang, J. S. Hwang, D. E. Wemmer, and J. D. Keasling. *Shewanella oneidensis* MR-1 fluxome under various oxygen conditions. *Appl Environ Microbiol*, 73(3):718–29, Feb 2007.
- [99] Y. J. Tang, A. L. Meadows, and J. D. Keasling. A kinetic model describing *Shewanella oneidensis* MR-1 growth, substrate consumption, and product secretion. *Biotechnol Bioeng*, 96(1):125–33, Jan 2007.
- [100] Y. J. Tang, A. L. Meadows, J. Kirby, and J. D. Keasling. Anaerobic central metabolic pathways in *Shewanella oneidensis* MR-1 reinterpreted in the light of isotopic metabolite labeling. *J Bacteriol*, 189(3):894–901, Feb 2007.
- [101] T. K. Teal, D. P. Lies, B. J. Wold, and D. K. Newman. Spatiometabolic stratification of *Shewanella oneidensis* biofilms. *Appl Environ Microbiol*, 72(11):7324–30, Nov 2006.

- [102] D. K. Thompson, A. S. Beliaev, C. S. Giometti, S. L. Tollaksen, T. Khare, D. P. Lies, K. H. Nealson, H. Lim, 3. r. d. Yates J, C. C. Brandt, J. M. Tiedje, and J. Zhou. Transcriptional and Proteomic Analysis of a Ferric Uptake Regulator (Fur) Mutant of *Shewanella oneidensis*: Possible Involvement of Fur in Energy Metabolism, Transcriptional Regulation, and Oxidative Stress. *Appl Environ Microbiol*, 68(2):881–892, Feb 2002.
- [103] K. M. Thormann, S. Duttler, R. M. Saville, M. Hyodo, S. Shukla, Y. Hayakawa, and A. M. Spormann. Control of formation and cellular detachment from *Shewanella oneidensis* MR-1 biofilms by cyclic di-GMP. *J Bacteriol*, 188(7):2681–91, Apr 2006.
- [104] K. M. Thormann, R. M. Saville, S. Shukla, D. A. Pelletier, and A. M. Spormann. Initial Phases of Biofilm Formation in *Shewanella oneidensis* MR-1. *J Bacteriol*, 186(23):8096–8104, Dec 2004.
- [105] K. M. Thormann, R. M. Saville, S. Shukla, and A. M. Spormann. Induction of Rapid Detachment in *Shewanella oneidensis* MR-1 Biofilms. *J Bacteriol*, 187(3):1014–1021, Feb 2005.
- [106] J. M. Tiedje. *Shewanella*—the environmentally versatile genome. *Nat Biotechnol*, 20(11):1093–4, Nov 2002.
- [107] T. Tolker-Nielsen, U. C. Brinch, P. C. Ragas, J. B. Andersen, C. S. Jacobsen, and S. Molin. Development and dynamics of *Pseudomonas* sp. biofilms. *J Bacteriol*, 182(22):6482–9, Nov 2000.
- [108] T. Tolker-Nielsen and S. Molin. Spatial Organization of Microbial Biofilm Communities. *Microb Ecol*, 40(2):75–84, Aug 2000.
- [109] A. I. Tsapin, I. Vandenberghe, K. H. Nealson, J. H. Scott, T. E. Meyer, M. A. Cusanovich, E. Harada, T. Kaizu, H. Akutsu, D. Leys, and J. J. Van Beeumen. Identification of a small tetraheme cytochrome c and a flavocytochrome c as two of the principal soluble cytochromes c in *Shewanella oneidensis* strain MR1. *Appl Environ Microbiol*, 67(7):3236–44, Jul 2001.
- [110] H. C. van der Mei, D. J. White, J. Atema-Smit, E. van de Belt-Gritter, and H. J. Busscher. A method to study sustained antimicrobial activity of rinse and dentifrice components on biofilm viability in vivo. *J Clin Periodontol*, 33(1):14–20, Jan 2006.
- [111] K. Venkateswaran, D. P. Moser, M. E. Dollhopf, D. P. Lies, D. A. Saffarini, B. J. MacGregor, D. B. Ringelberg, D. C. White, M. Nishijima, H. Sano, J. Burghardt, E. Stackebrandt, and

- K. H. Nealson. Polyphasic taxonomy of the genus *Shewanella* and description of *Shewanella oneidensis* sp. nov. *Int J Syst Bacteriol*, 49 Pt 2:705–24, Apr 1999.
- [112] J. Vieira and J. Messing. New pUC-derived cloning vectors with different selectable markers and DNA replication origins. *Gene*, 100:189–94, Apr 1991.
- [113] R. T. Villavicencio. The history of blue pus. *J Am Coll Surg*, 187(2):212–6, Aug 1998.
- [114] N. S. Webster and A. P. Negri. Site-specific variation in Antarctic marine biofilms established on artificial surfaces. *Environ Microbiol*, 8(7):1177–90, Jul 2006.
- [115] E. J. Wentland, P. S. Stewart, C. T. Huang, and G. A. McFeters. Spatial variations in growth rate within *Klebsiella pneumoniae* colonies and biofilm. *Biotechnol Prog*, 12(3):316–21, May 1996.
- [116] E. Werner, F. Roe, A. Bugnicourt, M. J. Franklin, A. Heydorn, S. Molin, B. Pitts, and P. S. Stewart. Stratified Growth in *Pseudomonas aeruginosa* Biofilms. *Appl Environ Microbiol*, 70(10):6188–6196, 10 2004.
- [117] C. B. Whitchurch, T. Tolker-Nielsen, P. C. Ragas, and J. S. Mattick. Extracellular DNA required for bacterial biofilm formation. *Science*, 295(5559):1487, Feb 2002.
- [118] M. Whiteley, M. G. Bangera, R. E. Bumgarner, M. R. Parsek, G. M. Teitzel, S. Lory, and E. P. Greenberg. Gene expression in *Pseudomonas aeruginosa* biofilms. *Nature*, 413(6858):860–4, Oct 2001.
- [119] K. D. Xu, P. S. Stewart, F. Xia, C. T. Huang, and G. A. McFeters. Spatial physiological heterogeneity in *Pseudomonas aeruginosa* biofilm is determined by oxygen availability. *Appl Environ Microbiol*, 64(10):4035–9, Oct 1998.
- [120] J. M. Yarwood, E. M. Volper, and E. P. Greenberg. Delays in *Pseudomonas aeruginosa* quorum-controlled gene expression are conditional. *Proc Natl Acad Sci U S A*, 102(25):9008–13, Jun 2005.
- [121] A. Yoshida and H. K. Kuramitsu. *Streptococcus mutans* biofilm formation: utilization of a gtfB promoter-green fluorescent protein (PgtfB::gfp) construct to monitor development. *Microbiology*, 148(Pt 11):3385–94, Nov 2002.